Elucidation of Orthopoxvirus Adaptation Mechanisms by Proteomics and Genomics

vorgelegt von
Dipl.-Ing.
Marica Grossegesse
geb. in Hildesheim

Von der Fakultät III – Prozesswissenschaften
der Technischen Universität Berlin
zur Erlangung des akademischen Grades

Doktor der Ingenieurwissenschaften
- Dr.-Ing. -

Genehmigte Dissertation

Promotionsausschuss:

Vorsitzender:	Prof. Dr. Peter Neubauer
Gutachter:	Prof. Dr. Andreas Nitsche
Gutachter:	Prof. Dr. Juri Rappsilber
Gutachter:	Prof. Dr. Roland Lauster

Tag der wissenschaftlichen Aussprache: 08.12.2017

Berlin 2017

Abstract

Adaptive changes of viruses enable the virus-host coevolution and infection of new host species. While viruses with an RNA genome adapt primarily by genomic variabilities, adaptation mechanisms of viruses with a DNA genome have remained largely elusive. Since genomes of DNA viruses are more stable compared to genomes of RNA viruses, it is assumed that mechanisms other than genomic changes underlie the adaptation of DNA viruses. However, these mechanisms have hardly been investigated so far. Since isolated virus particles are capable of crossing the species barrier, it is assumed that adaptive changes can be identified in the virus particles themselves. Therefore, this study aimed to elucidate adaptation mechanisms of DNA virus particles by proteomics and genomics technologies. While next-generation sequencing technologies are frequently used to analyze genomic changes of viruses, adaptive changes of virus particles by mass spectrometry-based proteomics have not been analyzed yet.

In the present study, cowpox virus (CPXV) was used as a model virus and cell culture as a model system to study adaptive changes of DNA virus particles. CPXV is a member of the genus Orthopoxvirus (OPV) and is able infect a remarkably broad range of host species, e.g. rats, cats, elephants and humans. Increasing numbers of CPXV infections in Europe underline the need for a comprehensive understanding of OPV adaptation mechanisms.

CPXV particles were isolated from a rat, which is a natural host of these viruses, and serially passaged five times in a rat and a human cell line. During passaging, an increase in viral fitness was observed exclusively in human cells, suggesting an adaptation of virus particles. Strikingly, proteome analysis revealed that the composition of virus particles changed in a cell line-specific manner, while the viral genome remained overall stable during passaging in both cell lines. Because several ubiquitination sites in virus proteins were identified, the role of ubiquitin for CPXV infection was analyzed. It was shown by the first global ubiquitination site analysis of virus particles that ubiquitin is a major conserved CPXV modification. Additionally, the dependence of CPXV replication on this protein modification was verified, making ubiquitination changes an attractive hypothesis of OPV adaptation. Furthermore, it was shown that CPXV particles incorporate intact transcripts, which presumably enable the rapid expression of viral immunomodulatory proteins upon infection.

Summarized, the results of the present study lead to new findings about OPV adaptation mechanisms *in vitro*. These mechanisms may also apply to *in vivo* adaptation of DNA viruses and may enable, for example, a crossing of the species barrier. The methods established in this study enable the further characterization of OPV adaptation and, moreover, can be applied to elucidate adaptation mechanisms of viruses belonging to other families.

Zusammenfassung

Adaptive Veränderungen von Viren ermöglichen eine Virus-Wirt Koevolution und die Infektion neuer Spezies. Während der Adaption von Viren mit RNA Genom primär eine genomische Variabilität zugrunde liegt, sind Adaptationsmechanismen von Viren mit DNA Genom bislang nur wenig erforscht. Da das Genom von DNA-Viren stabiler ist als das von RNA-Viren, wird vermutet, dass der Adaptation von DNA-Viren andere Mechanismen zugrunde liegen als rein genomische Veränderungen. Weiterhin ist anzunehmen, dass adaptive Veränderungen im Viruspartikel selbst zu identifizieren sind, da isolierte Viruspartikel in der Lage sind die Speziesbarriere zu überwinden. Das Ziel der hier vorliegenden Studie war es daher Adaptationsmechanismen von DNA-Viren mittels Proteomik und Genomik aufzuklären. Während genomische Veränderungen von Viren häufig mittels Next Generation Sequencing analysiert werden, wurden proteomische Veränderungen viraler Partikel bislang noch nicht mit Massenspektrometrie-basierten Methoden analysiert.

Als Modell-DNA-Virus für die hier vorliegende Studie wurde das Kuhpockenvirus (CPXV) gewählt und Zellkultur als System um adaptive Veränderungen zu untersuchen. CPXV gehören zum Genus der Orthopockenviren (OPV) und können eine Vielzahl von Spezies infizieren, z.B. Ratten, Katzen, Elefanten und Menschen. Die Anzahl an CPXV-Infektionen in Europa nimmt stetig zu, weshalb es notwendig ist Adaptionsmechanismen von OPV aufzudecken.

CPXV Partikel wurden aus einer Ratte isoliert und für fünf Passagen in einer humanen und in einer Ratten Zelllinie vermehrt. Dabei konnte ausschließlich in humanen Zellen eine Steigerung der viralen Fitness beobachtet werden, was auf eine Adaptation der Viren hindeutet. Die Proteomanalyse zeigte, dass sich die Viruspartikel während des Passagierens Zelllinien-spezifisch veränderten, während das virale Genom jedoch insgesamt stabil blieb. Da mehrere Ubiquitinierungsstellen in viralen Proteinen detektiert wurden, wurde die Rolle von Ubiquitin für die CPXV Infektion untersucht. Mittels der ersten globalen Ubiquitinomanalyse von Viruspartikeln konnte gezeigt werden, dass Ubiquitin eine konservierte Modifikation in CPXV Proteinen ist, dessen biologische Relevanz in weiteren Experimenten bestätigt werden konnte. Veränderungen der Ubiquitinierung stellen somit eine attraktive Hypothese zur Adaptation von OPV dar. Darüber hinaus konnte gezeigt werden, dass CPXV Partikel Transkripte inkorporieren, die vermutlich eine schnelle Expression viraler Immunmodulatoren ermöglichen.

Die Ergebnisse der vorliegenden Studie führen zu neuen Erkenntnissen über die Adaptationsmechanismen von OPV *in vitro*, die möglicherweise auch für die Adaption von DNA-Viren *in vivo* gelten. Die im Rahmen dieser Arbeit etablierten Methoden können weiterhin dazu genutzt werden, um die Adaptation von OPV näher zu charakterisieren und um die Adaptation von Viren anderer Familien zu untersuchen.

Table of Contents

1. Introduction

1.1. Cell culture propagation of viruses

1.1.1. History of virus propagation in cell culture

Viral infections have always been one of the biggest threats to humankind. The permanent coevolution of viruses and their hosts results in the constant risk of virus adaptation to new hosts, e.g. humans [1,2]. To develop therapeutic approaches and vaccines, mechanisms of pathogenesis and host range, which is the spectrum of species that can be infected by a virus strain, need to be elucidated. However, only in rare cases the amount of virus particles isolated from a clinical sample is sufficiently large for further characterization studies [3]. Hence, virus propagation is a common prerequisite for investigating viral infection. For this purpose, cell culture techniques are generally used, which are applied in research and vaccine production [4,5]. Additionally, virus stocks produced in cell culture guarantee a better standardization of subsequent experiments.

Until the 1950s, virus propagation was carried out *in vivo* in laboratory animals or embryonated chicken eggs, providing the host cells for virus replication [6]. Nowadays, virus propagation is usually carried out *in vitro* in cell culture, because it is easier to handle, less expensive, and spares animals' lives. In most cases well-established cell lines are used, e.g. HEp-2 (human epidermoid carcinoma cell line) or Vero E6 (African green monkey kidney cell line) [6-10].

In the early 1900s it was discovered that cells can be grown *in vitro* and that they can be used for virus propagation [6]. Nevertheless, animal tissues or whole animal embryos were needed for this purpose, because cell lines had not been established at that time. Vaccinia Virus (VACV), which has been used for smallpox eradication, was the first virus grown *in vitro* in 1913 [11]. Thereby, Steinhardt and colleagues used rabbit and guinea pig cornea, which they immersed in VACV suspension. Infectivity of the *in vitro* cultivated virus was proven by infection of rabbits and calves [11]. The breakthrough of cell culture in virology was the discovery that poliovirus proliferated in cell cultures, which were not derived from neural cells in 1949 [12]. Although the first immortal cell line was isolated from a cervix carcinoma of Henrietta Lacks (HeLa) in 1951 [13], it took until 1970 to improve cell culture techniques and to commercialize reagents and cell lines, paving the way for virus propagation in cell culture as a standard method in virology (**Figure 1.1**) [6,14].

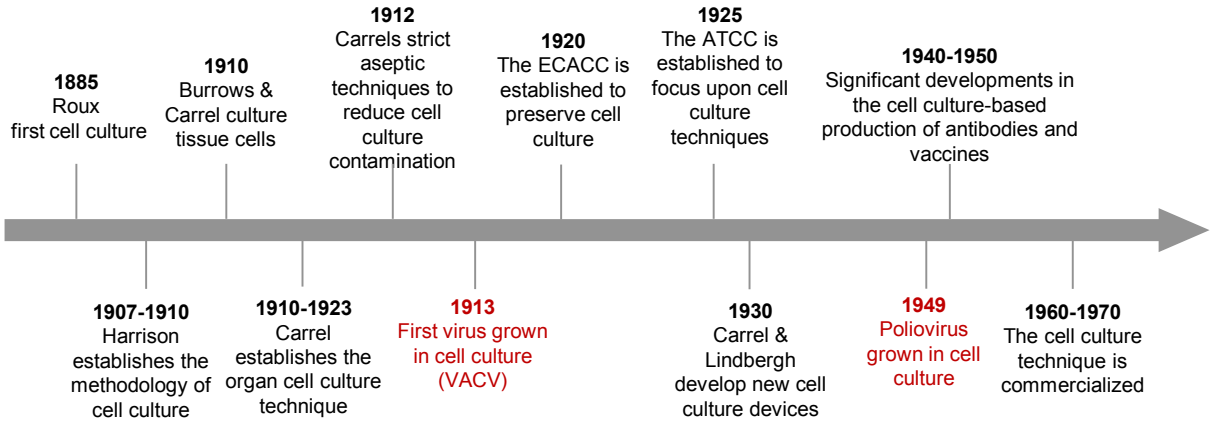

Figure 1.1. Landmarks of cell culture passaging and virus propagation in cell culture. Landmarks of cell culture passaging are shown in black, landmarks of virus propagation in cell culture in red. Modified from [15].

1.1.2. Virus adaptation in cell culture

Already in the very early days of studying viral infection in cell culture an adaptation of the virus to the host cell was observed. In 1946, it was reported that *in vitro* passaging of West Nile virus resulted in altered pathogenicity in mice [16] and initially poor growth of VACV improving over passages was observed in 1960 [17]. Moreover, numerous reports about viral adaptation in cell culture can be found throughout the history of *in vitro* virus propagation [18-21]. Adaptation may result in altered phenotypic properties, like an increase of the cytopathic effect (CPE), which is the visible morphological change of cells following infection [7,22]. On the one hand, these adaptations may be useful, because they can lead to less virulent particles, resulting in live attenuated vaccines like the vaccine virus strain for measles [19]. On the other hand, these adaptations may be detrimental as they can lead to differences in pathogenesis and host range compared to the clinically occurring virus [23,24].

Even though viral cell culture adaptation is not a controversial issue, but rather a known and generally accepted fact, it has hardly ever been investigated comprehensively. However, this issue concerns all virologists working with viruses obtained from cell culture and is therefore important to be investigated closely, because the virus used for research purposes may be not the same as the one originally isolated. Its properties may have been altered in a way that research results may vary greatly from *in vivo* processes and therefore might be misleading or even erroneous [23]. In the worst case, the cell culture-adapted virus strain might no longer be infectious *in vivo* [25].

Although virus adaptation in cell culture has been known for at least 70 years [16], distinct underlying mechanisms often remain unclear. More studies were carried out on the adaptation of RNA viruses than on the adaptation of DNA viruses and hence especially DNA virus adaptation mechanisms remain elusive [26]. Nevertheless, there are three main hypotheses about the

mechanisms underlying viral adaptation in cell culture, which apply also to virus adaptation *in vivo* [27]:

- Adaptation is caused by *de novo* mutations.
- Adaptation is induced by changes of the virus proteome.
- Adaptation is a selection process of pre-existing genomic variants.

RNA virus adaptation mainly takes place by selection of genomic variants from a heterogeneous virus population. Viral quasispecies result from the low-fidelity viral RNA polymerase (Pol) leading to mutation rates ranging from 10^{-6} to 10^{-4} substitutions per nucleotide per replication cycle [28,29]. In comparison, genomes of DNA viruses are generally more stable and possess mutation rates of about 10^{-8} substitutions per nucleotide per replication cycle [30]. These low mutation rates mainly result from the viral DNA-dependent Pol 3'-5' exonuclease activity correcting for incorrectly incorporated nucleotides [31]. Additionally, some viruses, like poxviruses, encode proteins involved in DNA repair mechanisms [32]. Hence, it seems conclusive that DNA viruses may primarily adapt via mechanisms other than *de novo* mutations and viral quasipecies formation.

Apart from genomic changes, proteomic changes may lead to viral adaptation. Generally, proteomic changes refer to altered protein expression, altered protein stability or changes in posttranslational modifications (PTMs). Altered protein expression in turn includes an altered expression level or an altered time point of expression during infection. Changes of PTMs may result either from host switch or genomic mutations resulting in amino acid changes, which may alter binding sites of PTMs. Proteomic changes may occur during the infection process and hence are not necessarily identifiable in virus particles. However, proteomic changes may also be identifiable in virions (extracellular virus particles) themselves. Besides an altered virion proteome composition, including the incorporation of host cell proteins [33,34], changes in PTMs of virion proteins present a conceivable adaptation mechanism. Although it is known that PTMs, like phosphorylation, glycosylation and ubiquitination, play important roles in viral infection, global changes as a result of cell culture adaptation have not been analyzed yet. This may also be due to the fact that except two virion phosphoproteome analysis, global PTMs in virion proteins have not been analyzed [35,36].

Furthermore, transcript incorporation of viral and host RNAs has been described for large DNA viruses belonging to the family of *Herpesviridae* [37-40] and *Mimiviridae* [41,42]. Intact virion-packaged transcripts are released upon entry into the host cell, enabling the rapid expression of according proteins [38,40]. Therefore, transcript incorporation also represents a plausible viral adaptation mechanism.

The different hypothesis about viral adaptation mechanisms are summarized in **Figure 1.2.** These mechanisms do not exclude each other, but may coexist and even depend on each other. For

example, a heterogeneous virus population is based on *de novo* mutations. Moreover, *de novo* mutations may influence proteomic differences. Hence, reality might be somewhere in between the different mechanisms.

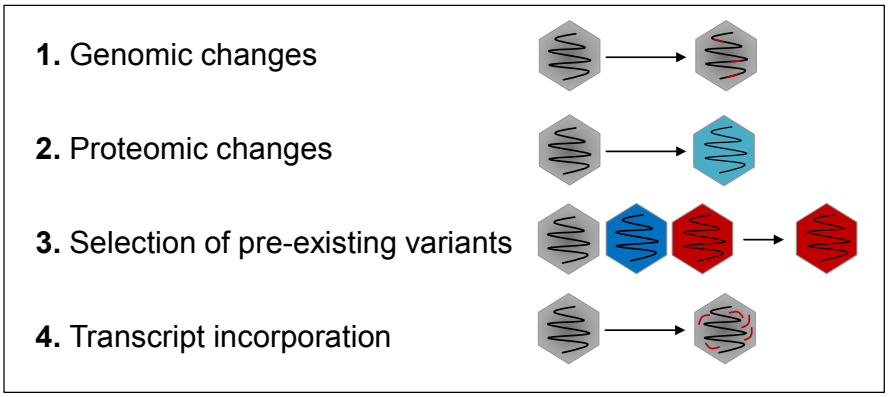

Figure 1.2. Main hypothesis about viral adaptation mechanisms. While RNA virus adaptation mainly takes place by selection of pre-existing variants, DNA virus adaptation mechanisms have hardly been investigated so far.

1.2. Virion characterization by genomics and proteomics

Although viral adaptation may manifest during the infection process, the basis for these changes has to be located in the virion itself if the host does not change. This applies to virus propagation in the same cell line, except the first passage after isolation. Generally, during the first passage, the environment of the virus changes from natural to artificial [43]. In case of a permissive cell, meaning a cell in which the virus is able to replicate efficiently, viral adaptive changes during further cell culture passaging have to occur in the virion itself. Hence, a comprehensive characterization of the virion is a prerequisite to analyze viral adaptation mechanisms in cell culture. This includes the analysis of the viral genome, the virion proteome and also PTMs. For this purpose, next-generation sequencing (NGS) and mass spectrometry-based proteomics are applied.

1.2.1. Next-generation sequencing

First generation DNA sequencing, also called Sanger sequencing, was introduced by Frederick Sanger in 1977. It is based on chain-termination sequencing, which is achieved by incorporation of fluorescently-labeled dideoxynucleotidetriphosphates (ddNTPs) lacking the 3'-OH group necessary for chain elongation. In that way fragments are synthesized which differ by one nucleotide in length. These fragments are separated by capillary electrophoresis and the fluorescence, which is specific for each nucleotide, is detected. Using Sanger sequencing DNA fragments of up to 1,000 bases can be sequenced with a raw accuracy of >99.999 % [44]. For sequencing of longer sequences, like whole genomes, the DNA has to be fragmented. This fragmentation is generally carried out randomly resulting in shorter fragments (shotgun

sequencing), which are assembled to longer sequences. However, for the analysis of whole genome sequences or transcriptomes, the Sanger method is not suited since it is expensive and time-consuming. This is because parallelization is restricted and fragments need to be clonally amplified in bacteria prior to sequencing. Instead, Sanger sequencing is suited for sequencing of PCR fragments. Nevertheless, the first complete human genome, consisting of about three billion base pairs (bp), was analyzed with Sanger technology, what took about 13 years [45].

Second generation DNA sequencing technologies are referred to as NGS. These technologies were commercially introduced between 2005 and 2010 and are based on shotgun sequencing. NGS uses massive parallel sequencing, resulting in more time and cost effective sequencing, but shorter read lengths compared to Sanger sequencing. Raw accuracy of NGS depends on the platform, but is usually between 99.0-99.9 % [46]. The data output of high throughput NGS platforms greatly exceeds those of Sanger sequencing and ranges between several hundreds of gigabyte up to terabytes [47]. However, for signal detection, DNA fragments need to be amplified by PCR prior to sequencing.

In 2005, 454 Life Sciences (soon taken over by Roche) launched the first commercial NGS machine. It was based on pyrosequencing technology, which uses an enzymatic reaction to detect the pyrophosphate resulting from nucleotide incorporation [48]. One year later, in 2006, Solexa (2007 purchased by Ilumina) launched the Genome Analyzer machine. The Illumina technology is based on massive parallel sequencing of a pool of adaptor-ligated DNA fragments (library) by cyclic reversible termination. For this purpose, modified nucleotides are used that possess a fluorophore (one color for each nucleotide) and a 3’ termination group. The termination group ensures the incorporation of one single nucleotide at a time and thus enables the addition of all four nucleotides in parallel. After nucleotide detection via total internal reflection fluorescence, the termination group is removed for the next step of nucleotide incorporation. To be able to detect the fluorescence signal, DNA fragments are amplified by bridge PCR prior to sequencing. The SOLiD (Sequencing by Oligonucleotide Ligation and Detection) technology was launched in 2007 by Applied Biosystems and uses fluorescently-labeled probes, which are ligated to primers. These probes are degenerated except of two bases. Using ladder primer, overlapping sequence information is generated and the fragment sequence is deduced. In contrast, the Personal Genome Machine (PGM) released by Life Technologies in 2010 relies on the Ion Torrent semiconductor technology, which detects the pH change resulting from proton release upon nucleotide incorporation [44,49].

In 2013, Roche shut the 454 sequencing business down. Nowadays, the Illumina technology is most commonly applied [50,51]. Generally, in a paired-end run DNA fragments are sequenced from both ends resulting in up to 2 × 300 bp per fragment. Depending on the platform, the number of generated reads varies between 25 million (MiSeq) and more than five billion (HiSeq). Hence,

for small genomes, like viral genomes, the MiSeq platform is well-suited, while large eukaryotic genomes require sequencing on a HiSeq platform [52].

NGS plays a key role in virology and greatly advanced the understanding of viruses. It is applied for diverse purposes, e.g. the detection of new viruses, viral metagenome analysis, transcriptome analysis of infected cells, whole viral genome sequencing and diagnostics [53]. Moreover, deep sequencing by NGS is applied to elucidate rare viral variants and quasispecies [54-56]. In June 2017, the NCBI viral genome database contained 7349 complete viral genomes. Hence, to analyze genomic adaptation of viruses, NGS is the method of choice. Recently, for example, Wang and colleagues [21] compared the genome sequences of human cytomegalovirus (CMV) of low passages and after more than 40 passages in cell culture. They elucidated two mutations in coding sequences (CDS), which were presumably related to increased amounts of infectious virus observed during passaging. Other examples include the NGS-based elucidation of gene amplification during VACV passaging in cell culture [57] and the recently reported genomic adaptation of Marburg virus during *in vivo* and *in vitro* passaging [58].

1.2.2. Mass spectrometry-based proteomics

In 1996, Wilkins and colleagues coined the word proteome to describe the entity of proteins from a genome, cell or tissue [59]. In contrast to the genome, the proteome is highly variable and differs among tissues. Moreover, the proteome depends on intra- and extracellular stimuli and hence may also differ from cell to cell [60]. The proteome is far more complex than the genome. While the human genome encodes about 20,000-25,000 genes [45], the number of different proteins is estimated to be about one million [61] and even up to 1.5 million in human plasma [62]. This complexity results from genetic variation, alternative splicing and protein modifications. Different molecular forms of a protein are referred to as proteoforms [63]. Proteomics is the field dealing with the analysis of the proteome in all its complexity. Protein abundances span orders of magnitude, e.g. more than ten orders in serum and about seven orders in cell lines and tissues, making the detection of low abundant proteins in the presence of high abundant proteins challenging [64]. Moreover, while genomics benefits from PCR technology, proteomics lacks an amplification technique prior to analysis [65]. Therefore, the experimental and technological requirements are more complex in proteomics compared to genomics [65]. At present there is no method that is able to analyze the proteome in all its complexity, including protein sequence, abundance, modifications and interactions [66]. Nevertheless, technical and bioinformatics developments in the field of proteomics steadily enable the analysis of an increasing part of the proteome [65]. The technological milestone, which first revealed the proteome complexity, was two-dimensional gel electrophoresis invented 1975 [67,68]. At that time, however, it was not possible to identify the protein spots in the gel. This was first made

possible by technological developments in mass spectrometry (MS), which is the most important technology in proteomics today.

MS is used to determine the mass of ions in a three-step process:

(I) Conversion of the analyte into gas-phase ions.

(II) Separation of ions according to their mass-to-charge (m/z) ratio.

(III) Detection of ions.

MS has been already applied in the early 20th century to analyze the atomic weight of elements, leading to the discovery of isotopes. Since the 1950s, MS has been applied to analyze small biomolecules and from 1960 on MS enabled sequencing of small peptides. However, for generation of gas-phase peptide ions, extensive derivatization was required and larger peptides were not ionizable without decomposition [69]. This changed with the invention of two soft ionization methods at the end of the 1980s: Matrix-assisted laser desorption ionization (MALDI) [70] and electrospray ionization (ESI) [71], which enabled the MS-based analysis of proteins and peptides. For MALDI analysis, peptides are embedded in an UV-absorbing crystalline matrix, which is subjected to UV-light laser shots under vacuum. In contrast to the pulsed ionization of MALDI, ESI uses a high electric field to ionize peptides under atmospheric pressure directly from solution in a continuous fashion. Therefore, ESI can be coupled online to liquid chromatography (LC) to separate peptides prior to MS analysis [72]. The coupling of ESI with tandem mass spectrometry (MS/MS), which already had been invented in 1966 [73], together with the development of database search algorithms in 1993 [74] marked the beginning of shotgun proteomics. Analogous to shotgun sequencing in genomics, shotgun proteomics is based on the digestion of complex protein mixtures into smaller peptides, a technique also known as bottom-up proteomics. Peptide sequences are obtained by MS/MS fragment spectra from which proteins are inferred. Protein inference is based on database search comparing recorded spectra to theoretical ones. These theoretical spectra originate mostly from genomics analysis, demonstrating the dependency of discovery proteomic from genomics [74].

Sensitivity of LC-ESI-MS/MS (short LC-MS/MS) was greatly enhanced by the invention of nanospray-ESI in the mid-1990s [75]. In 1999, the orbitrap mass analyzer was invented by Makarov and commercialized by Thermo Fisher Scientific in 2005 [60,76]. The orbitrap combines accurate mass (< 1 ppm mass deviation) and high resolution (up to one million full width at half maximum) and hence is commonly used in proteomics nowadays [76,77]. Although fragmentation of peptides in the orbitrap mass analyzer is possible, it is advantageous to combine it with faster mass analyzers, like quadrupole or linear ion trap, which are used for ion manipulation, e.g. selection or fragmentation [76]. Orbitrap hybrid machines were used to analyze the first proteome of a eukaryotic organism (*Saccharomyces cerevisiae*) in 2008 [78] and to identify more than 10,000 proteins from HeLa cells in 2011 [79]. The first drafts of the human

proteome, analyzing the protein expression in diverse human tissues, body fluids and cell lines, were published in 2014 [80,81].

MS-based proteomics steadily gains popularity in virology research, which is mostly the result of improved workflows and MS instrumentations rather than the availability of viral genome sequences (**Figure 1.3**). MS-based proteomics has, for example, been applied to analyze proteomic changes in cells upon infection and to elucidate virus-host protein interactions [82]. Moreover, the proteomic composition of diverse viruses has been analyzed by LC-MS/MS, including adenovirus [83], herpesvirus [84,85], coronavirus [86], mimivirus [87] and poxvirus [88-91] virions. However, there is not a single report dealing with global proteomic changes of the virus particle itself as a result of cell culture propagation. In terms of PTM analysis in virion proteins only two global phosphorylation site analysis of VACV virion proteins have been published [35,36]. Other PTMs in virion proteins have not been analyzed globally yet.

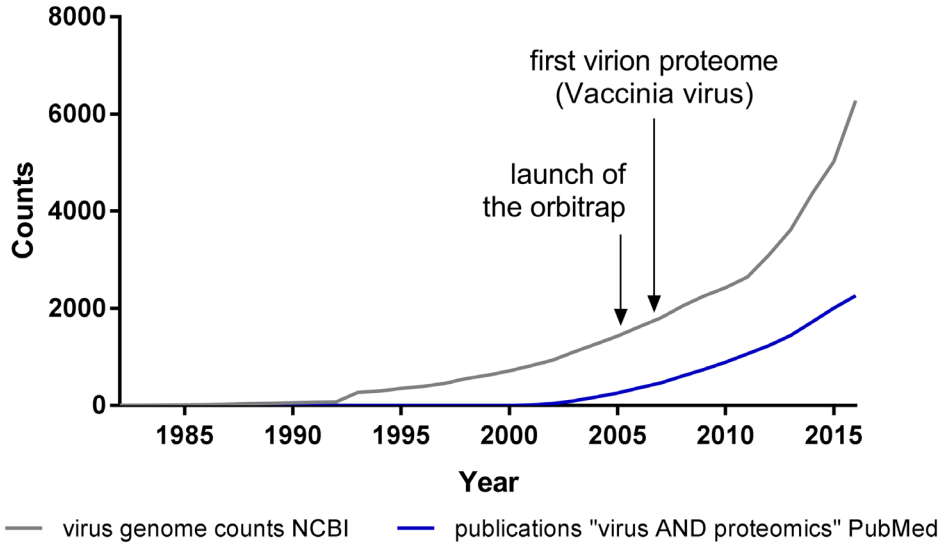

Figure 1.3. Increasing popularity of proteomics in virology.

1.3. Orthopoxviruses

As a member of the *Poxviridae* family the genus of Orthopoxviruses (OPV) comprises highly complex DNA viruses. The most prominent member of OPV is the smallpox-causing variola virus (VARV) which led to the death of hundreds of millions of people in the 20th century. VACV, an OPV member that less virulent than VARV, was used for smallpox eradication by vaccination. The WHO-led global eradication campaign was declared successful in 1979 [92]. Smallpox remains the first and only human disease eradicated by vaccination, what is considered the biggest achievement in international public health [93]. However, the mechanisms underlying VARV virulence and host range, which is limited to humans, are still unknown [94]. Underlined by the fact that routine vaccination has been discontinued, the use of VARV in biological warfare or bioterrorism is a permanent threat nowadays [95].

Besides VARV, the genus OPV comprises several animal-borne viruses with zoonotic potential meaning that these viruses are transmittable from animal to human. Most current OPV infections are caused by VACV, monkeypox virus (MPXV) or cowpox virus (CPXV) [96-98]. Moreover, concerns have been raised recently about the emergence of VARV-like viruses from zoonotic OPV by natural evolution [99]. CPXV is especially suited to fill the biological niche that VARV eradication has left, because it possesses the largest genome of OPV including all open reading frames (ORFs) of VARV [100]. Additionally, CPXV encodes the largest set of immunomodulatory proteins and has the broadest host range among OPV [98,101]. While wild rodents are the natural reservoir of CPXV [102], also domestic animals like cats [103] or pet rats [104] and zoo animals [105] can be infected. The number of zoonotic CPXV infections in Europe is increasing [106]. CPXV infection may lead to local skin lesions, which become covered by a crust (**Figure 1.4**). However, also generalized CPXV infections in humans [107,108] and even fatal cases in immunocompromised patients [109] have been reported. CPXV is transmitted primarily by skin contact [110], but a direct human-to-human transmission has not been reported yet [106,111].

Figure 1.4. Skin lesions caused by CPXV infection. (**A,B**) Skin lesions observed in a rat. (**C,D**) Skin lesions of zoonotic CPXV infections. Pictures were taken in the Consultant Laboratory for Poxviruses at the Robert Koch Institute (ZBS 1).

1.3.1. Virion structure and replication

OPV particles are brick-shaped and measure about 360 × 270 × 250 nm. The dsDNA genome of about 200 kb length encodes more than 200 genes [32]. The genome ends are covalently linked and contain inverted terminal repeats (ITRs). Conserved OPV genes are generally localized in the genome center, while non-conserved genes localize at the genome ends and encode proteins that are important for virulence and host range [32,112]. The viral DNA is associated with proteins and packaged in a capsid (core). The core is surrounded by one or two membranes, resulting in intracellular mature virions (IMV) or extracellular enveloped virions (EEV), respectively. Two lateral bodies (LBs) are located between core and membrane which are supposed to deliver viral enzymes into the host cell cytoplasm early in infection [113] (**Figure 1.5**).

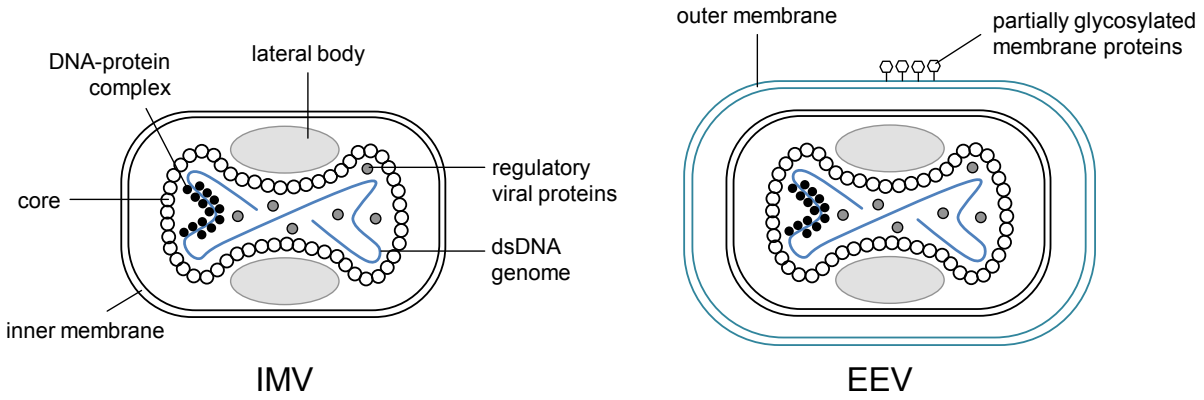

Figure 1.5. Schematic presentation of OPV particles. Two infectious virion forms exist: intracellular mature virions (IMV) with one membrane and extracellular enveloped virions (EEV) with two membranes. Modified from [32].

OPV replication exclusively takes place within the cytoplasm of the host cell. For this purpose, OPV encode their own transcription and replication machinery [110]. However, transcription of viral genes belonging to the intermediate and late class depends also on host factors [114-116]. Upon infection, the intact core is released into the cytoplasm, followed by early viral gene expression inside the core. After release of the viral DNA by core uncoating, intermediate and viral genome replication, followed by late protein expression, proceeds in distinct cytoplasmic areas called virus factories (VF) [32,117,118]. In that process, the cascade-like protein expression is regulated by different viral promoters, which are referred to as early, intermediate and late promoters [119]. IMVs are the prevalent infectious form of OPV and released by lysis of the host cell. Alternatively, IMV particles are wrapped with a second membrane resulting in EEV particles which are released by exocytosis (**Figure 1.6**) [120].

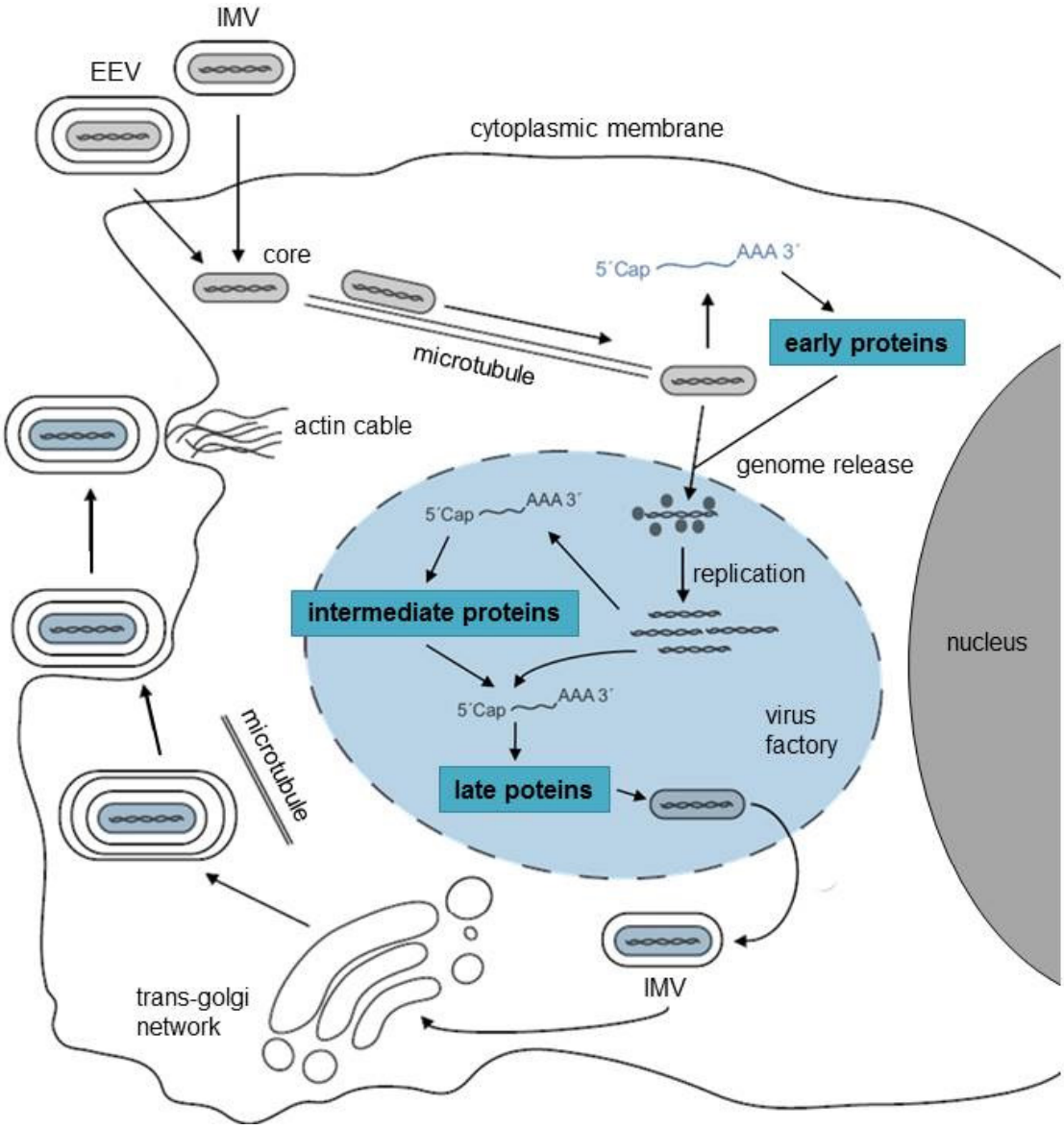

Figure 1.6. Schematic presentation of OPV replication. Upon entry, the virus core containing the dsDNA virus genome is released into the cytoplasm. Early viral proteins are expressed while the virus core is still intact. After core disintegration, viral genome replication takes place and intermediate and late viral proteins are expressed. Subsequently, virus particles are assembled and wrapped with one (intracellular mature virions, IMV) or two membranes (extracellular enveloped virions, EEV). Modified from [32].

1.3.2. The Orthopoxvirus mature virion proteome

To date, six studies have been published that analyzed the proteome composition of purified OPV IMV particles using MS-based proteomics [36,88-90,121,122]. Proteome analysis of EEV particles has not been performed, because the outer EEV membrane is highly fragile and hence not stable during purification [34]. The most comprehensive study conducted by Doellinger and colleagues analyzed the proteome of three VACV and three CPXV strains, identifying 133 common viral proteins in purified IMV preparations as well as diverse host proteins [88]. Moreover, species-specific viral proteins and abundance differences of viral IMV proteins were identified, indicating that the OPV IMV proteome is rather dynamic [88]. In the following, OPV proteins are named according to the CPXV GRI-90 reference strain if not stated otherwise.

Viral membrane proteins and structural core proteins are most abundant in OPV IMV particles. Additionally, the G17 phosphoprotein, which is presumably an LB scaffold protein, is highly abundant in IMV particles [88,113]. Besides highly abundant structural proteins, IMV particles contain multiple proteins associated with transcription and host-virus interaction, but also numerous proteins of unknown function [88]. Since early viral genes are trancribed inside the intact core, OPV particles need to contain all proteins necessary for the transcription of early genes. Viral proteins interacting with the host also include diverse immunomodulatory proteins, which act during infection to evade the host immune response. CPXV encode at least 30 immunomodulatory proteins, from which at least 20 have been detected in IMV particles (**Table 1.1**) [88,123]. Immunomodulatory proteins in IMV particles include apoptosis inhibitors, a tumor necrosis factor (TNF)-binding protein, a chemokine-binding protein, interferon (IFN)- and interleukin (IL)-binding proteins, NF-κB inhibitors and multiple proteins for the modulation of the IFN and innate immune response. The J1 protein is the most abundant immunomodulatory protein in CPXV IMV particles. J1 inhibits activation of the transcription factor STAT1 in the course of interferon signal transduction. With more than 2×10^5 copies/virion J1 reaches copy numbers of strucutral virion components like the core protein A4. Moreover, A49, B12, F3, D1/I5 and Q1, which act at diverse levels of immune evasion have been found in comparably high copy numbers ($> 10^4$ copies/virion) in CPXV IMV particles [88].

Table 1.1. Orthopoxvirus immunomodulatory proteins.[a]

Protein CPXV GRI-90	Gene VACV WR	Function	CPXV IMV proteome[b]
Apoptosis inhibitors			
B12	195	Serin proteinase inhibitor, caspase-1 und -8 inhibitor, CrmA	+
B20	205	Serin proteinase inhibitor	+
Q1	028	Inhibitor of TNF-R and TLR signaling	+
G1	040	Mitochondria-associated apoptosis inhibitor	+
T1	-	Apoptosis inhibitor, Golgi transmembrane protein	-
C7	-	E3 ubiquitin-protein ligase p28-like	-
Tumor necrosis factor-binding proteins			
A56	179	TNF receptor, CrmC	-
D2/I4	215	TNF- and chemokine-binding protein, CrmB	-
K2	-	TNF- and chemokine-binding protein,, CrmD	-
K3	-	TNF receptor, CrmE	+
Chemokine-binding proteins			
A43	166	CC- and CXC-chemokine-binding protein	-
D1/I5	218	CC- chemokine-binding protein	+
Interferon-binding proteins			
B7	190	IFN-γ receptor	+
B17	200	IFN-α/β receptor	+
Interleukin-binding proteins			
B14	197	IL-1β-binding protein	+
C8	-	IL-18-binding protein	+
Modulation of interferon response			
C4/C13	021	Interferon antagonist	+
F3	059	dsRNA binding protein, PKR inhibitor	+
J1	099	Tyr/ser protein phosphatase, dephosphorylation of STAT1	+
M1	032	Interferon antagonist	+
M3	034	eIF-2α homolog, PKR inhibitor	-
Inhibition of innate immune response			
A36	158	Inhibitor MHC class II antigen presentation	-
A47	170	Steroid hormone synthesis	
B8	191	Inhibition of intracellular MHC class I trafficking	+
C2	-	Inhibition of NK-induced lysis of infected cells	+
D10	-	Inhibition release of MHC class I complex from PLC	-
Inhibition NF-κB			
A49	172	Inhibition NF-κB and IRF3 activation by interaction with MyD88, TIRAP/TRIF, TRAM	+
A55	178	Inhibition NF-κB activation by interaction with IRAK2,TRAF6	+
B13	196	Inhibition NF-κB activation by interaction with IKK complex	+
M6	039	Inhibition NF-κB and IRF3 activation by interaction with IRAK2, TRAF6, DDX3	-
Q1	028	Inhibition NF-κB and IRF3 activation by interaction with IKK complex and TBK1	+

[a] Modified from [123]
[b] Detected in highly purified CPXV IMV virions [88]

1.3.3. The role of the ubiquitin-proteasome system during Orthopoxvirus infection

The ubiquitin-proteasome system (UPS) is exploited by members of most virus families [124] and is essential for the replication of different virus families, including *Reo*- [125], *Corona*- [126] and *Poxviridae* [127-129]. The UPS is highly modulated during OPV infection, e.g. by virus-encoded ubiquitin ligases like the CPXV p28 protein or viral BTB/kelch and ANK/PRANC proteins interacting with cellular ubiquitin ligases [130,131]. OPV do not encode viral ubiquitin, but host ubiquitin was reported to locate to VACV replication sites during infection [132]. Additionally, several proteome studies identified ubiquitin as part of the VACV and CPXV mature virion [88-90] and it was found to be more than 100-fold enriched in VACV and CPXV particles compared to human cells [88]. Although ubiquitin presumably is a major poxvirus protein modification, only sparse information about ubiquitinated virus proteins is available.

Most research regarding the role of the UPS in OPV infection was done with the best-characterized OPV member VACV, showing that treatment of HeLa cells with proteasome inhibitors led to reduced viral titers and impaired intermediate and late viral protein expression, while early viral gene expression still occurred. Also, the prevention of VACV-DNA replication and VF formation has been observed in the context of proteasome inhibition [127-129]. This is consistent with the finding that proteasome activity is required for VACV genome uncoating [129]. Furthermore, proteins in the viral core fraction of purified VACV IMV particles contain K48-linked polyubiquitin which is associated with proteasomal degradation [129]. These findings lead to the hypothesis that proteasome-mediated degradation of K48-linked polyubiquitinated core proteins is a prerequisite for OPV genome uncoating and replication [129] (**Figure 1.7**).

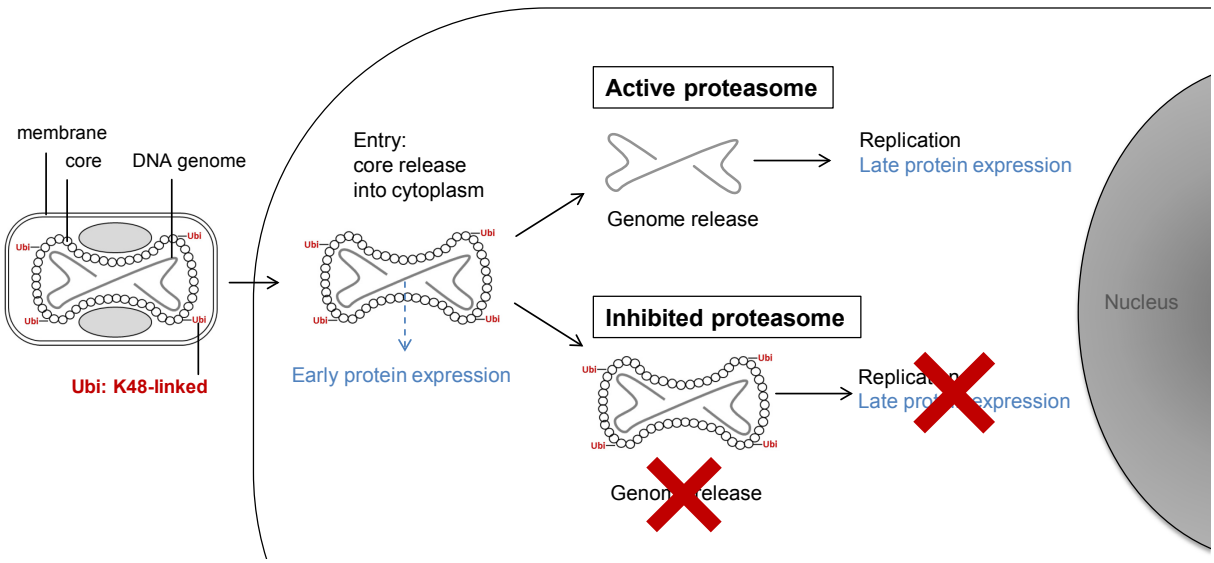

Figure 1.7. Hypothesis of CPXV genome release. Structural core proteins are polyubiquitinated with K48-linked ubiquitin and degraded by the proteasome upon infection, resulting in viral DNA replication and late viral protein expression.

1.3.4. Orthopoxvirus adaptation

The first descriptions of smallpox in India, China, Egypt and Middle East reach back before Christ. Although the origin of VARV is unknown, it presumably arose from a CPXV-like ancestor by genome reduction and mutation [94]. With about 10^{-8} substitutions per nucleotide per replication, mutation rates of OPV are rather low [30,133]. Besides the proofreading activity of the viral DNA Pol [31], OPV encode at least four proteins involved in DNA repair mechanisms [134]. These include the Holliday junction resolvase A23 which removes branches from DNA molecules [135], the nicking-joining enzyme M4 which cleaves and rejoins crosslinked replicative DNA intermediates [136], the deoxyuridine triphosphatase (dUTPase) G2, which minimizes dUTP incorporation in DNA and the uracil DNA glycosylase (UDG) E4. UDG excises uracil from DNA, which may arise by cytosine deamination or nucleotide misincorporation [118,137]. Moreover, as UDG is part of the DNA Pol holoenzyme, DNA replication and repair may be directly coupled in poxvirus replication [138,139]. Whether poxviruses also exploit the host DNA repair machinery is not known [140].

OPV can rapidly adapt to evolving host defense mechanisms. As the mechanism underlying this rapid evolution the transient gene expansion, also referred to as copy number variation (CNV), has been suggested [57]. This mechanism describes the multiplication of gene copies. Although CNV has been shown in cell culture applying high selective pressure to distinct genes [57,133,141], it has not been detected in naturally occurring OPV, possibly because it is a transient event [133]. Analogous to gene expansion in terms of CNV, the reduction of OPV genes during evolution is another mechanism of OPV adaptation [142]. Recombination of co-infecting OPV also represents an adaptation mechanism, which has already been described in 1958 [143]. OPV recombination has been observed *in vitro,* e.g. between VARV and CPXV [144], but also naturally occurring recombinant OPV have been described [145]. Although OPV recombination is a frequent event, only a single responsible enzyme has been described in this context, which is the viral DNA Pol [146]. Selective inhibition of the exonuclease activity of the DNA Pol reduces poxvirus recombination frequency *in vitro* [146]. Nevertheless, detailed mechanisms underlying DNA Pol-promoted recombination and whether it is involved in CNV still need to be investigated [146]. Moreover, recombination may also result in horizontal transfer of host genes [95], what is underlined by a variety of OPV genes showing considerable similarity to eukaryotic genes, e.g. immunomodulatory genes [147] and subunits of the RNA Pol [148,149].

Summarized, gene amplification and reduction in combination with the accumulation of random mutations and recombination are assumed to be the mechanisms underlying OPV adaptation [94]. However, these mechanisms rely on genomic changes and since OPV genomes are highly stable, they do not explain the rapid adaptation of OPV in the absence of genomic changes.

1.4. Aims

Production of sufficient virus amounts for further investigations is usually done by cell culture propagation, what is known to result in adaptation of the virus to the host cell. These adaptations can cause changes in the viral phenotype which may be linked to differences in virulence and host range compared to the clinically occurring virus (**Figure 1.8**).

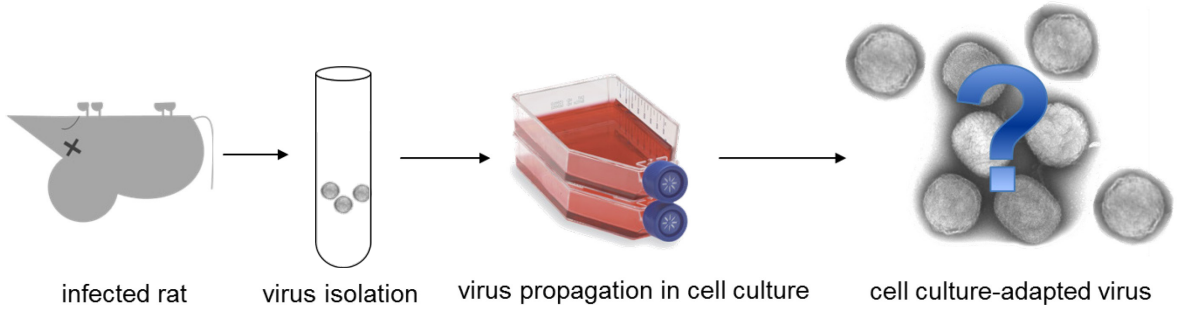

Figure 1.8. Illustration of virus adaptation in cell culture. Mechanisms underlying the adaptation of virus particles, especially DNA viruses, as a result of cell culture propagation are not completely understood.

While RNA virus adaptation mostly takes place by selection of genomic variants resulting from a less stable genome compared to DNA viruses [28], DNA virus adaptation mechanisms remain largely elusive. However, DNA virus adaptation may result from one or multiple of the mechanisms described in section 1.1.2. Therefore, the present study aims to elucidate DNA virus adaptation mechanisms in cell culture using modern -omics techniques. CPXV is used as a model DNA virus, because it has an exceptionally broad host range and, moreover, causes zoonotic infections illustrating its adaptive potential *in vivo*.

In detail the aims of this study include:

- **Analysis of adaptive CPXV IMV changes during passaging in cell culture by a combined proteomics/genomics approach.**

  Global proteomic differences of any virus particles during cell culture passaging have not been analyzed yet. Hence, in this study they shall be investigated by LC-MS/MS using CPXV isolated from a natural host (rat). Additionally, the genome stability of CPXV during passaging shall be analyzed by NGS. Moreover, using a rat and a human cell line for passaging, species-specific adaptations shall be analyzed.

- **Analysis of ubiquitination sites in CPXV IMV proteins and verification of the biological relevance of ubiquitin for CPXV infection.**

  Ubiquitin is essential for OPV infection [127,128]. However, the role of ubiquitin during CPXV infection has hardly been investigated [128] and, moreover, the role of the UPS during CPXV infection has remained elusive. Hence, conserved ubiquitination sites in CPXV virion proteins shall be elucidated by LC-MS/MS. Furthermore, the biological relevance of

ubiquitination for CPXV infection shall be proven by investigating the effects upon proteasome inhibition as described in section 1.3.3.

- **Analysis of transcript incorporation in CPXV particles.**
  Although transcript incorporation has been shown for other large DNA viruses [39], it has never been investigated for OPV. Therefore, an NGS-based protocol to analyze transcripts in CPXV IMV particles shall be established and transcripts in CPXV IMV particles propagated in different cell lines shall be elucidated.
- **Analysis of the selection of pre-existing variants during CPXV passaging.**
  Selection of pre-existing variants can only be proven if distinct genomic variants are known. Hence, variants shall be simulated by different CPXV strains, which are mixed and passaged in different cell lines. The strain ratio before and after passaging in different cell lines shall be determined by NGS.

The results of this study shall support the assessment of DNA virus changes during cell culture passaging and, moreover, shall be used to generate hypothesis about *in vivo* DNA virus adaptation mechanisms (**Figure 1.9**).

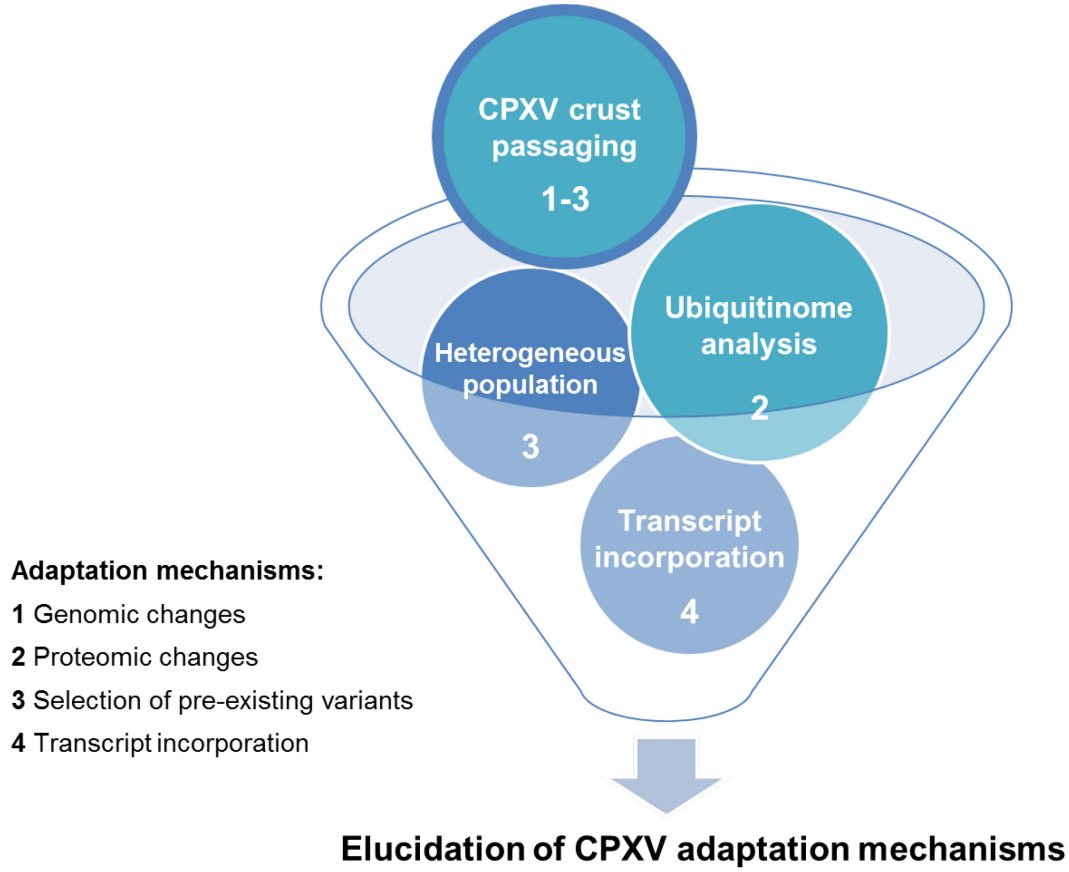

Figure 1.9. Overview of experiments to elucidate CPXV adaptation mechanisms. Proteomics (turquoise) and genomics (blue) methods were used to analyze adaptation mechanisms (1-4) of CPXV in cell culture. The numbers associated with each experiment refer to the according underlying adaptation hypothesis that is analyzed in the experiment.

2. Materials and Methods

Standard consumables and standard laboratory equipment are not listed separately.

2.1. Chemicals and reagents

Table 2.1. Chemicals and reagents.

Name	Producer
2-Chloroacetamid (CAA)	Sigma-Aldrich
Acetic acid	Sigma-Aldrich
Acetonitrile (ACN), LC-MS CHROMASOLV®	Sigma-Aldrich
Ammonium bicarbonate (ABC)	Sigma-Aldrich
Bortezomib	New England Biolabs
Carboxymethyl cellulose (CMC)	BDH Chemicals
Cesium chloride (CsCl)	Sigma-Aldrich
Dimethylsulfoxid (DMSO)	Roth, Pierce
Ethanol (EtOH)	Roth
Formic acid (FA), LC-MS grade	Pierce
HALT protease inhibitor cocktail (100 ×)	Thermo Fisher Scientific
Lane Marker Reducing Sample Buffer	Thermo Fisher Scientific
L-Tryptophan	Sigma-Aldrich
Methanol (MeOH), LC-MS grade	Sigma-Aldrich
MG-132	Merck
Naphtol blue black	Sigma-Aldrich
P1 buffer	Quiagen
PageRuler™ Prestained Proteinladder	Thermo Fisher Scientific
Paraformaldehyde (PFA)	VWR Chemicals
Phenylmethylsulfonylfluorid (PMSF)	Thermo Fisher Scientific
RIPA buffer	Thermo Fisher Scientific
Sodium acetate	Sigma-Aldrich
Sodium dodecyl sulfate (SDS)	Sigma-Aldrich
Sucrose BioUltra for molecular biology	Sigma-Aldrich
SuperSignal Molecular Weight Proteinladder	Thermo Fisher Scientific
SuperSignal West Dura Extended Duration Substrate	Thermo Fisher Scientific
Tansfer buffer (5x)	BioRad
Trifluoroacetic acid (TFA)	Sigma-Aldrich
Tris(2-carboxyethyl)phosphine (TCEP)	SERVA
Trizma® base	Sigma-Aldrich
Tween20	Sigma-Aldrich
Urea	Sigma-Aldrich
Water, LC-MS grade	Sigma-Aldrich, Pierce
β-Mercaptoethanol	Sigma-Aldrich

2.2. Enzymes, molecular biological kits and antibodies

Table 2.2. Enzymes.

Name	Producer
AgPath-ID™ One-Step RT-PCR Reagents	Life Technologies
Platinum Taq	Invitrogen
RNase A	Quiagen
SuperScript™ II Reverse Transcriptase	Invitrogen
Trypsin Gold, MS grade	Promega
Trypsin/LysC Mix, MS grade	Promega

Table 2.3. Molecular biological kits.

Name	Producer
CellTiter-Glo® Luminescent Cell Viability Assay	Promega
High Sensitivity DNA Analysis Kit	Agilent Technologies
Kapa Library Quant. Kit	PeqLab
LDH Cytotoxicity Assay Kit	Pierce
Min Elute Reaction Cleanup Kit	Quiagen
MiSeq Reagent Kit v3 (600 cycle, 25 Mio Cluster)	Illumina
NEBNext® mRNA Second Strand Synthesis Module	New England Biolabs
Nextera® XT DNA Library Preparation Kit	Illumina
Nextera® XT Index Kit	Illumina
NucleoSpin® RNA II Total RNA Isolation Kit	Macherey-Nagel
PhiX Control Kit v3	Illumina
Proteasome 20S Activity Assay	Sigma-Aldrich
PTMScan® Ubiquitin Remnant Motif (K-ε-GG) Kit	New England Biolabs
PureLink® Viral RNA/DNA Mini Kit	Invitrogen
Qubit® dsDNA HS Assay Kit	Life Technologies
Turbo DNA-free™ Kit	Ambion

Table 2.4 Antibodies.

Name	Source	Producer
Anti-rabbit-HRP	Goat	Cell Signaling technology #7074
OPV-A33R antibody	Rabbit	Daniel Stern, Robert Koch Institute
OPV-L1R antibody	Rabbit	Daniel Stern, Robert Koch Institute

2.3. Consumables, culture media and solutions

Table 2.5. Consumables.

Name	Producer
3M Mili-SPE Extraction Disc Cartridge (C18 SD)	Sigma-Aldrich
96-Well Polystyrene Plates, White Opaque	Pierce
Agencourt AMPure XP	Beckman Coulter
Analytical column (Reprosil-Pur 120 C18-AQ, 2.4 µm, 300 mm x 75 µm)	Dr. Maisch
Empore™ SPE Disks, C18	Sigma-Aldrich
Glass beads, 1 mm diameter	Sigma-Aldrich
Microcon® YM-30 Centrifugal Filter Unit	Merck Millipore
Precise Protein Gels, 4-20 %, 10-Well	Pierce
Stainless steel emitters, O.D. 150 µm, I.D. 30 µm	Thermo Fisher Scientific
Ultracentrifuge tubes SW28, SW40, SW60	Beckman Coulter
Zirconium Beads	OPS Diagnostics

Table 2.6. Media and solutions.

Name	Producer
Dulbecco's Modified Eagle Medium (DMEM)	Gibco
Eagle's Minimal Essential Medium (EMEM)	Gibco
Fetal calf serum (FCS)	PAA, Biochrom
L-glutamine	PAA
Penicillin-Streptomycin, 100x (Pen-Strep)	Gibco
Phosphate buffered saline without Mg^{2+} and Ca^{2+} (PBS)	Robert Koch Institute
Trypsin solution	Robert Koch Institute

2.4. Nucleic acids

Table 2.7. Nucleic acids.

Name	Sequence (5'> 3')	Application
P4A F	TAA TAC TTC gAT TgC TCA TCC Agg	Poxvirus reference sequence [150]
P4A R	ACT TCT CAC AAA Tgg ATT TgA AAA TC	
P4A probe	Fam-TCC TTT ACg TgA TAA ATC AT-MGB	
CCforSE01	CAA ggg gTA CCA AgA AAA TgA AgA AGG C	Detection of CCHF RNA [151]
CCrevSE02	gCC ACA ggg ATT gTT CCA AAg CAg AC	
CCprobeSE01	FAM-TgT CAA CAC AgC Agg gTg CAT gTA gAT-BHQ1	
CCprobeSE03	FAM-TgT AAg CAC ggC Agg gTg CAT gTA AAT-BHQ1	
CCprobeSE04	FAM-ATC TAT ATg CAC CCC gCT gTg TTA ACA-BHQ1	
CCprobeSE0A	FAM-ACT CCA ATg AAg Tgg ggg AAg AAg CT-BHQ1	

2.5. Eukaryotic cell lines

Table 2.8 Eukaryotic cell lines.

Cell line	Culture media	Description	ATCC#[b]
HEp-2	DMEM + 2 mM L-Gln + 5 % FCS[a]	Human (HeLa derivative)	CCL-23
Rat-2	DMEM + 2 mM L-Gln + 5 % FCS[a]	Rat embryonic fibroblast	CRL-1764
Vero E6	DMEM + 2 mM L-Gln + 5 % FCS	African green monkey kidney	CRL-1586
HeLa	EMEM + 2 mM L-Gln + 10 % FCS	Human cervix carcinoma	CCL-2

[a] During CPXV crust passaging 1 % Pen-Strep was added
[b] American Type Culture Collection (ATCC) reference number

2.6. Viruses

Table 2.9. Viruses.

CPXV strain	Name short	Description	Zoonotic context	Reference
Brighton Red	BR	Reference strain; isolated in 1937 from a human [152]	Cattle - human	ATCC # VR-302
RatHei09/1	Hei	Isolated in the Consultant Laboratory for Poxviruses from a rat in Heidelberg, Germany, in January 2009	Rat - human	NCBI GenBank: KC813504.1
RatKre08/2	Kre	Isolated in the Consultant Laboratory for Poxviruses from a pet rat in Krefeld, Germany, in February 2008	Rat - human	NCBI GenBank: KC813505.1
HumBer07/1	Ber	Isolated in the Consultant Laboratory for Poxviruses from a human in Berlin, Germany, in January 2008	Cat - human	NCBI GenBank: KC813509.1
HumGri07/1	Gri	Isolated in the Consultant Laboratory for Poxviruses from a human in Grimmen, Germany, in July 2008	Elephant - human	NCBI GenBank: KC813511.1
BRFseR	BRFseR	Recombinant CPXV expressing RFP under an early and GFP under a late viral promotor	none	Karsten Tischer, Freie Universität Berlin

2.7. Technical equipment, software and databases

Table 2.10. Technical equipment.

Name	Producer
2100 Bioanalyzer	Agilent Technology
ABI 7500 real-time PCR sytem	Applied Biosystems
AxioCam Erc5s light microscope camera	Zeiss
ChemiDoc™ MP Imaging System	Bio-Rad
Cup Sonifier	Branson
EASY-nanoLC	Proxeon
FastPrep® FP120 Homogenizer	MP Biomedicals
Illumina MiSeq sequencer	Illumina
LSM 780 confocal microscope	Zeiss
LTQ Orbitrap Discovery™	Thermo Fisher Scientific
Mr. Frosty Cryo Freezing Container	Thermo Fisher Scientific
Nanodrop™ ND-1000	Peqlab
Qubit® 2.0 Fluorometer	Life Technologies
Tecan Infinite® M1000 PRO & Infinite 200	Tecan
TransBlot® Turbo™ Transfer System	Bio-Rad
Ultracentrifuge	Thermo Scientific, Beckman Coulter
Univapo vacuum centrifuge	UniEquip
xCELLigence™ RTCA SP	Roche Diagnostics

Table 2.11. Software.[a]

Name	Developer or producer
ABI 7500 v2.0.5	Applied Biosystems
Bowtie 2 v2.2.6 [153]	John Hopkins University
Gene-Heatmap Plugin for Geneious	Robert Koch Institute
Geneious v9.1.3	Biomatters
GraphPad Prism 5	GraphPad Software
Image Lab	Bio-Rad
MaxQuant v1.5.1.2/1.5.2.8 [154]	Max Planck Institute of Biochemistry
Motif-x Logo v1.2 10.05.06 [155]	Harvard Medical School
Perseus v1.5.0.31 [156]	Max Planck Institute of Biochemistry
Proteome Discoverer v2.1	Thermo Fisher Scientific
RAMBO-K v1.2 [157]	Robert Koch Institute
RTCA v1.2	Roche Diagnostics
SPAdes v3.6.2 [158]	St. Petersburg State University
STRING DB v10.0 [159]	STRING Consortium
Velvet v1.2.09 [160]	European Bioinformatics Institute

[a] Standard software is not listed separately

Table 2.12. Databases.

Database	Source
Reference proteome *Homo sapiens* (70,956 entries)	UniProt
Reference proteome *Rattus norvegicus* (31,664 entries)	UniProt
Genome *Homo sapiens* GRCh38 reference assembly	NCBI
Genome *Rattus norvegicus* Rnor_6.0 reference assembly	Ensembl
CPXV BR[a]	UniProt
CPXV Hei, Kre, Ber, Gri[a]	Translated from genome sequence
CPXV crust Hei with isoforms[a,b]	Translated from genome sequence
Contaminant database (247 entries)	cRAP (http://www.thegpm.org/crap/)

[a] Annotation according to CPXV GRI-90

[b] Mutations resulting in amino acid changes were added as isoforms

2.8. Cytological methods

2.8.1. Cultivation of eukaryotic cell lines

Adherent cells were cultured in 25, 75 or 175 cm^2 cell culture flasks at 37 °C and 5 % CO_2 in a humidified incubator. Cells were splitted before reaching confluence in a ratio of 1:2 to 1:10, depending on cell growth and demand. Cells were washed with PBS and incubated with trypsin until rounding was observed. Depending on the dilution factor a respective volume of cell suspension was transferred into fresh culture medium.

The cell number was determined by counting 8 big squares of a Neubauer chamber. If necessary, cells were diluted 1:5 or 1:10 prior to counting. The cell number per mL was calculated by multiplying the average cell number with the chamber factor (10^4) and the dilution factor.

For cryopreservation, cells were cultured in 175 cm^2 cell culture flasks to 90 – 100 % confluence, washed with PBS and trypsinized. For trypsin inactivation 8 mL medium were added and cells were pelleted at 300 × g and 4 °C for 6 min. The cell pellet was resuspended in 5 mL pre-cooled freeze mix (1:10 DMSO in FCS) and 1 mL aliquots were slowly frozen (1 °C/min) to -80 °C using Mr. Frosty Freeze Drying container. For long-term storage cells were transferred to liquid nitrogen (-196 °C). Cells were thawed and transferred to a falcon tube with 10 mL medium. After centrifugation at 300 × g for 7 min the cell pellet was resuspended in 1 mL medium and transferred to a 25 cm^2 cell culture flask containing 3 mL medium. Cells were routinely tested for mycoplasma and simian virus 5 (SV5) contamination before cryopreservation and after thawing.

2.8.2. Treatment of cells with proteasome inhibitors

MG-132 and Bortezomib were dissolved in DMSO, diluted 1:10 with EMEM and sterile filtered through a 0.2 µm filter. If not other stated, HeLa cells were treated with proteasome inhibitors simultaneously to infection. Control cells of all experiments were treated with the same amount of DMSO as inhibitor-treated cells.

2.8.3. Analysis of proteasome activity

The chymotryptic proteasome activity was analyzed using the Proteasome 20S Activity Assay according to manufacturer's instructions. Briefly, 10,000 HeLa cells per well were seeded into a 96-well opaque black plate and incubated overnight. After three wash steps with PBS, cells were treated with 1 and 10 µM MG-132 or 0.01, 0.1 and 1 µM Bortezomib in medium without FCS, and the proteasome activity was measured 24 h post inhibitor addition. Cells were incubated at 37 °C for 4 h with 100 µL/well Proteasome Assay Loading Solution protected from light, and the fluorescence intensity was measured at 525 nm with excitation at 490 nm.

2.8.4. Analysis of cell viability

The cellular ATP content was analyzed using the CellTiter-Glo® Luminescent Cell Viability Assay (Promega). Briefly, 10,000 HeLa cells per well in a 96-well white opaque plate were treated with 1 and 10 µM MG-132 or 0.01, 0.1 and 1 µM Bortezomib for 24 h and the ATP content was measured according to manufacturer's instructions.

2.8.5. Analysis of proteasome inhibitor-induced cytotoxicity

Lactate dehydrogenase (LDH) is a cytoplasmic enzyme which is released upon plasma membrane damage and hence can be used as biomarker for cytotoxicity. The release of LDH was measured using the LDH Cytotoxicity Assay Kit according to the Chemical Compound-Mediated Cytotoxicity Assay Protocol in the manufacturer's instructions. In summary, 10,000 HeLa cells per well in a clear 96-well plate were treated with 10 µM MG-132 or 1 µM Bortezomib. After 24 h the LDH release was analyzed according to manual instructions.

2.8.6. Effect of proteasome inhibition on GE and PFU

HeLa cells in 24-well plates were infected in triplicate with CPXV BR at a multiplicity of infection (MOI) of 1 in the presence or absence of 10 µM MG-132 or 1 µM Bortezomib. After incubation at 4 °C for 1 h the virus suspension was removed and cells were washed gently with PBS and incubated with or without proteasome inhibitors for 4 or 24 h. The supernatant was centrifuged at 1,000 × g for 5 min and analyzed for genome equivalents (GE) and plaque forming units (PFU).

2.9. Molecular biological and biochemical methods

2.9.1. Extraction of nucleic acids from CPXV

Viral DNA was isolated from virus suspensions using the PureLink® Viral RNA/DNA Mini Kit with or without carrier RNA according to manufacturer's instructions (**Table 2.13**).

Table 2.13. Overview of DNA extraction with PureLink® Viral RNA/DNA Mini Kit.

Experiment	Extraction volume [µL]	Virion purity	Elution volume [µL]	Carrier RNA
CPXV crust passaging	20 (P1), 2 (P2), 1 (P3-P5)	non-purified[a]	50	+
NGS CPXV crust passaging	5	sucrose gradient	50	-
GE-to-PFU ratio	100	non-purified[a]	50	+
Heterogeneous virus population	20	sucrose gradient	50	+

[a] Virions after cell lysis

Viral RNA was isolated from highly pure virus particles in 60 µL P1 buffer with or without RNase using the NucleoSpin® RNA kit according to manufacturer's instructions. DNA was eluted in 40 µL RNase-free water using the high yield and high concentration protocol.

2.9.2. Synthesis of cDNA

For first-strand synthesis Super Script II™ reverse transcriptase was used according to the manufacturer's instructions including 10 µM random hexamer primers without RNaseOut reagent. For second-strand synthesis NEBNext® mRNA Second Strand Synthesis Module was used according to the manufacturer's instructions. Double stranded cDNA was stored at -80 °C and purified using the MinElute Reaction Cleanup Kit prior to library preparation.

2.9.3. Quantitative real-time PCR

Viral genome equivalents (GE) were quantified using an OPV real-time PCR (qPCR) assay [150]. Briefly, 2.5 µL of extracted DNA were added to 22.5 µL reaction mix (**Table 2.14**) and amplified according to the thermal profile in **Table 2.15** using an ABI 7500 system. By measuring plasmid standards in the range of 10^1 to 10^6 copies per reaction the amount of GE was calculated. If no plasmid standard was analyzed simultaneously, the amount of GE was approximated using the following equation calculated from repetitive standard curve measurements in the Consultant Laboratory for Poxviruses (Robert Koch Institute, ZBS 1): $C_t = -1.433\ln(x) + 37.8$.

Table 2.14. Reaction mixture OPV qPCR.

Reagent	Volume/reaction [µL]
H_2O (PCR-grade)	14.15
10 x PCR buffer	2.5
$MgCl_2$ (50 mM)	2
dNTPs (2.5 mM)	2
F primer (10 µM)	0.75
R primer (10 µM)	0.75
Probe (10 µM)	0.25
Platinum Taq (5 U/µL)	0.1

Table 2.15. Thermal profile OPV qPCR.

Temperature [°C]	Time [s]	Cycle
95	600	1 ×
95	10	45 ×
60	35	

Crimean-Congo hemorrhagic fever virus (CCHF) RNA was detected using a one-step qPCR [151]. Briefly, 3 µL extracted RNA were added to 22 µL reaction mix (**Table 2.16**) and amplified according to the thermal profile in **Table 2.17** using an ABI 7500 system.

Table 2.16. Reaction mixture CCHF qPCR.

Reagent	Volume/reaction [µL]
H_2O (PCR-grade)	3.5
RT buffer	2.5
Enhancer	1
CCforSE01	1.50
CCrevSE02	1.50
CCprobeSE01	0.25
CCprobeSE03	0.25
CCprobeSE04	0.25
CCprobeSE0A	0.25
Enzyme mix	1.00

Table 2.17. Thermal profile CCHF qPCR.

Temperature [°C]	Time [s]	Cycle
45	900	1 ×
95	600	1 ×
94	20	45 ×
59	30	

2.9.4. Determination of protein and peptide concentration

Peptide concentrations of desalted samples were determined by absorbance measurement at 280 nm using a Nanodrop. The protein content of lysates was determined by tryptophan fluorescence measured with a microplate reader [88,161]. Briefly, protein lysates in 4 % SDS, 100 mM Tris pH 7.6, 10 mM TCEP and 40 mM CAA were mixed with 8 M urea in 50 mM Tris pH 8.5 (UA) to a final volume of 200 µL. The fluorescence was measured at 350 nm with 295 nm excitation in a white opaque 96-well plate and the tryptophan content was determined by measuring a tryptophan standard curve ranging from 0.1 to 0.9 µg tryptophan. Calculation of protein content was done by assuming a tryptophan weight content of 1.3 % for virus [88] and 1.19 % for cell lysates [161].

2.9.5. Confocal laser scan microscopy

A total of 60,000 HeLa cells per well were seeded on sterile cover slips in a 24-well plate. Cells were infected with sucrose cushion-purified CPXV BRFseR at an MOI of 5 in the presence or absence of 10 µM MG-132 or 1 µM Bortezomib. After 8 h cells were washed thrice with PBS and fixed in 4 % PFA in PBS for 1 h. PFA was removed by washing thrice with PBS. Coverslips were removed from the 24-well plate and washed carefully with Millipore water. Cells were mounted with MOWIOL/DAPI, coverslips placed on clean microscopy slides and allowed to dry overnight protected from light. Fluorescence was observed with a LSM 780 confocal microscope.

2.9.6. Transmission electron microscopy

Transmission electron microscopy (TEM) was done in the core facility of advanced Light and Electron Microscopy (Robert Koch Institute, ZBS 4). For verification of virus particle purity, approximately 10^9 PFU of CsCl-purified IMV particles were inactivated in 2 % PFA in 0.25 M HEPES at RT for 3 h and analyzed using TEM. To analyze the effect of proteasome inhibition on CPXV core uncoating, HeLa cells were propagated in T25 cm^2 cell culture flasks and pretreated with or without 10 µM MG-132 for 1 h prior to infection with CPXV BRFseR at an MOI of 100. After 4 h of incubation in presence or absence of MG-132 cells were fixed in 2.5 % glutaraldehyde in 0.05 M HEPES pH 7.2 at RT for 2 h. The samples were post fixed with 1 % osmium tetroxide in distilled water for 1 h, 0.1 % tannic acid in 0.05 M Hepes for 30 min and 1 % uranyl acetate in distilled water for 2 h, followed by stepwise dehydration in a graded ethanol series and embedding in epon resin, which was subsequently polymerized at 60 °C for 48 h [162]. Thin sections were produced with an ultramicrotome (UC7, Leica) and counterstained with uranyl acetate and lead citrate and examined using a Tecnai12 transmission electron microscope operated at 120 kV. For quantification of intact virus cores and VF, 100 cells were randomly chosen and analyzed.

2.10. Virological methods

2.10.1. Virus propagation and purification

Cells were cultured in T175 cm^2 cell culture flasks and infected at an MOI of 0.01 - 0.1. Four days postinfection (p.i.) cells were scraped in culture medium, pelleted at 300 × g for 6 min and resuspended in 10 mM Tris pH 9.0. Cells were disrupted with glass beads and vigorous vortexing for 90 s. After sonication for 1 min glass beads and cell debris were pelleted at 1,000 × g and 4 °C for 5 min. Purification of IMVs was done by rate-zonal sucrose gradient centrifugation [163] in sterile SW28 centrifuge tubes followed by isopycnic CsCl density gradient centrifugation [90] in sterile SW40 or SW60 centrifuge tubes (**Figure 2.1**). For crude purification, the supernatant was centrifuged through a 36 % sucrose cushion at 32,900 × g and 4 °C for 80 min and the virus pellet was resuspended in 1 mL of 10 mM Tris pH 9.0. The virus suspension was sonicated for 1 min and stored in aliquots at -80 °C or alternatively layered on a 24 % - 40 % continuous sucrose gradient made with a gradient mixer, and centrifuged at 26,000 × g and 4 °C for 50 min. The virus band was collected and stored at 4 °C while the pellet was resuspended in 1 mL of 10 mM Tris pH 9.0, sonicated for 1 min and centrifuged through a fresh 24 % - 40 % continuous sucrose gradient as described before. The virus bands were pooled and concentrated at 32,900 × g and 4 °C for 60 min. The pellet was resuspended in 1 mL of 10 mM Tris pH 9.0 and stored in aliquots at -80 °C or purified further through a 1.23 - 1.29 g/mL continuous CsCl gradient at 180,000 × g and 4 °C for 4 h. IMV particles of a density about 1.27 g/mL were aspirated and concentrated through 17 mL of a 36 % sucrose cushion as described. The pellet was resuspended in 1 mL of 10 mM Tris pH 9.0 and stored in aliquots at -80 °C.

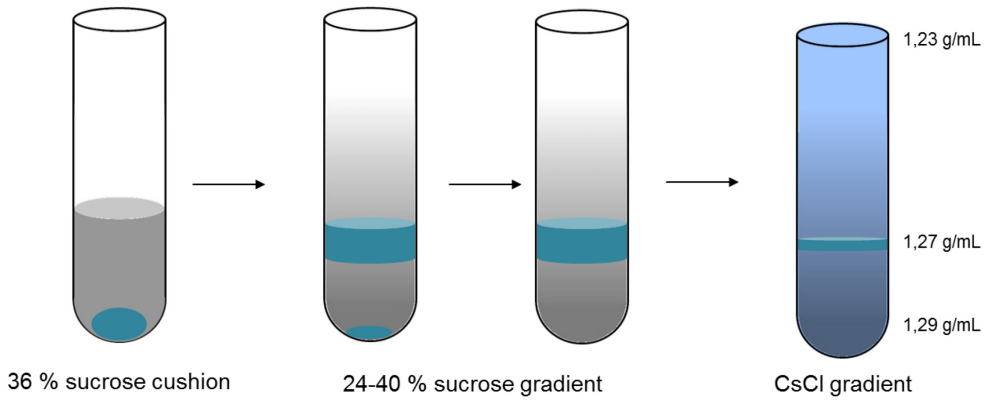

Figure 2.1. CPXV IMV purification by gradient ultracentrifugation. Crude purification was done by sucrose cushion, followed by further purification using sucrose gradient centrifugation. The pellet from the first sucrose gradient was purified through a second sucrose gradient. Virus particles from both bands were finally centrifuged through an isopycnic cesium chloride (CsCl) gradient. Turqouise: IMV particles.

2.10.2. Virus isolation from CPXV crust

CPXV particles were purified from a crust originating from a Wistar rat (sample #5262) that has been intradermally infected with CPXV Hei within the context of the doctoral thesis of Astrid Puppe [164]. Seven days p.i. the crust was excised and stored at -80 °C. For the isolation of CPXV particles the crust was cutted into small pieces and homogenized with 20 - 25 ceramic beads in 500 µL of 10 mM Tris pH 9.0 at 6.0 m/s for 6 × 20 s using a FastPrep instrument. After 3 min of sonication the beads were pelleted and the supernatant was saved. The homogenized crust was washed twice with 500 µL of 10 mM Tris pH 9.0 and the supernatants of the wash steps were saved. To maximize virus yield, the crust was vortexed thrice in 500 µL of 10 mM Tris pH 9.0 for 30 s and washed again twice with 500 µL of 10 mM Tris pH 9.0. All Supernatants including those from washing steps were pooled and nuclei and cell debris were pelleted at 5,000 × g and 4 °C for 5 min. The supernatant was sonicated for 1 min and IMV particles were purified by sucrose gradient as described and stored in aliquots at -80 °C until serial passaging and further experiments (**Figure 2.2**).

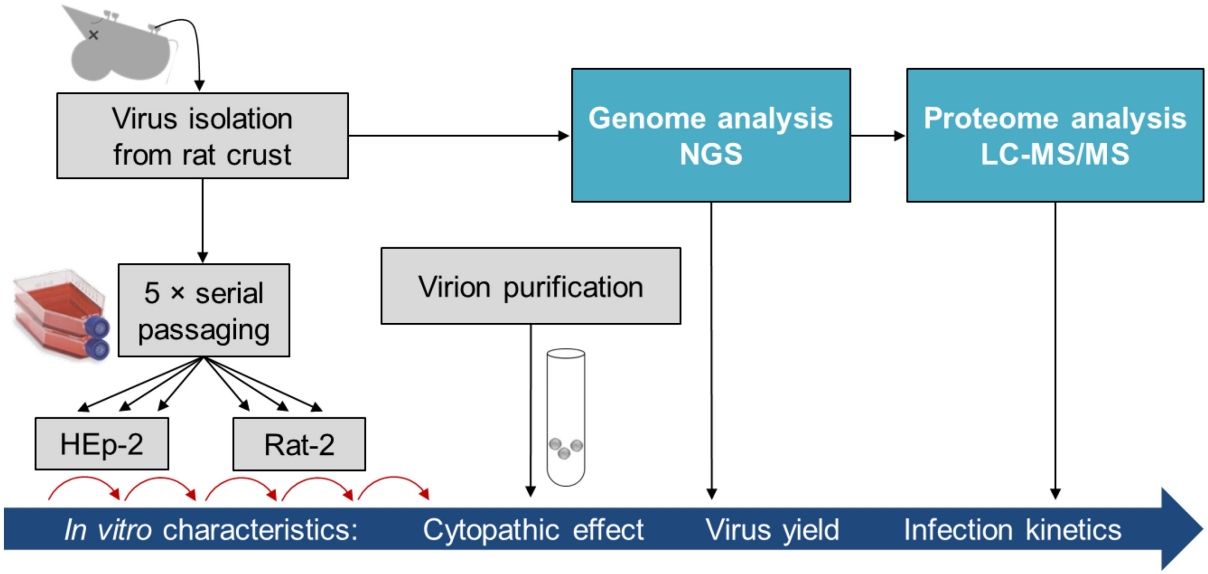

Figure 2.2. Experiment overview: passaging of CPXV particles isolated from a rat crust. CPXV were isolated from a rat crust, purified by sucrose gradient ultracentrifugation and passaged five times in triplicate in HEp-2 and Rat-2 cells. During passaging, the cytopathic effect was documented and the virus yield of each passage was determined by qPCR. After purification of IMV particles from cell culture, the genome and proteome of the crust and each passage was analyzed by next-generation sequencing (NGS) and tandem mass spectrometry (LC-MS/MS), respectively. Furthermore, infection kinetics of purified crust and passages were performed by real-time cell analysis.

2.10.3. Serial passaging CPXV isolated from a rat crust

For the analysis of CPXV adaptation in cell culture, purified virus particles from the crust were serially passaged in triplicate in HEp-2 and Rat-2 cells (**Figure 2.2**). HEp-2 cells are generally used for CPXV propagation and Rat-2 cells were chosen because of their closer relatedness to the natural host (rat). For infection of the first passage, 2×10^6 cells of each cell line were mixed with purified CPXV crust particles in 4 mL of medium at an MOI of 0.1 assuming a GE-to-PFU ratio of 1:1. Cells were incubated in a T25 cm^2 cell culture flask for 4 d and the CPE was documented daily. Non-infected control cells served as a reference for CPE documentation. For virus isolation, cells were scraped into medium and pelleted at 1,000 × g and 4 °C for 5 min. The cell pellet was resuspended in 1mL of 10 mM Tris pH 9.0 and disrupted using glass beads. After pelletizing of glass beads, viral DNA was extracted from the supernatant and the amount of GE per mL was determined by qPCR. Assuming a PFU-to-GE ratio of 1:82 in HEp-2 and 1:17 in Rat-2 cells as determined in section 2.10.4, the next passage was infected at an MOI of 0.1. The according virus amount was added to the medium of an 80 – 90 % confluent cell monolayer and incubated with daily CPE documentation for 4 d. The procedure of cell disruption, GE determination and infection of fresh cells was repeated 4 × for a total of 5 passages. Thereby, the number and size of cell culture flasks per replicate and passage was increased as following: 1 × T25 cm^2 (P1), 1 × T75 cm^2 (P2), 5 × T175 cm^2 (P3-5).

2.10.4. Determination of the GE-to-PFU ratio in the supernatant

To speed-up CPXV passaging, the time-consuming plaque assay was replaced by faster qPCR. Therefore, the ratio of GE-to-PFU was determined, which is the ratio of infectious to non-infectious virus particles. Briefly, HEp-2 and Rat-2 cells in T25 cm^2 cell culture flasks were infected in quadruplicates with CPXV Hei at an MOI of 0.1. Cells were disrupted using glass beads and vigorous vortexing 4 d p.i.. The supernatant after glass beads pelleting was subjected to plaque assay and qPCR (**Table S1**).

2.10.5. Plaque assay

The number of PFU, which resembles the number of infectious particles, was determined by infecting 3×10^5 Vero cells per well in a 24-well plate with 200 µL virus suspension using serial dilutions ranging from 10^{-3} to 10^{-9} depending on the expected titer. Medium containing 1.6 % (w/v) CMC was added 4 h p.i. and cells were incubated for 4 d. Fixation of cells was done in 3.5 % formaldehyde in PBS for 20 min followed by 20 min incubation with staining solution (0.1 % (w/v) naphtol blue black, 1.36 % (w/v) sodium acetate and 6 % (v/v) acetic acid). Plaques resulting from CPE become visible as holes in the cell monolayer. The number of PFU was calculated as shown below using the mean of at least 2 wells of the same dilution.

$$Titer\left(\frac{PFU}{ml}\right) = \frac{\sum plaques \times lowest\ countable\ dilution}{volume\ [ml]}$$

2.10.6. Real-time cell analysis

The xCELLigence RTCA (real-time cell analysis) system was used to analyze and compare the cell status of CPXV-infected cells. The system is based on electrical impedance measurement by microelectrodes embedded at the bottom of a 96-well plate (E-plate). The output is a unitless number called the Cell Index (CI) which represents the background corrected relative impedance. The CI increases with increasing interaction of cells with the electrodes and vice versa and hence depends on cell status parameters like cell number, morphology and adhesion (**Figure 2.3**).

Initially background measurement was done with 50 µL medium per well in a 96-well E-Plate. For all experiments 10,000 cells (HEp-2 or Rat-2) per well in 100 µL medium were added and the CI was monitored every 15 min. After overnight incubation cells were infected with different CPXV at an MOI of 0.1, 1 or 5 in 50 µL medium and impedance measurement was continued for up to 160 h. For infection sucrose cushion-purified stocks of CPXV BR, Hei, Kre, Gri or Ber were used or alternatively sucrose gradient-purified stocks of CPXV crust and passages.

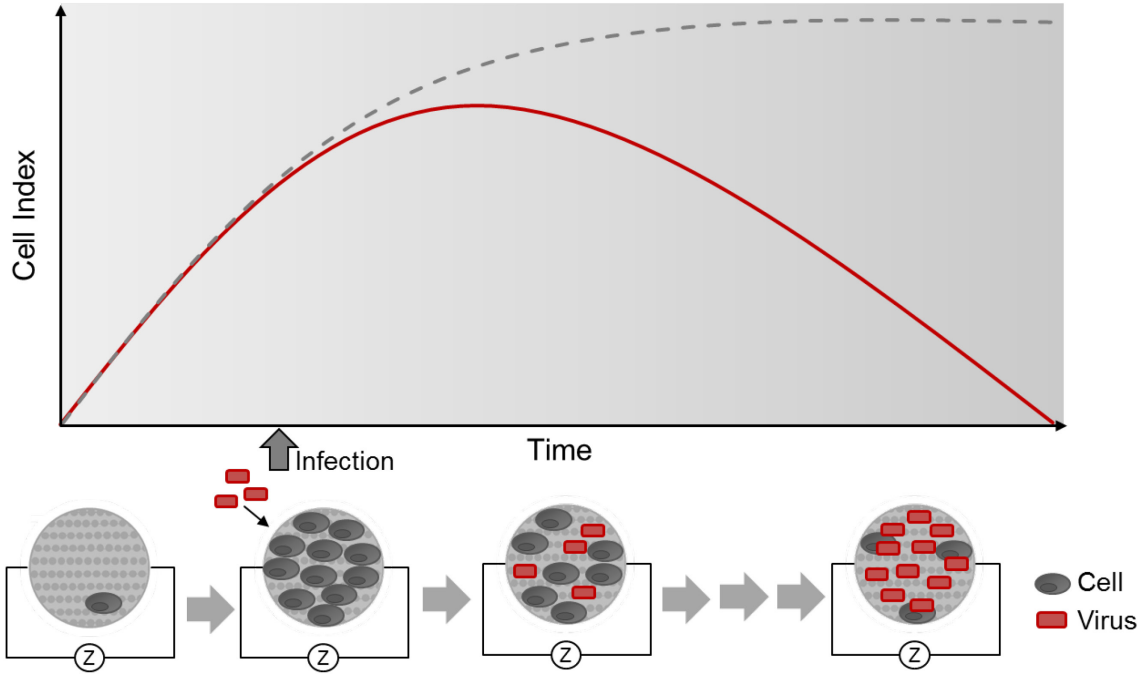

Figure 2.3. Principle of real-time cell analysis using the xCELLigence system. The cell index increases as a result of cell proliferation. Infection of cells leads to a decrease of cell index resulting from morphological changes. Grey dashed line: non-infected cells. Red line: infected cells. Z: impedance.

2.10.7. Simulation of a heterogeneous virus population

Because it is not possible to separate distinct virus variants in heterogeneous CPXV populations with NGS - unless detected variants are located in the same read - a heterogeneous CPXV population was simulated by mixing 5 CPXV strains with known genome sequence. Subsequently

the CPXV mixture was passaged 4 or 5 times in HEp-2 or Rat-2 cells with an infection time of 12 h per passage which corresponds to one replication cycle of CPXV.

Five CPXV strains (BR, Kre, Hei, Ber and Gri) were chosen on the basis of their genomic heterogeneity derived from a published phylogenetic analysis [88]. Equally PFU of sucrose cushion-purified virus stocks were pooled in a way that MOI was 1 for each CPXV strain resulting in a total MOI of 5. HEp-2 or Rat-2 cells were infected in duplicates in a low volume, incubated for 1 h and washed 3 × with PBS before addition of fresh medium. After 12 h p.i. cells were scraped in medium and lysed with glass beads and vigorous vortexing. The virus suspension was purified with sucrose cushion (see section 2.10.1) and PFU were determined for infection of the next passage at an MOI of 5. In total, the virus mix was passaged 5 times in duplicates in HEp-2 cells. In Rat-2 cells one replicate could be passaged only 4 times since PFU were too low for infection of the fifth passage.

2.10.8. Analysis of transcript incorporation in CPXV particles

To analyze the presence of transcripts in CPXV particles without prior sequence knowledge, an NGS-based protocol was developed. In summary, RNA outside of virus particles was removed, RNA extracted and the viral DNA digested before NGS analysis (**Figure 2.4**).

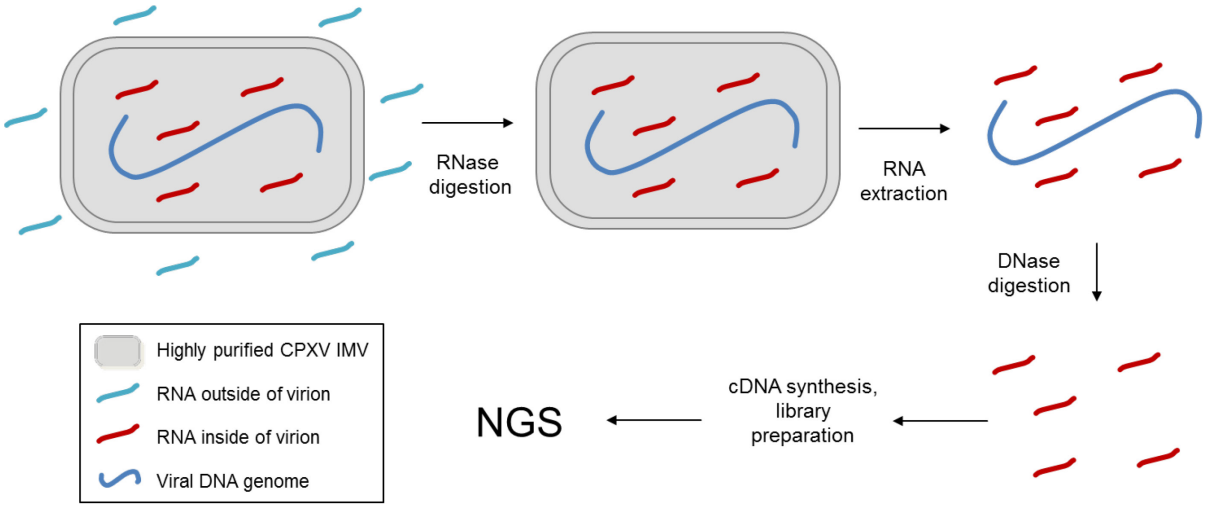

Figure 2.4. Sample preparation for the analysis of transcript incorporation in CPXV particles. RNA outside of highly pure CPXV particles was digested with RNase prior to RNA extraction. Viral DNA was digested and the leftover RNA analyzed with next-generation sequencing (NGS).

A total of 10^8 - 10^9 PFU of heat inactivated (1 h 60 °C) CsCl-purified CPXV BR in 500 µL 50 mM Tris pH 8.5 were pelleted at 25,000 × g and 4 °C for 30 min. The pellet was resuspended in 60 µL of buffer P1 with or without 100 µg/µL RNase A and incubated at 37 °C for 30 min. Alternatively, the virus pellet was dissolved in 25 µL of 50 mM Tris pH 8.0 containing 0.25 µg of trypsin and incubated at RT for 5 min. Trypsin was inactivated by adding PMSF to a final concentration of 1 mM. Virus particles were pelleted at 25,000 × g and 4 °C for 10 min and

resuspended in buffer P1 for RNase digestion as described. Subsequently, RNA was extracted and eluted in 60 µL of RNase free water. For digestion of viral DNA, 3 µL of Turbo DNase buffer and 1 µL of Turbo DNase were added to 27 µL of eluate and incubated at 37 °C for 30 min. To stop the digestion 5 µL of inactivation reagent were added and incubated at RT for 5 min with occasionally flipping of the tube. The inactivation reagent was pelleted at 10,000 × g for 1.5 min and 10 µL of the supernatant was used for cDNA synthesis.

Removal of RNA by digestion and RNA stability during DNase digestion were verified by spike-in RNA control. Briefly, 10^7 copies of plasmid-derived CCHF RNA were added before RNase or DNase digestion and assayed for CCHF RNA before and after digestion using qPCR. Removal of genomic CPXV DNA was analyzed using an OPV qPCR.

2.11. Genomic methods

2.11.1. Next-generation sequencing

CPXV genome sequences as well as transcripts incorporated in CPXV were analyzed by the sequencing core facility (Robert Koch Institute, ZBS 1) using an Illumina MiSeq machine.

For library preparation, the Nextera® XT DNA Library Preparation Kit was used according to the manufacturers' instructions. Briefly, DNA was fragmented by transposomes and adaptor-tagged in a single step called tagmentation. Tagmentation results in DNA fragments of approximately 300 bp size which are amplified by PCR. Thereby, index adaptors and adaptors for cluster generation by bridge PCR are introduced generating the DNA library. After library clean-up using AMPure XP beads, samples were equally pooled and checked for size distribution on a Bioanalyzer using a High Sensitivity DNA chip. Samples were sequenced after cluster generation by bridge PCR amplification on a flow cell.

2.11.2. Analysis of next-generation sequencing data

All raw reads were demultiplexed using CASAVA v1.8 (Illumina), trimmed using Trimmomatic v0.33 [165] and controlled for quality using FastQC v0.11.5 [166] from the Bioinformatics Service Unit (Robert Koch Institute).

De novo assembly of CPXV genomes and variant analysis

Separation of viral and host reads was done using RAMBO-K (Read Assignment Method Based On K-mers) [157]. Viral reads were *de novo* assembled using SPAdes v3.6.2 [158] and Velvet v1.2.09 [160]. Bowtie2 v2.2.6 [153] was used both for the confirmation of read separation by RAMBO-K and for the verification of *de novo* assemblies. Annotations were transferred from the CPXV GRI-90 reference strain (NCBI GenBank: X94355.2). As consensus sequences of replicates matched, reads of the triplicate per passage and cell line were summarized for further

analysis. To identify genomic changes during CPXV passaging, assembled genomes were analyzed for variants/SNPs using the ”find variations/SNPs” feature in Geneious v10.0.5 [167]. The minimum coverage was set to 100 with a minimum variant frequency of 0.01. Maximum variant p-value was 10^{-6} and minimum strand-bias p-value 10^{-5} when exceeding 65 % bias. All consensus sequences containing variant annotations (11 sequences) were aligned using MAFFT high speed multiple sequence alignment program v1.3.5 with default parameters. Variant annotations were exported and manually reviewed. In the analysis, tandem repeats were defined as repetitive regions of at least one nucleotide with at least four repetitions. Mutations resulting in amino acid changes were included as isoforms in the proteomic database.

Transcript analysis in CPXV particles

Trimmed reads were mapped to both the CPXV BR reference genome and either the *Homo sapiens* reference genome assembly (GRCh38) or the *Rattus norvegicus* reference genome assembly (Rnor6.0), using the split read mapper TopHat2 [168] with standard parameters. Additionally, reads were mapped to reference sequences of human and rat 18S and 28S ribosomal RNA (rRNA), since annotations for these genes are not available in ENSEMBL (www.ensembl.org). Reads mapping to the host and the virus genome were identified and extracted using a custom python script. The number of reads mapping to each gene was counted based on ENSEMBL annotations for the human and rat genomes. This included the mapping to 18S and 28S and annotation from the CPXV BR reference sequence genome, using the tool featureCounts [169]. Read counts were normalized for sequencing depth and gene length (reads per kilobase million, RPKM) and sorted by RPKM. In order to filter out spurious hits, only the top transcripts making up 90 % of the RPKM in the sample were considered for further analysis

Simulation of a heterogeneous CPXV population

The mix ratio of 5 CPXV strains before and after passaging was analyzed by the Bioinformatics Service Unit (Robert Koch Institute). In principle, the CPXV strains were differentiated by 214 SNPs which were used to build an overdetermined system of equations with the strain proportions as the only unknowns which is exemplary shown in the following.

The underlying assumption of the analysis is that for every position in the genome should hold:

$$(1)\ \frac{\sum reads\ with\ base\ X\ at\ position\ Y}{\sum reads\ mapping\ at\ position\ Y} = \sum Proportion\ of\ strain\ with\ base\ X\ at\ position\ Y$$

In other words: The proportion of reads with base X at position Y equals the proportion of strains in the mix that have base X at this position. For all positions in which the strains do not differ from each other, this simply evaluates to 1=1, giving no information. However, for positions at which at least one strain has a different base than the others, this leads to an equation where the only unknowns are the proportions of each strain in the mix. For instance, at position 1366 the BR

strain contains an A while the other 4 strains contain a G. This would lead to the following two equations:

$$(2)\ \frac{\sum reads\ with\ base\ G\ at\ position\ 1366}{\sum reads\ mapping\ at\ position\ 1366} = \sum Proportions\ of\ CPXV\ Ber, Kre, Gri\ and\ Hei$$

$$(3)\ \frac{\sum reads\ with\ base\ A\ at\ position\ 1366}{\sum reads\ mapping\ at\ position\ 1366} = Proportion\ of\ CPXV\ BR$$

Since the proportions of the strains in the mix are constant across all equations, formulating such equations for each position leads to a large number of equations with only five unknowns. Such an overdetermined system of equations can be solved using the ordinary least squares method. When the overdetermined system is written in matrix form Ax = b, the solution x can be determined using the formula

$$(4)\ x = (A^T A)^{-1} A^T b$$

with A^T is the transpose of matrix A and A^{-1} is the inverse of matrix A. In the example equations (2) and (3) are written in matrix form as follows:

$$(5)\ \begin{matrix} \\ A \\ C \\ G \\ T \end{matrix}\begin{matrix} \begin{matrix} BR & Ber & Kre & Gri & Hei \end{matrix} \\ \begin{bmatrix} 1 & 0 & 0 & 0 & 0 \\ 0 & 0 & 0 & 0 & 0 \\ 0 & 1 & 1 & 1 & 1 \\ 0 & 0 & 0 & 0 & 0 \end{bmatrix} \end{matrix} \begin{bmatrix} \%\ BR \\ \%\ Ber \\ \%\ Kre \\ \%\ Gri \\ \%\ Hei \end{bmatrix} = \begin{bmatrix} \%\ A\ at\ pos.1366 \\ \%\ C\ at\ pos.1366 \\ \%\ G\ at\ pos.1366 \\ \%\ T\ at\ pos.1366 \end{bmatrix}$$

2.12. Proteomic methods

2.12.1. Sample preparation for mass spectrometry

Purified virus particles were pelleted in 500 µL of 10 mM Tris pH 9.0 at 25,000 × g and 4°C for 30 min. Virus pellets were lysed in 30 - 90 µL of lysis buffer (4 % SDS, 10 mM TCEP, 40mM CAA in 100 mM Tris pH 7.6) by heating at 95 °C for 5 min. For cell lysis, a pellet to lysis buffer ratio of 1:3 (vol:vol) was used. While the anionic SDS supports protein denaturation, TCEP reduces disulfide bridges which become alkylated by CAA resulting in carbamidomethyl-modified cysteine residues [170]. The lysates were sonicated for 1 min (virus lysates) or 3 min (cell lysates), clarified at 16,000 × g for 5 min, and prepared for MS analysis using a modified Filter Aided Sample Preparation (FASP) method [171]. Briefly, 30 µL of lysate (< 200 µg of protein) were filled up with 200 µL of 8M Urea in 100 mM Tris pH 8.5 (UA) and loaded onto a Microcon Centrifugal Filter Unit with 30 kDa MWCO. SDS was removed by washing three times with 200 µL UA. Urea was replaced by washing thrice with 50 mM ammonium bicarbonate (ABC) and digestion was performed overnight at 37 °C in a wet chamber with Trypsin/Lys-C Mix in 40 µL ABC using a protein:enzyme ratio of 25:1. Tryptic peptides were recovered by centrifugation and eluted twice with 40 µL of ABC. Peptides were desalted with 3M Mili-SPE

Extraction Disc Cartridges (C18-SD) [171] or 200 µL StageTips with two Empore™ SPE Disks C18 [172] and dried in a vacuum concentrator. Concentrated peptides were stored at -80 °C until enrichment of ubiquitinated peptides or LC-MS/MS analysis.

2.12.2. Immunoaffinity purification of ubiquitinated peptides

Enrichment of ubiquitinated peptides was done with the PTMScan® Ubiquitin Remnant Motif (K-ε-GG) Kit according to the manufacturer's instructions. The method is based on an antibody specific for the di-glycine tag at lysine residues (diGly(K)) which results from tryptic digestion of ubiquitinated proteins (**Figure 2.5**). Briefly, desalted tryptic peptides were reconstituted in 1.4 mL IAP buffer and incubated with washed motif antibody-bead slurry at 4 °C for 2 h. After three washes with IAP buffer and three washes with MS-grade water, diGly(K) peptides were eluted in 55 µL of 0.15 % TFA followed by a second elution step with 50 µL of 0.15 % TFA. DiGly(K) enriched peptides were desalted using 200 µL StageTips with two Empore™ SPE C18 disks [172] and concentrated in a vacuum concentrator.

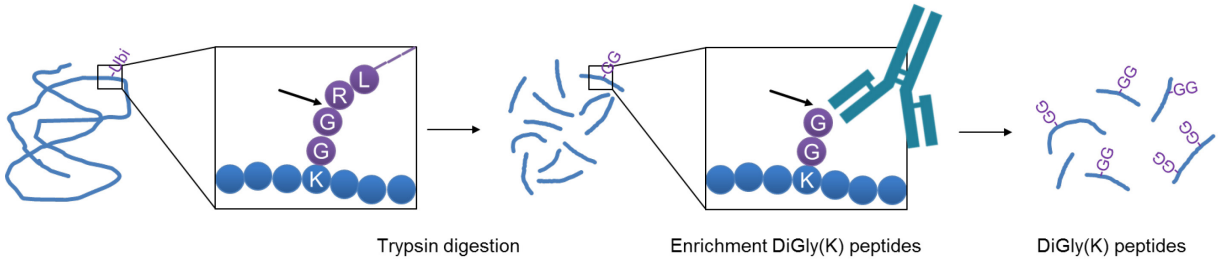

Figure 2.5. Schematic presentation of diGly(K) peptide enrichment. Peptides with diGly(K) residues resulting from tryptic digestion of ubiquitinated proteins were enriched using a motif-specific antibody.

2.12.3. LC-MS/MS analysis

Shotgun proteome analysis was performed using nano liquid chromatography (nLC) coupled to tandem mass spectrometry (MS/MS). Peptides were separated on a reversed-phase analytical column build of a stationary silicagel matrix modified with C18 residues. Peptides binding to the stationary phase via hydrophobic side chains were eluted based on hydrophobicity, size and charge with an increasing linear solvent gradient. DMSO was added during nLC separation to improve ionization efficiency resulting in more protein identifications [173,174]. For background ion reduction an ABIRD device was used. The parameters for nLC separation are listed in **Table 2.18**. Peptides eluting from the nLC were ionized by ESI generating gas phase peptide ions which were analyzed in an LTQ Orbitrap Discovery™ mass spectrometer. The LTQ Orbitrap is a hybrid mass spectrometer composed of two mass analyzers. Peptide ions are scanned out with high mass accuracy and high resolution in the Orbitrap mass analyzer (MS^1 spectra). Dependent on intensity, charge and dynamic exclusion, fragmentation of the top N peptide ions is performed in the faster linear ion trap (LTQ) analyzer using collision-induced dissociation (CID). Thereby, peptide ions collide with helium atoms resulting primarily in fragmentation at the peptide bond.

Fragment ions are scanned out in the LTQ (MS^2 spectra). The parameters applied for LC-MS/MS analyses are shown in **Table 2.18**.

Table 2.18. Parameters LC-MS/MS.

nLC separation	
Analytical column	Reprosil-Pur 120 C18-AQ, 2.4 µm, 300 mm x 75 µm
Emitter tip	Stainless steel emitter, O.D. 150 µm, I.D. 30 µm
Solvent A	0.1 % FA, 3 % DMSO in H_2O
Solvent B	0.1 % FA, 3 % DMSO in ACN
Flow rate	225 nL/min | 200 nL/min
Gradient	0-29 % B in 4 h | 0-40 % B in 90 min
Sample load	2 µg in 4 µL in 0.1 % FA | 1 µg in 4 µL in 0.1 % FA
LTQ Orbitrap	
Top N iontrap	7 | 12
Resolution orbitrap	30000
Scan rate ion trap	normal
Ion charge	+2, +3 | ≥ +2
AGC MS target value	1.00E+06
AGC MS^2 target value	5.00E+03
MS^2 threshold	5.00E+02
Mass range	400-1400 m/z | 300-1250 m/z
Normalized collision energy CID	35 %
Max. ion accumulation time MS	500 ms
Max. ion accumulation time MS^2	100 ms | 150 ms
Exclusion duration	120 s
Spray voltage	2.0 kV
Capillary temperature	275 °C

Blue: adjusted parameters for the analysis of diGly(K) peptides

2.12.4. Proteomic data analysis

Quality control of proteomic data was routinely performed using the Proteomics Quality Control Pipeline (PTXQC) [175].

Analysis with MaxQuant

Identification and label free quantification (LFQ) of CPXV IMV proteins and ubiquitinated peptides in CPXV-infected HeLa cells was done with Andromeda [176] and MaxLFQ algorithm [177], respectively, implemented in MaxQuant computational proteomics platform [154] using the parameters in **Table 2.19**. For LFQ samples are analyzed separately by LC-MS/MS and the peak areas of MS^1 peptide ions are compared after normalization (**Figure 2.6**). The prerequisites for accurate LFQ based on peptide peak areas as performed by MaxLFQ are sufficient resolution and highly reproducible LC-MS/MS performance, especially retention time and signal stability.

Table 2.19. Parameters MaxQuant.

RAW files	3× crust (technical replicates) 15× HEp-2 P1-P5 15× Rat-2 P1-P5	3× control 3× MG-132
Databases	Human, rat, CPXV_crust Hei, contaminant | Human, CPXV BR, contaminant	
Digestion mode, enzyme	Specific, trypsin/P	
Max missed cleavages	2	
Variable modifications	Oxidation (M), acetylation (protein N-term), diGly(K)	
Fixed modification	Carbamidomethyl (C)	
Mass tolerance parent ions	6 ppm | 4.5 ppm	
Mass tolerance fragment ions	0.5 Da	
Peptide FDR	0.05 | 0.01	
Protein FDR	0.01 | 1	
Site decoy fraction	0.01	
LFQ min. ratio count	1	
Match between runs	ON	
Match time window [min]	2.5 | 0.7	
Alignment time window [min]	20	
Peptides for quantification	Unique + razor	
Use only unmodified peptides for quantification	OFF	

Blue: adjusted parameters for the analysis of ubiquitinated peptides in CPXV-infected HeLa cells

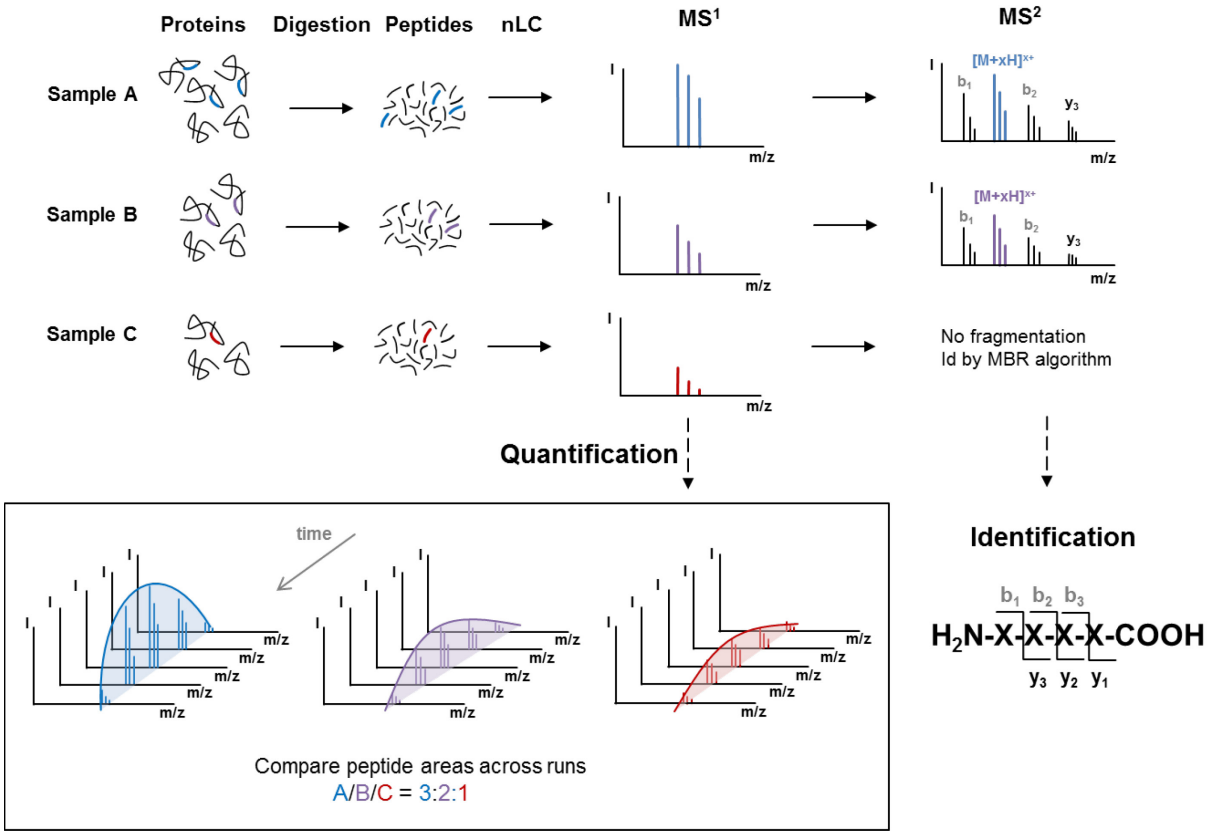

Figure 2.6. Principle of label-free quantification (LFQ) in shotgun proteomics. Proteins from virions or infected cells were lysed, digested and peptides separated by nLC. LFQ was done by comparing areas of identical peptides across runs. For feature identification in samples without MS^2 sequence information, peptide identifications were transferred between samples using the match between runs (MBR) algorithm.

Further bioinformatic analysis of protein and peptide identifications was done in Perseus as described in the following.

Bioinformatic analysis: CPXV crust passaging

LFQ values were filtered for reverse, contaminants and proteins only identified by site. Log_2 transformed protein intensities were separated in (i) crust + HEp-2 passages (18 samples) and (ii) crust + Rat-2 passages (18 samples). Each group was analyzed identically according to the following. Rows were categorically annotated in crust (technical triplicate) and P1-P5 (biological triplicate each) and filtered for at least 3 valid values in at least one group. As linear correlation between crust and passaged virus was only between 0.4-0.6 (Pearson correlation), viral proteins were analyzed separately from host proteins. Missing values were imputed from normal distribution with default values mimicking low abundance measurements (width 0.3, down shift 1.8) and median column normalization was performed to account for different sample loads. Pearson correlation of viral proteins was acceptable (> 0.8) for further analysis. Principal component analysis (PCA) was done prior to z-score normalization. Significant differences of z-score normalized protein intensities were analyzed using an ANOVA test with 5 % permutation-based FDR, 250 randomizations and S0 = 2. ANOVA significant protein intensities were averaged over the group mean and courses were correlated to the reference profiles shown in **Figure 2.7**. Proteins with a distance ≤ 0.1 to the reference profiles were defined as being adaptation-specific. Identical viral proteins correlating to the same reference profiles in HEp-2 and Rat-2-passaged cells were defined as comparable between cell lines.

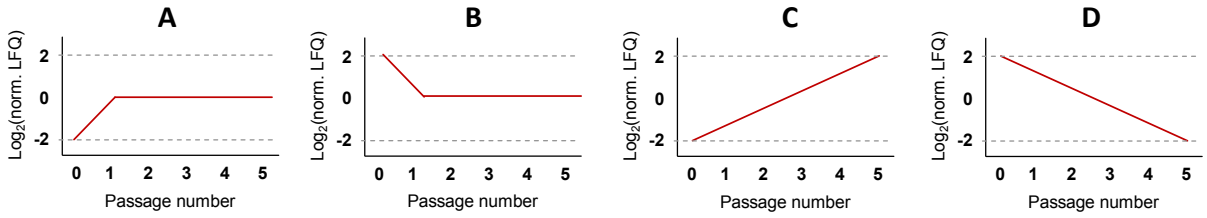

Figure 2.7. Reference profiles of adaptation-specific viral proteins. (**A,B**) Reference profiles of viral proteins showing adaptation upon change from crust to cell culture. (**C,D**) Reference profiles of viral proteins showing a continuous adaptation during passaging.

Host proteins were analyzed analogously to viral proteins. The crust was excluded from the analysis, because of the low linear correlation compared to cell culture passaged virus. LFQ values were filtered additionally for rat proteins in HEp-2 samples and vice versa to remove host-unspecific proteins. Rows were filtered for at least 12 valid values and ANOVA test was performed applying 1 % FDR-adjusted p-value with 2500 permutations and S0 = 0. Mean values of ANOVA significant proteins were hierarchically clustered using Euclidean distance and 300 clusters. Protein clusters including host proteins increasing or decreasing during passaging were defined as adaptation-specific host proteins

To elucidate differences in ubiquitination, viral peptide intensities were filtered for at least 3 valid values in at least one group and host proteins for at least 12 total valid values followed by mean column subtraction. Abundance differences of diGly(K) peptides were analyzed by ANOVA test (S0 = 0; 5 % permutation-based FDR with 250 (viral peptides) and 2,500 (host peptides) randomizations). ANOVA significant peptides were z-score normalized and plotted in GraphPad Prism.

Bioinformatic analysis: ubiquitinated peptides in CPXV-infected HeLa cells

Peptide raw intensities were filtered for reverse and contaminant peptide hits. Log_2-transformed peptide intensities were normalized by median column subtraction and peptides with at least one diGly(K) modification were kept for further analysis. Categorically annotated control and inhibitor-treated replicates were filtered for at least three valid values in at least one group and normalized by median row subtraction. Missing values were imputed from normal distribution (width 0.3, down shift 1.8). Significant differences of ubiquitinated peptides were analyzed using a two-sided t-test with 5 % permutation-based FDR, 250 randomizations and S0 = 2.

CPXV IMV ubiquitinome data analyses using Proteome Discoverer

Ubiquitinated viral proteins were identified with SEQUEST database search algorithm implemented in Proteome Discoverer computational proteomics platform. MS^2 spectra of technical duplicates were searched against the human UniProt complete proteome set with isoforms, the protein sequences of the respective CPXV strain and a contaminant database. The enzyme specificity was set to trypsin (full) allowing for 2 missed cleavages. Mass tolerances were 10 ppm for parent ions and 0.6 Da for fragment ions. The maximum number of dynamic modifications per peptide was set to 4 including methionine oxidation, protein N-terminus acetylation and diGly modification of lysine residues. Cysteine carbamidomethylation was set as static modification. Peptides were identified with a false discovery rate (FDR) of 1 % estimated by Percolator algorithm [178] and peptide areas were calculated using the Precursor Ions Area Detector node.

Protein quantification using the total protein approach (TPA)

The TPA concept was used to estimate protein concentrations without spike-in standard [179,180] and calculated according to the following:

$$Protein\ concentration\ (i)\left[\frac{mol}{g\ total\ protein}\right] = \frac{LFQ\ intensity\ (i)}{Total\ LFQ\ intensity \times MW(i)}$$

3. Results

3.1. Passaging of CPXV isolated from a rat crust in different cell lines

CPXV IMV particles were isolated from a rat crust resulting in 2.8×10^8 viral GE measured with qPCR. Purified virions were serially passaged five times in triplicate in HEp-2 and Rat-2 cells. To estimate changes in viral fitness during passaging, the CPE was documented and the virus yield determined. In the following, samples are abbreviated according to cell line and passage, e.g. "RP1" for first passage in Rat-2 cells.

3.1.1. CPE and virus yield during passaging

From the first passage on, a CPE was detectable in both cell lines. Neither the first day of CPE appearance nor the characteristics changed during passaging. But while Rat-2 cells showed a CPE already on the first day p.i., a CPE in HEp-2 cells was not detected until day three p.i.. Furthermore, upon CPE appearance, Rat-2 cells rapidly detached from the surface and formed aggregates (**Figure 3.1**). In contrast, HEp-2 cells barely detached from the surface after CPE appearance, but formed syncytia (multinucleated enlarged cells) instead, which were hardly detectable in aggregated Rat-2 cells.

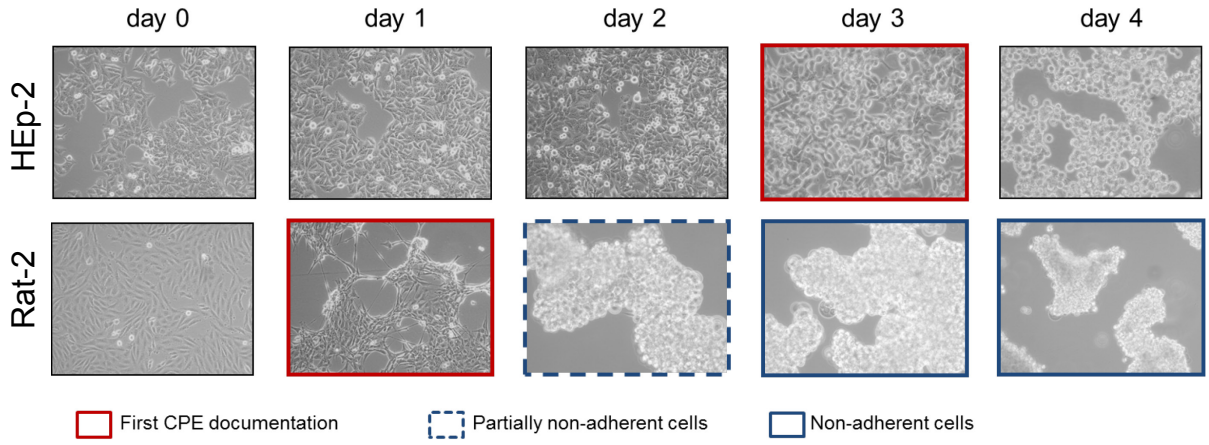

Figure 3.1. CPE documentation during passaging of CPXV isolated from a rat crust. HEp-2 and Rat-2 cells were infected with purified CPXV isolated from a rat crust (day 0) at an MOI of 0.1 and the cytopathic effect (CPE) was documented daily until harvesting (day 4).

Although HEp-2 and Rat-2 cells showed diverse CPE appearance, the total virus yield in both cell lines was comparable, except a higher virus yield in HEp-2 cells in the last passage. The virus yield in HP5 was significantly higher than in all other samples, indicating replication gains of CPXV in human cells. In contrast, the virus yield in Rat-2 cells showed no significant difference during passaging (**Figure 3.2**).

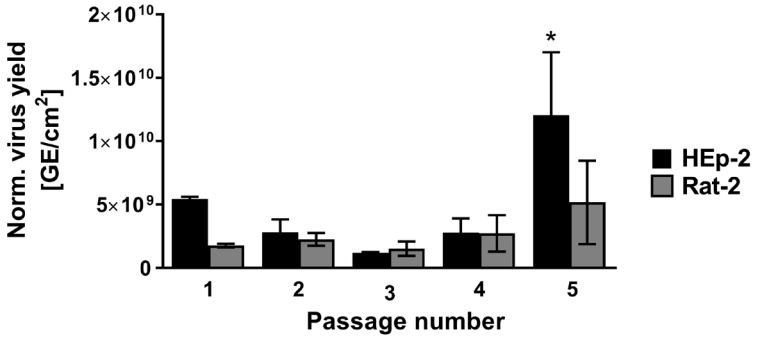

Figure 3.2. Virus yield during passaging of CPXV isolated from a rat crust. Viral genome equivalents (GE) in each passage were determined by qPCR after cell lysis. Error bars indicate mean ± standard deviation of three biological replicates. Statistics: One-way ANOVA and Bonferroni's multiple comparison test (*p ≤ 0.05).

3.1.2. Real-time cell analysis of passaged and non-passaged CPXV

To elucidate changes in viral fitness during passaging, passaged and non-passaged virions were compared using RTCA, which measures the adherence of cells over time. Passaged virions were analyzed with the same cells they had been propagated in previously, revealing an overall faster detachment of Rat-2 cells compared to HEp-2 cells. Apart from these differences, passaged virions showed comparable courses in both cell lines. In contrast, replicates of the non-passaged virions showed clearly heterogeneous courses, which split up into two distinct courses: one representing the course of the passages and another showing significantly faster cell detachment (referred to as crust_I and crust_II in **Figure 3.3**). These heterogeneities were confirmed in repetition of the experiment (**Figure S1**).

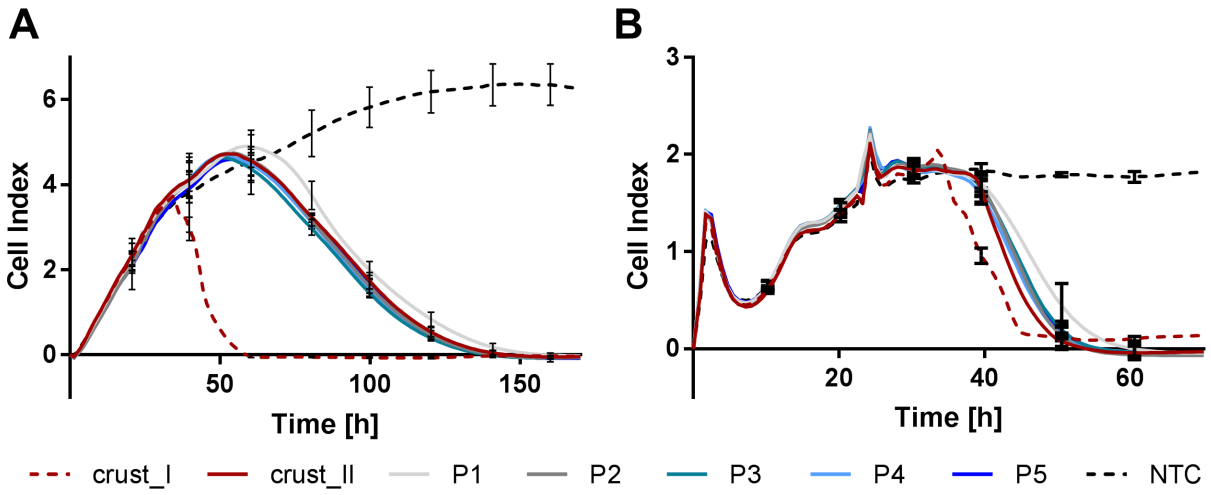

Figure 3.3. Real-time cell analysis of passaged and non-passaged CPXV in HEp-2 and Rat-2 cells. (**A**) HEp-2 and (**B**) Rat-2 cells were seeded in 96-well E-plates and the cell adherence was measured over time. An increasing Cell Index implies increasing cell adhesion to the well bottom and vice versa. About 24 h after seeding, cells were infected with purified CPXV originating from a rat crust or from different passages (P1-P5) in the corresponding cell line at an MOI of 0.1. Error bars indicate mean ± standard deviation of three biological replicates of passaged virions or six technical replicates of the non-passaged virions, which split up into two different courses (crust_I and II) with each n = 3.

3.1.3. Genome analysis of passaged and non-passaged CPXV

To elucidate possible genomic changes underlying the increased viral fitness in HP5 and, moreover, to elucidate possible changes in virus particles occurring in the absence of yield changes, NGS of the crust and each passage was performed. Deep sequencing resulted in about 1-7 million viral reads per sample with a mean genome coverage of > 2,500 in passages and about 1,300 in the crust (**Table S2**). *De novo* assembled viral genomes had a length of > 216,300 bp except for RP1 with 209,458 bp. In comparison, the genome size of the CPXV strain RatHei09/1 used is specified with 208,980 bp in the NCBI database (GenBank: KC813504.1), showing that *de novo* assembly performed well. All 206 unique CDS of the GRI-90 reference strain could be transferred to assembled genomes, except RP1. Here sequence information of the terminal five genes was missing. Note that the terminal five CPXV genes D1L to D5L are inverted versions of I1R to I5R located in the ITR region. Since these five genes occur in one copy at both ends of the genome, *de novo* assembly restricted reads to either left or right site of the genome, resulting in higher coverage at one end of the genome (**Figure 3.4**).

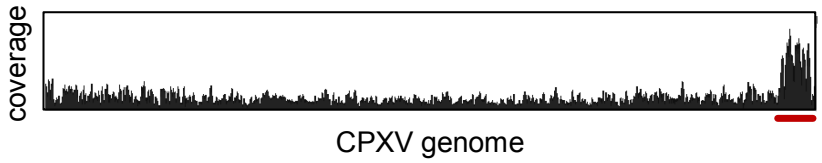

Figure 3.4. Exemplary coverage across *de novo* assembled CPXV genome. Duplicated genes clearly show an increased coverage (red).

Copy number variation (CNV)

CNV in terms of gene expansion may be identified by *de novo* assembly, because reads covering two adjacent gene duplicates should be identified, or by increased read depth in the alignment [57]. However, *de novo* assembled viral genome sequences did not reveal any gene expansion. Assemblies were verified by alignment of reads to the genome sequence whereby duplicated genes resulted in clearly higher coverage as demonstrated by the five genes with known duplication (**Figure 3.4**). Coverage of these genes was constantly higher than the mean coverage across the genome adding two standard deviations. However, no other gene with comparable increased read depth was identified in any of the samples, indicating that CNV did not occur during passaging of the CPXV crust isolate.

Variant analysis

Comparison of consensus sequences, which represent the major variants in a heterogeneous sequence pool, revealed six differences between passaged and non-passaged virion genomes. Strikingly, all six variants were insertions or deletions localized in repetitive sequences outside of CDS. Notably, HP5 and RP5 consensus sequences differed only by two and four nucleotides from the crust consensus sequence, implying the overall genome stability of CPXV isolates propagated in cell culture. Nevertheless, variant analysis revealed 27 variants in the CPXV crust and a mean of about 28 variants in each passage irrespective of the cell line used for propagation. Moreover, a total of eight variants in the crust and a mean of about five variants per passage were localized in a CDS (**Table 3.1**).

Table 3.1. Number of variants in crust and passaged CPXV.

Sample[a]	Total	CDS[b]	*De novo*[c]	Sample[a]	Total	CDS[b]	*De novo*[c]
HP1	27	4	6	RP1	27	5	22
HP2	23	3	6	RP2	30	4	17
HP3	37	7	31	RP3	27	7	14
HP4	29	4	6	RP4	24	6	6
HP5	27	6	7	RP5	32	4	10
Mean	28.6	4.8	11.2	Mean	28	5.2	13.8
Crust	27	8					

[a] H: HEp-2; R: Rat-2; P: passage
[b] Variants in coding sequence
[c] First time detected in this passage

Identified variants included insertions and deletions (indels), substitutions and SNPs. With a mean of over 50 % SNPs represented the most frequent variant type in all samples, followed by indels with about 40 %. Substitutions made up a mean of 5 % in passaged virions, but were absent in the non-passaged virions. Notably, about 72 % of all variants were found in tandem repeats. Among a total of 78 different variants in HEp-2 and 89 in Rat-2 cells, 54 were identical in both cell lines, showing also reproducible variant frequencies (**Figure 3.5**).

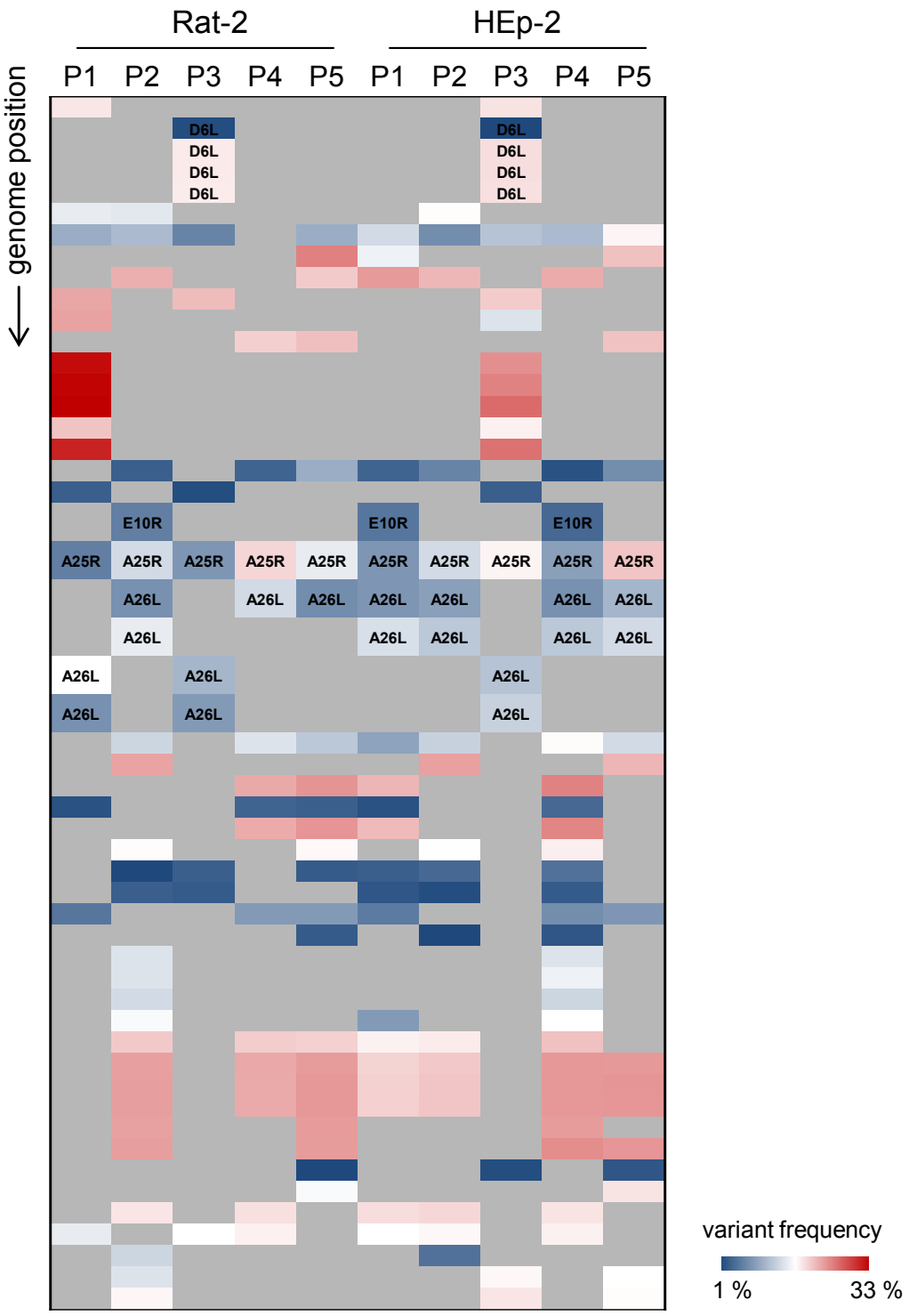

Figure 3.5. Heatmap visualization of minor variants during passaging. The frequency of 54 variants detected in both cell lines is shown according to the genome position. Frequencies are comparable, but variants appeared mostly in different passages. If no gene name is shown variants are in non-coding regions. Grey: variant not detected.

Altogether 14 mutated CDS were identified, from which 12 resulted in an amino acid change. Surprisingly, nine mutations were found in conserved genes and seven were essential genes associated mostly with transcription (**Table 3.2**).

Table 3.2. Overview of genes with amino acid changes in CPXV crust and passages.

Sample[a]	Gene	Description	Function	Essential	Conserved
C	J4L	RNA polymerase-associated protein	Transcription	+	+
	L6L	Telomere-binding protein	Viral reproduction	+	+
H	C1L	Putative uncharacterized protein	Unknown	-	-
	H3R	Late transcription elongation factor	Transcription	+	+
	A12R	Membrane biogenesis protein	Morphogenesis	+	+
R	A9R	Intermediate transcription factor 3 small subunit	Transcription	+	+
	J6R	DNA topoisomerase 1B	DNA replication	-	+
	O4R	DNA-directed RNA polymerase 147 kDa polypeptide	Transcription	+	+
H/R	D6L	Putative uncharacterized protein	Unknown	-	-
C/H/R	A25R	DNA-directed RNA polymerase 133 kDa polypeptide	Transcription	+	+
	A26L	A-type inclusion protein	Viral reproduction	-	-
	E10R	mRNA decapping protein	Transcription	-	+

[a] C: crust; H: HEp-2; R: Rat-2

De novo mutations and selection of pre-existing variants

The term *de novo* mutation is used in the following to describe variants appearing for the first time in a passage. *De novo* mutations were identified in both cell lines in the A26L gene encoding the A-type inclusion protein, the uncharacterized D6L gene and the E10R gene encoding an mRNA decapping enzyme. Additionally, A26L, E10R and the A25R gene encoding the RNA Pol 133 kDa polypeptide contained variants that were also detected in the crust, indicating pre-existing variants rather than *de novo* mutations. Interestingly, a frequency accumulation of a single variant was observed. This was an A→C transversion at position 269 in the A25R gene leading to a K→T substitution at amino acid position 90 (Lys90Thr). While variant frequency in the crust was 3.1 % for this SNP, HP5 displayed a frequency of 11.4 % and RP4 9.5 % variant frequency. The Lys90Thr in the A25R gene was the only CDS-localized mutation detected in every sample and, moreover, the only that increased in frequency during passaging, indicating a selective advantages of this mutation (**Table 3.3**).

Result summary: genomic adaptation of CPXV particles

- Stable virus genome, but multiple minor variants
- Variants largely reproducible between cell lines
- Tandem repeats more mutation-prone
- No gene duplications
- A25R & A26L major targets of mutations
- Transcription-associated genes targets of mutations

Table 3.3. Mutations in viral CDS during passaging of CPXV isolated from a rat crust.

CDS	Pos[a]	Change[b]	Type	R[c]	Protein effect	AA[d]	Variant frequency [%][e]										
							P0	HP1	HP2	HP3	HP4	HP5	RP1	RP2	RP3	RP4	RP5
A12R	728	A→G	SNP	+	Substitution	K→R										1.2	
A24R	1,149	(A)8→(A)9	Insertion	+	Frame Shift											1.4	
A25R	269	A→C	SNP	-	Substitution	K→T	3.1	2.7	4.2	6.4	2.9	11.4	2.2	4.2	2.7	9.5	4.6
A25R	4	(A)8→(A)9	Insertion	+	Frame Shift		1.3									1.4	
A26L	1,091	G→T	SNP	+	Substitution	H→Q	1.1										
A26L	1,118	$(GTT)_8$→$(GTT)_9$	Insertion	+	Insertion	P→P	3.1	2.7	2.9		2.6	3.4		2.6		4.2	2.5
A26L	1,115	$(GTT)_8$→$(GTT)_7$	Deletion	+	Deletion	QP→P	4.6	4.3	3.8		3.8	4.2		4.6			
A26L	1,093	$(TTG)_8$→$(TTG)_7$	Deletion	+	Deletion	Q→				3.7			5.0		3.4		
A26L	1,093	$(TTG)_8$→$(TTG)_9$	Insertion	+	Insertion	→Q				4.0			2.6		2.8		
A9R	259	(A)8→(A)9	Insertion	+	Frame Shift												1.5
C1L	465	C→A	SNP	+	Substitution	R→S						1.2					
C2L	168	C→T	SNP	-	None											1.5	
D6L	613	ATA→TCC	Substitution	-	Substitution	Y→G							1.9				
D6L	615	A→T	SNP	-	Truncation					1.0					1.1		
D6L	616	+TCC	Insertion	-	Insertion	→G				8.8					7.4		
D6L	611	C→T	SNP	-	Substitution	S→N				8.7					7.4		
D6L	606	G→A	SNP	-	None					8.5					7.1		
E10R	474	$(T)_7$→$(T)_8$	Insertion	+	Frame Shift		2.9	2.0			1.7			2.2			
E10R	481	$(T)_7$→$(T)_8$	Insertion	+	Frame Shift								2.6				
E10R	716	A→T	SNP	-	Substitution	E→V						1.8					
H3R	28	A→G	SNP	-	Substitution	N→D						1.3					
J4L	101	+GG	Insertion	-	Frame Shift		1.1										
J6R	319	A→G	SNP	-	Substitution	K→E											2.1
L6L	1,084	$(T)_{10}$→$(T)_{11}$	Insertion	+	Frame Shift		1.9										
O4R	1,648	T > C	SNP	-	Substitution	S→P										1.1	

[a] Position in CDS [b] Nucleotide change [c] Localization in tandem repeat [d] Amino acid change [e] P0: crust; H: HEp-2; R: Rat-2; P1-P5: Passage 1-5

3.1.4. Proteome analysis of passaged and non-passaged CPXV IMV virions

The proteome composition of passaged and non-passaged CPXV IMV was analyzed by LC-MS/MS to elucidate possible proteomic changes. A mean of 18,500 MS^2 spectra per sample was acquired from which a mean of 17.5 % was identified as highly confident peptide. From a total of 3,453 identified proteins 167 originated from CPXV while the residual 3,286 ones stemmed from the host (human or rat) or were contaminants. The sample order was shuffled during MS analysis to avoid systematic errors. However, proteins outside of virion particles may stick together with virion proteins and hence cannot be entirely removed during purification, which is why identified proteins may be incorporated in or associated with virions.

Adaptive changes of viral proteins in IMV particles

Mutations resulting in amino acid changes in viral proteins were included as isoforms in the viral protein database used for analysis. Not surprisingly, as mutation frequencies were low (≤ 11.4 %), no isoforms were identified in proteome analysis. A total of 167 highly confident CPXV proteins were identified. Proteins quantified in all three replicates in at least one sample were considered for quantification. Because linear correlation between passaged and non-passaged samples was rather low, as demonstrated by a Pearson correlation of 0.4 - 0.6, host proteins were removed from the analysis and separately analyzed, improving linear correlation of virus proteins to > 0.8 and even > 0.9 between replicates (**Figure 3.6**).

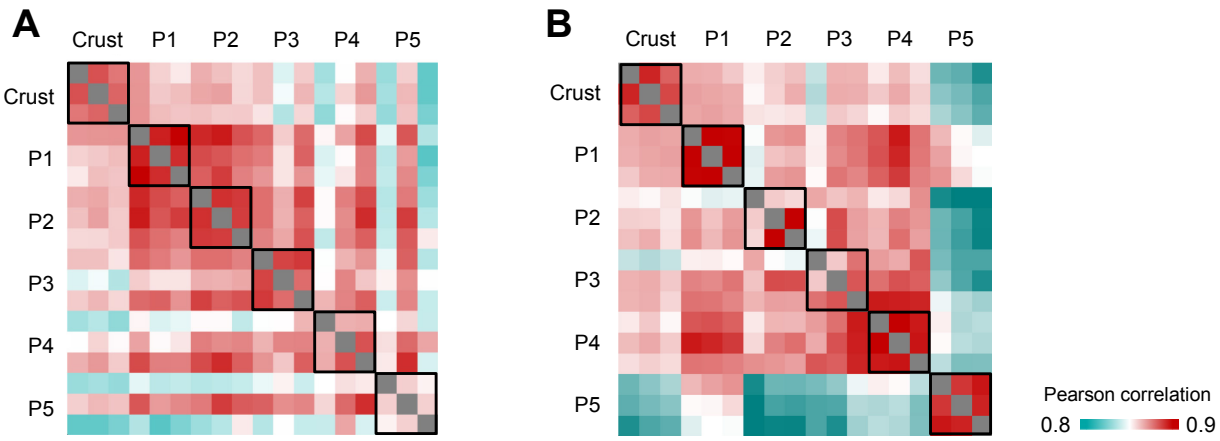

Figure 3.6. Linear correlation of viral protein intensities in IMV particles during passaging. Shown is the Pearson correlation of normalized viral LFQ intensities without missing values of non-passaged (crust) and passaged virions (P1-P5) in (**A**) HEp-2 and (**B**) Rat-2 cells. P1-5: Passage 1-5.

Surprisingly, PCA and hierarchical clustering of virus proteins revealed fairly good separability of CPXV particles from different passages (**Figure 3.7**). This suggested that the IMV proteome changed during cell culture passaging what is underlined by the heat map visualization in **Figure 3.7**, showing considerably differences between crust and passages and also differences among passages.

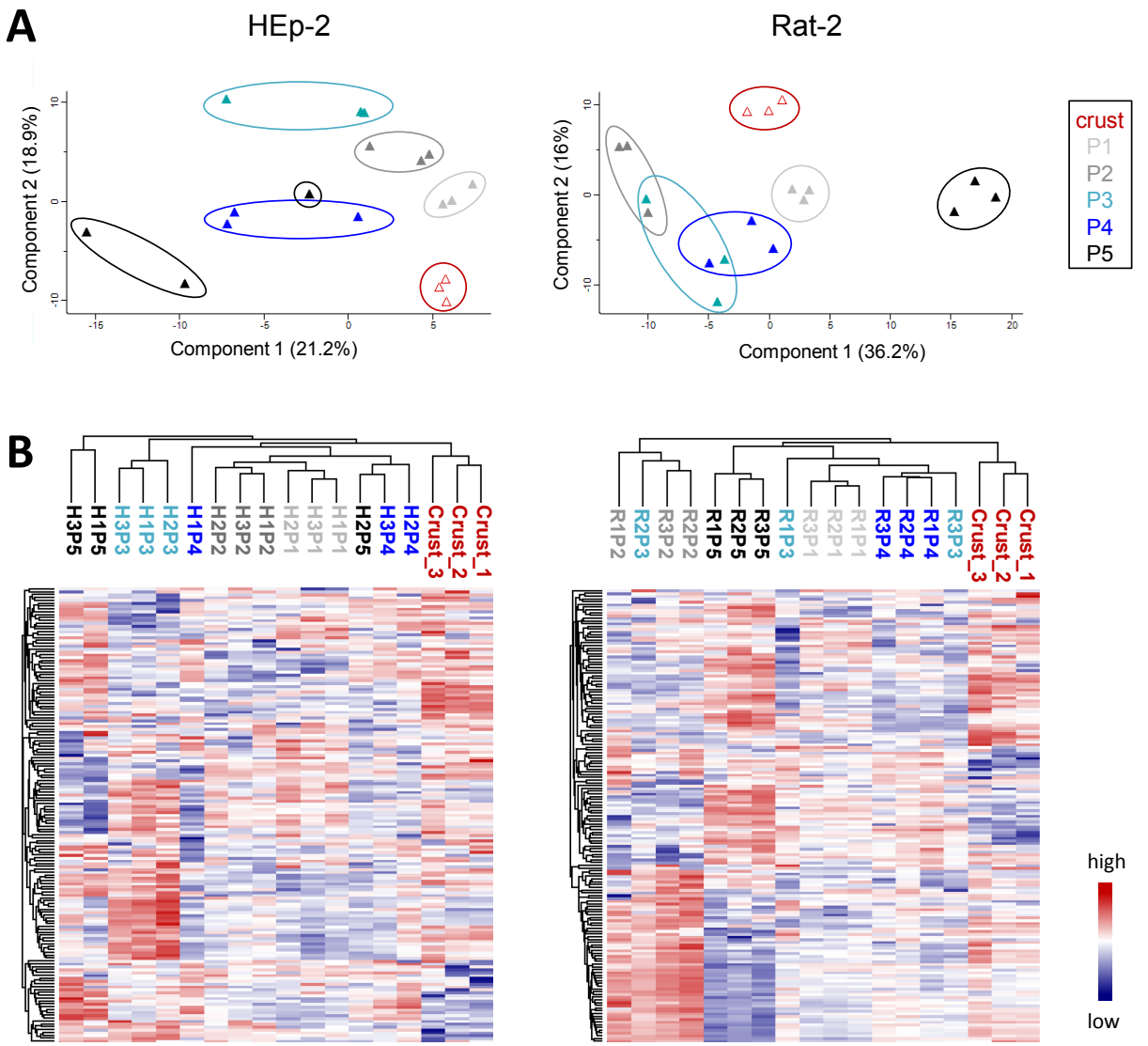

Figure 3.7. Principal component analysis and hierarchical clustering of viral CPXV IMV proteins. Normalized LFQ intensities of virus proteins without missing values were used for (**A**) principal component analysis prior to z-score normalization and (**B**) hierarchical clustering after z-score normalization. Both analyses demonstrate separability of passages, indicating proteomic differences during cell culture passaging. P1-5: Passage 1-5.

Significance of differences was analyzed by ANOVA and adaptation-related viral proteins were defined as proteins displaying a clear abundance trend during passaging or showing altered amounts upon host change, meaning different amounts in passaged and non-passaged virions. To identify common adaptation mechanisms, courses of viral proteins were compared between cell lines (see section 2.14.4). This led to the identification of the envelope protein G13, which changed comparably during passaging in both cell lines (**Figure 3.8A**). Proteins with different courses in cell lines during passaging were considered to be cell-line specific, resulting in 15 viral proteins in HEp-2-passaged virions and eight viral proteins in Rat-2-passaged virions (**Figure 3.8B,C**). Courses of these proteins revealed that the same number of viral proteins changed upon infection of the first passage (six proteins per cell line; **Figure 3.8B,C**), while more

viral proteins changed during passaging in HEp-2 cells (nine proteins; **Figure 3.8C**) compared to Rat-2 cells (two proteins; **Figure 3.8B**). Moreover, two proteins (A53 and Q1) changed in virions passaged in both cell lines, but showed different courses (**Figure 3.8B,C**).

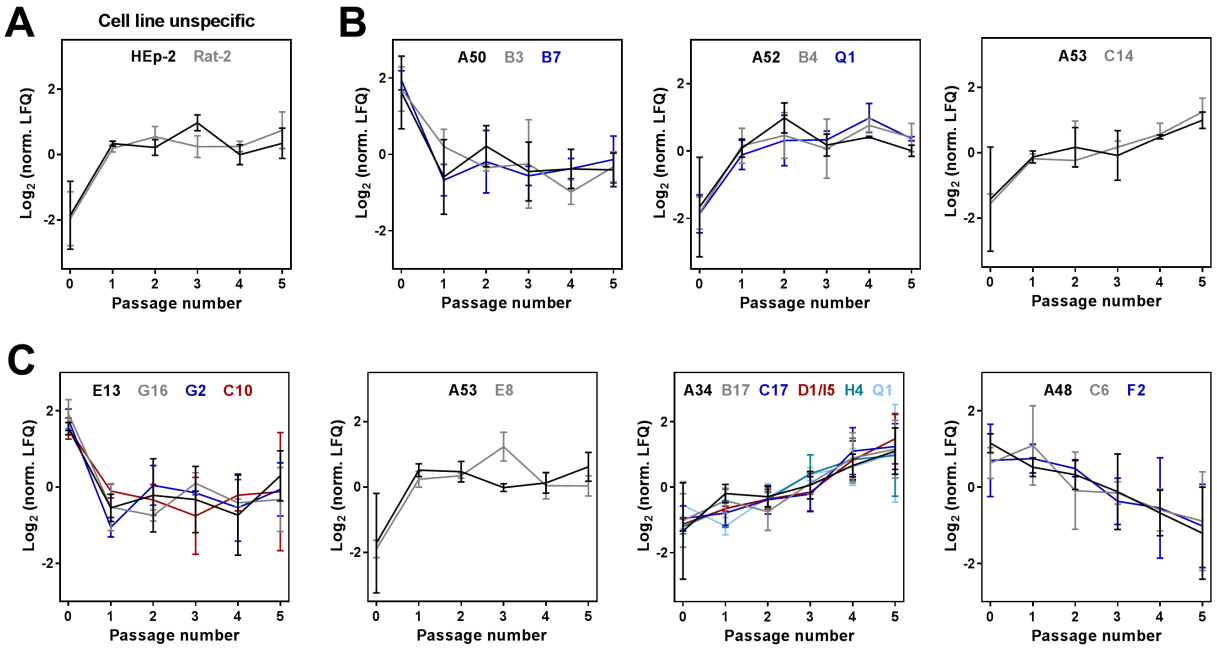

Figure 3.8. Viral proteins changing in an adaptation-associated manner during passaging in HEp-2 and Rat-2 cells. Proteins are sorted according to adaptation-associated time courses with distances ≤ 0.1 to reference profiles. (**A**) A single viral protein (G13) displays comparable courses during passaging in both cell lines (cell line unspecific). Proteins changing in a cell line-independent manner were identified in (**B**) Rat-2- and (**C**) HEp-2-passaged virions. Shown are normalized LFQ intensities (log_2) of ANOVA significant proteins. Error bars indicate mean ± standard deviation of three biological replicates (passage 1-5) or three technical replicates (passage 0: crust).

Sorting the viral proteins, which changed in a cell type-specific manner, according to their function revealed that proteins in both cell lines were associated with similar functions, including proteins of immunomodulatory, unknown and membrane-associated function (**Table 3.4**). Virions passaged in HEp-2 cells additionally showed changes of viral proteins associated with diverse other processes, including viral proteins with enzymatic activities. Strikingly, four out of the six viral proteins increasing in amounts during passaging in HEp-2 cells were associated with viral immune evasion.

Table 3.4. Function of viral proteins changing in a cell line-specific manner during passaging.

Protein	Description[a]	Function
HEp-2		
A34	EEV glycoprotein	Membrane
E8	Cell surface-binding protein	Membrane
E13	Scaffold protein	Membrane
B17	Soluble IFN-α/β receptor	Immune evasion
C17	Complement control protein	Immune evasion
D1/I5	Secreted chemokine-binding protein	Immune evasion
Q1	Inhibitor of TNF-R and TLR signaling	Immune evasion
C6	Uncharacterized protein	Unknown
C10	Uncharacterized protein	Unknown
F2	Uncharacterized protein	Unknown
G16	Uncharacterized protein	Unknown
A48	Cu-Zn superoxide dismutase-like protein	Others
G2	dUTPase	Others
H4	Glutaredoxin-2	Others
A53	DNA ligase	DNA replication
Rat-2		
B4	EEV type-I membrane glycoprotein	Membrane
A50	Uncharacterized protein	Unknown
A52	Uncharacterized protein	Unknown
B3	Uncharacterized protein	Unknown
C14	Uncharacterized protein	Unknown
B7	Interferon-γ receptor-like protein	Immune evasion
Q1	Inhibitor of TNF-R and TLR signaling	Immune evasion
A53	DNA ligase	DNA replication

[a] According to UniProt

Adaptive changes of host proteins in IMV particles

Compared to the passaged virions, the host proteome of non-passaged virions isolated from the rat crust was dominated by rat collagen-α 1 and 2, which is the predominant fibril-building collagen type of the skin. Therefore, it was no surprise to identify collagen-α in extraordinarily high amounts in a sample originating from a rat skin. For the analysis of changes in host protein abundance associated with CPXV IMV particles, the crust had to be excluded from the analysis, because similarity to the passaged virion host background was too low for comparison, as indicated by a poor Pearson correlation (< 0.5).

All passages, except P3 and P4 in Rat-2 cells, could be separated by PCA, indicating differences in host cell protein abundance associated with virus particles during passaging (**Figure 3.9**).

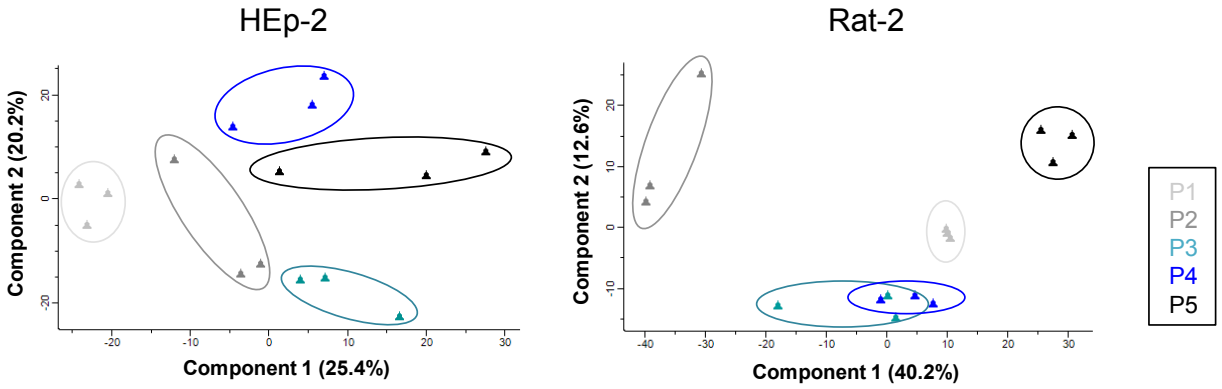

Figure 3.9. Principal component analysis of host proteins during passaging. Normalized LFQ intensities of virus proteins without missing values were used for principal component analysis, revealing separability of host cell proteins associated with CPXV IMV particles during passaging in HEp-2 and Rat-2 cells. P1-P5: Passage 1-5.

Significantly altered host proteins were analyzed for adaptation-associated cluster (see section 2.14.4). Because the crust had to be excluded from the analysis, host proteins with different amounts in virions isolated from the crust and in passaged virions could not be identified. Most host proteins did not show any adaptation-related courses. Nevertheless, host proteins with increasing or decreasing amounts during passaging were identified. In HEp-2-passaged virions 17 host proteins and in Rat-2-pasaged virions 24 host proteins showed adaptation-associated courses (**Figure 3.10**). Only the eukaryotic translation initiation factor 3 subunit B (EIF3B) changed in virions passaged in both cell lines, showing increasing abundance during passaging. Interestingly, a protein involved in cytoplasmic DNA sensing (XRCC5) increased and an apoptosis-associated protein (PDCD6) decreased in abundance in HEp-2-passaged virions. In contrast, in Rat-2-passaged virions a serin/threonine-protein phosphatase increased in abundance (Ppp2r4), while another decreased (Ppp2r1a) during passaging. Moreover, a regulatory subunit of the proteasome (Psmc5) increased during passaging in Rat-2 cells, while the proteasome activator complex subunit 4 (Psme4) decreased in abundance.

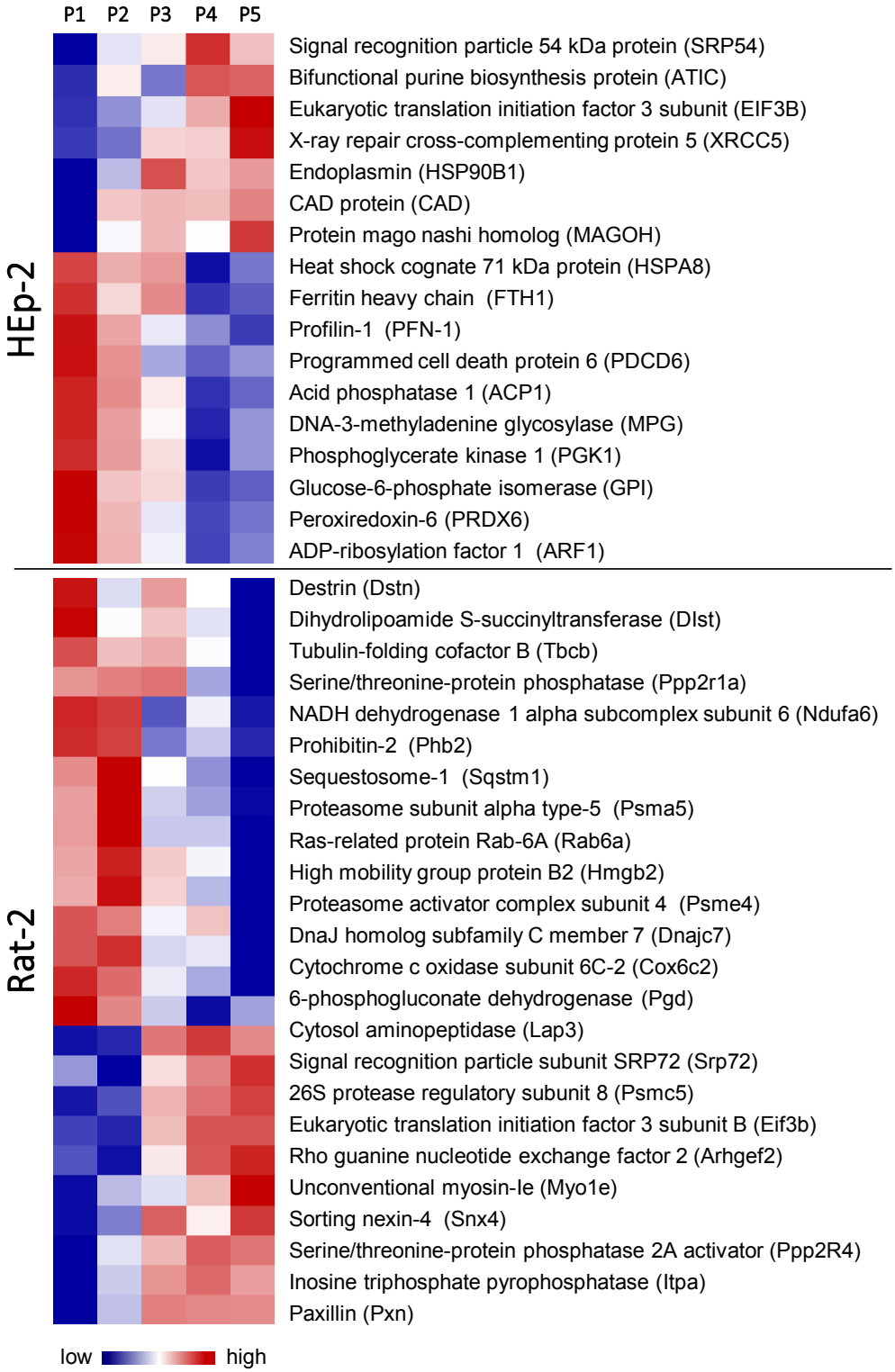

Figure 3.10. Heatmap visualization of host proteins changing during passaging. Host proteins with adaptation-associated courses (increasing or decreasing in abundance) were identified in purified CPXV IMV particles during passaging in HEp-2 or Rat-2 cells. Shown are mean values of three biological replicates of z-score normalized protein intensities (ANOVA significant). Ribosomal proteins and histones were removed. P1-P5: Passage 1-5.

Role of ubiquitination during CPXV passaging

Because ubiquitin has been identified in previous proteome analysis of CPXV IMV particles [88], the modification of lysine residues with diGly was included in the analysis to identify ubiquitination sites. A total of 124 ubiquitination sites were identified, including seven sites in five viral proteins. As a result of the MBR algorithm, diGly(K) peptides were identified in every sample, although LFQ values were not available for every sample. Three of five ubiquitinated virus proteins were membrane-associated (A14, E8 and J3), while one was a structural core component protein (A4) and one an immunomodulatory protein (Q1) (**Table 3.5**).

Table 3.5 Ubiquitinated virus proteins identified during CPXV crust passaging.

Protein	DiGly(K) position	Description
A14	49	Virion membrane protein
A4	111	Major core protein 4b
E8	13; 14	Cell surface-binding protein
J3	38; 46	IMV heparin-binding surface protein
Q1	70	Inhibitor of TNF-R and TLR signaling

Quantification of ubiquitinated peptides revealed that cell culture passaging lead to significant changes in the ubiquitination of A14, E8 and Q1 in both cell lines. Additionally, Rat-2 cells showed differences in the abundance of J3 ubiquitination. However, only ubiquitinated peptides of E8 and Q1 in HEp-2 cells showed a distance ≤ 0.2 to adaptation-related courses, indicating adaptive changes during passaging (**Figure 3.11A**).

Furthermore, the amount of ubiquitin itself significantly changed during cell culture passaging in both cell lines. Polyubiquitin linkages were identified at positions K48 and K11. Quantitative approximation of diGly(K) linkage-specific ubiquitin peptides indicated that K48-linked ubiquitination decreased during passaging in HEp-2 cells (**Figure 3.11B**).

Besides ubiquitin itself, amounts of ubiquitin-related proteins changed during passaging in Rat-2 cells. Here, differences in the abundance of the E3 ubiquitin-protein ligases NEDD4 and E3C, the ubiquitin-conjugating enzyme E2N and the ubiquitin-like modifier activating enzyme 1 (UBA1) were detected. However, courses of these proteins were not associated with adaptation. Moreover, the amount of Small ubiquitin-related modifier 2 (SUMO2) decreased during passaging in both cell lines, showing an adaptation-associated course during passaging in HEp-2, but not in Rat-2 cells (**Figure 3.11C**).

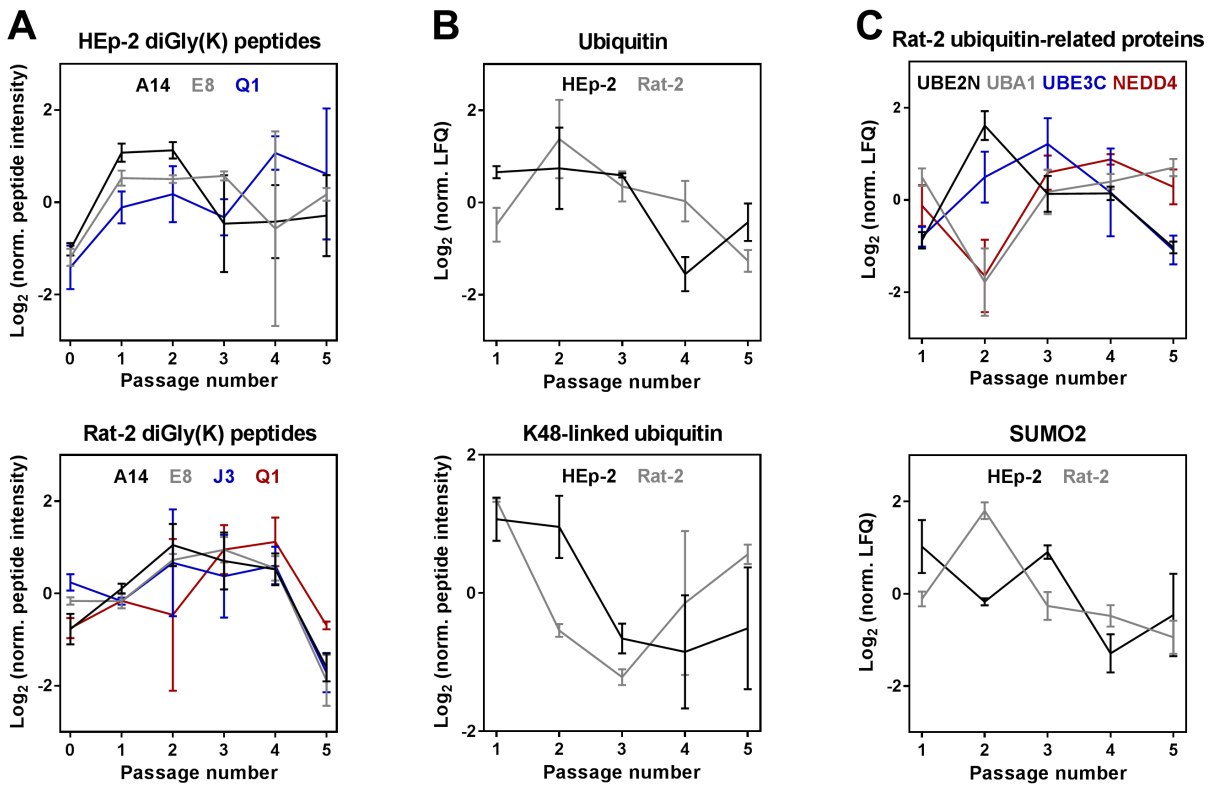

Figure 3.11. Amount of ubiquitin-associated proteins during cell culture passaging. Shown are z-score normalized peptide intensities (ANOVA significant). Error bars indicate mean ± standard deviation of three biological replicates (passage 1-5) or three technical replicates (passage 0: crust). (**A**) Amount of ubiquitinated viral peptides during passaging. (**B**) Total and K48-linked ubiquitin abundance during passaging in HEp-2 and Rat-2 cells. (**C**) Abundance of ubiquitin-related proteins during passaging in Rat-2 cells.

Result summary: proteomic adaptation of CPXV IMV particles

Cell type-independent:
- Adaptation upon switch from crust to cell culture and during passaging
- Increased amounts of viral membrane protein G13
- Increased amounts of host translation initiation factor 3 subunit B
- Possible role of ubiquitination during CPXV adaptation

Cell type-specific:
- Viral HEp-2: Adaptation of proteins associated with membrane and immune evasion
- Viral Rat-2: Adaptation of viral proteins with unknown function
- Host HEp-2/Rat-2: Adaptation of proteins with diverse functions

3.2. The role of ubiquitination in CPXV infection

Adaptation of CPXV may result from ubiquitinome changes as indicated by proteome analysis of the passaged crust (see section 3.1). However, distinct ubiquitination sites in poxvirus proteins have hardly been analyzed yet and underlying mechanisms remain elusive. Therefore, as a prerequisite to analyze adaptation-related changes in the ubiquitinome of poxviruses, the role of the UPS during CPXV infection and, moreover, the CPXV IMV ubiquitinome was analyzed. As described in section 1.3.3, the investigations were based on the hypothesis of ubiquitinated CPXV core proteins. Parts of the data shown in the following were generated by Annemarie Fritsch in the course of her master's thesis, which she made under my supervision [181]. Graphics resulting from data of her experiments include Figures 3.12, 3.13 and 3.14A,B.

3.2.1. The role of the UPS during CPXV infection

The role of the UPS during CPXV infection was investigated by analyzing the effect of proteasome inhibition on CPXV replication. Prior to infection experiments, different concentrations of MG-132 and Bortezomib were analyzed for their inhibition of the chymotryptic-like proteasome activity in HeLa cells. Both compounds inhibit primarily the chymotrypsin-like site of the 26S proteasome but may also act on the caspase-like site in a concentration-dependent manner [182]. As inhibitors were dissolved in DMSO, corresponding DMSO amounts were added to control samples. A complete inhibition of proteasome activity was only observed using 10 µM MG-132 and 1 µM Bortezomib, representing the highest tested inhibitor concentrations (**Figure 3.12A**), which have already been applied in previous studies [127,128]. Furthermore, the cell viability was analyzed to exclude cytotoxic effects of the proteasome inhibitors. Analysis of the ATP amount revealed about 80 % cell viability of inhibitor treated cells after 24 h of treatment (**Figure 3.12B**), while inhibitor induced cytotoxicity was below 5 %, confirming acceptable conditions for infection experiments (**Figure 3.12C**).

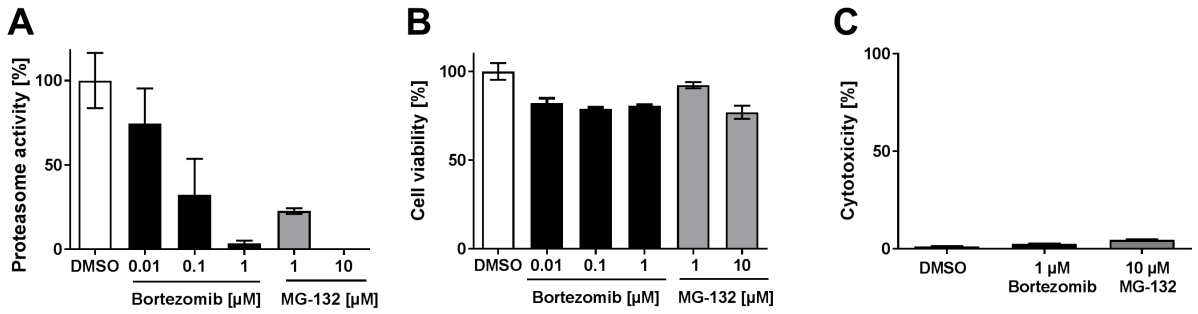

Figure 3.12. Effect of proteasome inhibitors on HeLa cells. HeLa cells were incubated 24 h in the presence of MG-132, Bortezomib or DMSO and assayed for (**A**) chymotrypsin-like proteasome activity, (**B**) ATP amount and (**C**) release of lactate dehydrogenase. Error bars indicate mean ± standard deviation of one experiment performed at least in triplicate. Experiments were performed by Annemarie Fritsch [181].

Since the reduction of CPXV PFU has only been described for proteasome inhibition with Bortezomib [128], the effect of MG-132 was analyzed, as it is the inhibitor primarily used for studies with VACV [127-129]. Thereby, the reduction of CPXV GE and PFU in HeLa cells treated with either Bortezomib or MG-132 was confirmed (**Figure 3.13**).

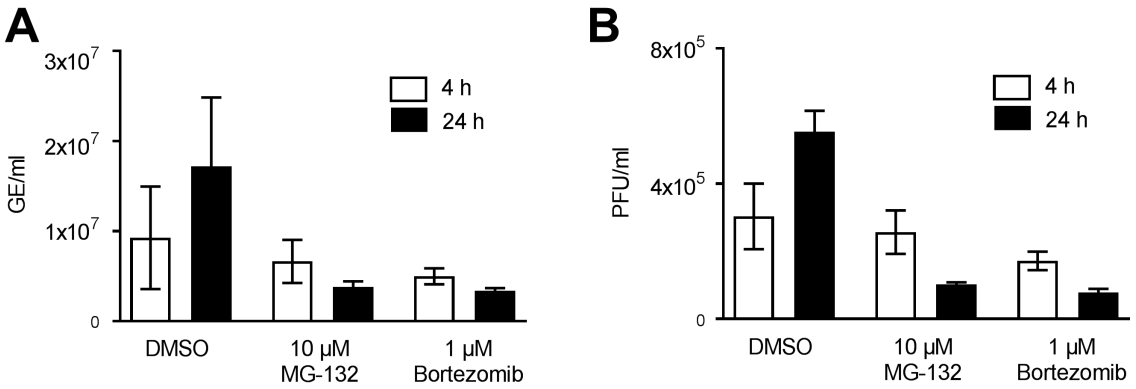

Figure 3.13. Effect of proteasome inhibition on CPXV GE and PFU. HeLa cells were infected with CPXV BR at an MOI of 1 in the presence or absence of 10 µM MG-132 or 1 µM Bortezomib. After 4 and 24 h p.i. the amount of (**A**) viral genome equivalents (GE) and (**B**) plaque forming units (PFU) in the supernatant was analyzed. Error bars indicate mean ± standard deviation of one experiment performed in triplicate. Experiments were performed by Annemarie Fritsch [181].

Inhibition of late protein expression has only been shown using MG-132 [128], while inhibition of VF formation has not been shown for CPXV at all. Analyzing HeLa cells infected with a recombinant CPXV, expressing RFP under an early and GFP under a late viral promotor, the absence of late protein expression in inhibitor treated cells could be shown, while early protein expression was still detectable. Additionally, VF were only detected in control cells with non-inhibited proteasome while VF were absent in cells with inhibited proteasome (**Figure 3.14A,B**). Additionally, the absence of late viral protein expression resulting from proteasome inhibition was confirmed by western blot (**Figure S2**). These results demonstrate that the effects of proteasome inhibition observed for VACV replication are transferable to CPXV.

The absence of late protein expression and viral genome replication has been hypothesized to result from the inability of core uncoating [127-129]. Therefore, the presence of intact CPXV cores in the cytoplasm of cells with inhibited proteasome was analyzed. Indeed, using electron microscopy intact viral cores in 72 % of MG-132 treated cells were detected, while only 1 % of cells with non-inhibited proteasome showed clearly intact core structures. Furthermore, VF were present in 77 % of cells with non-inhibited proteasome, while no VF were detected in MG-132-treated cells (**Figure 3.14C**). Both results suggest that CPXV replication is impaired by MG-132 treatment due to prevention of core uncoating. This agrees with the hypothesis of proteasomally degraded core proteins.

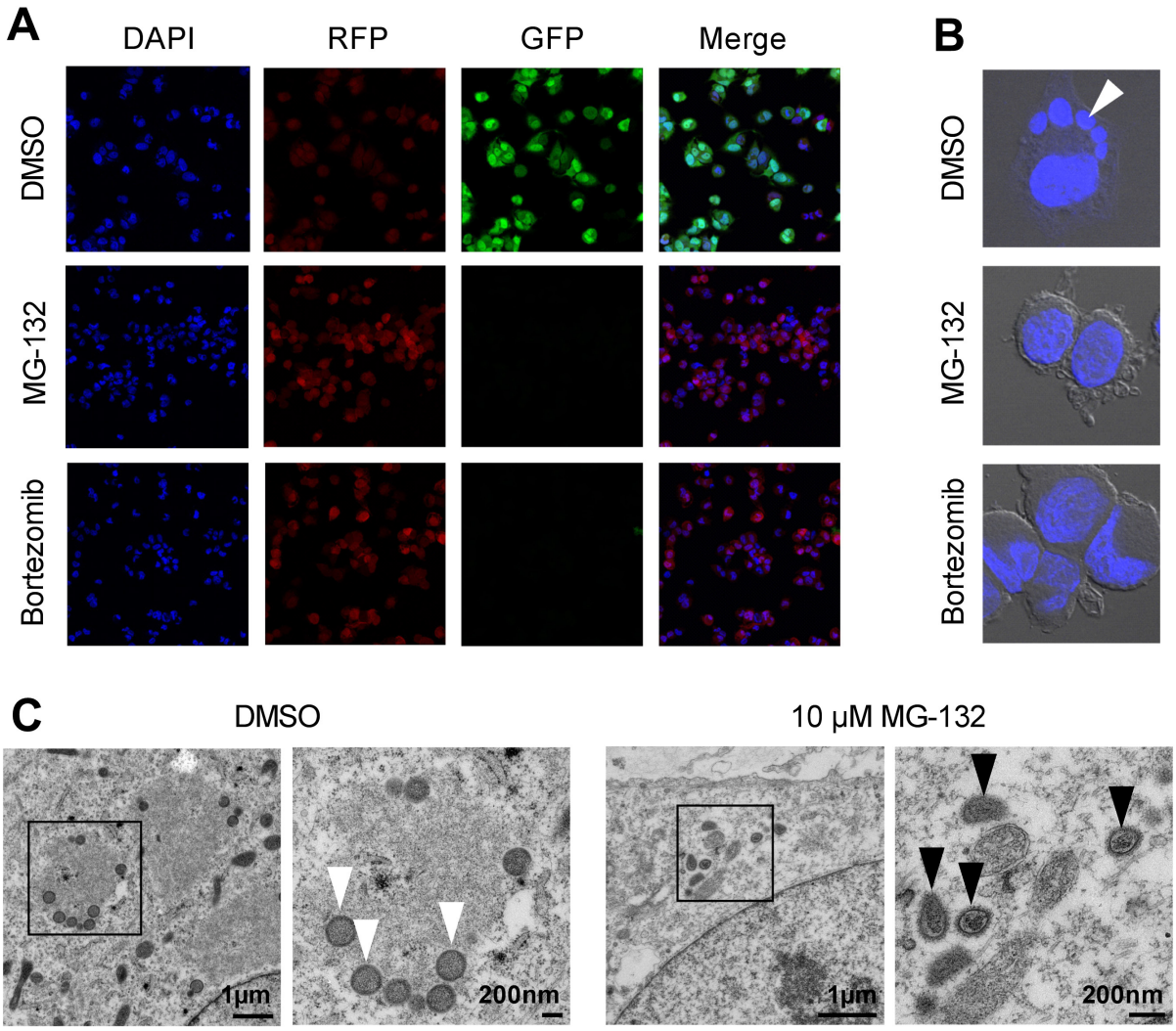

Figure 3.14. Effect of proteasome inhibition on viral protein expression, virus factory formation and uncoating. HeLa cells were infected with CPXV BRFseR expressing RFP under an early viral promotor and GFP under a late viral promotor at an MOI of 5 in the presence or absence of 10 µM MG-132 or 1 µM Bortezomib. After 8 h cells were fixed and stained with DAPI. (**A**) Inhibitor-treated cells show no late viral protein expression while early protein expression is still detectable. RFP fluorescence in control cells is overlaid by GFP fluorescence and hence appears less intense. (**B**) While cells with non-inhibited proteasome (DMSO) display typical virus factories in the cytoplasm (white arrow), these structures were absent in proteasome inhibitor-treated cells. (**C**) HeLa cells were infected with CPXV BRFseR at an MOI of 100 in the presence of 10 µM MG-132 or DMSO and subjected to transmission electron microscopy 4 h p.i. Virus factories and immature virus particles (white arrows) were detected in cells treated with DMSO, while intact cores (black arrows) were regularly found in cells treated with proteasome inhibitor MG-132. Pictures A and B were taken by Annemarie Fritsch [181].

3.2.2. Analysis of the CPXV mature virion ubiquitinome

Although K48-linked ubiquitin was identified in VACV core fractions [129], there is no information available about distinct ubiquitinated proteins in the core fraction that would proof the hypothesis of ubiquitinated structural core proteins. Therefore, the mature virion ubiquitinome of five CPXV strains was analyzed by LC-MS/MS to elucidate the conserved CPXV ubiquitinome. Besides the cell culture-adapted CPXV BR strain, representing the best characterized CPXV, four strains that were isolated between 2007 and 2009 in the Consultant

Laboratory for Poxviruses at the Robert Koch Institute, Germany, were analyzed. These four strains lead to documented zoonotic infections. If the hypothesis of ubiquitinated core proteins is true, ubiquitination sites in corresponding proteins should be identified. For this purpose, CPXV mature virus particles were purified by density gradient ultracentrifugation, lysed and proteins digested with trypsin. Ubiquitinated lysine residues result in diGly(K) remnants at peptides which were enriched via immunoaffinity purification and analyzed by LC-MS/MS.

In total between 656 and 1230 diGly(K) peptides were identified from about 12,000 to 14,500 fragment spectra, depending on the CPXV strain. A mean of about 50 % of all peptides based on peptide area quantification contained at least one ubiquitination site, indicating a successful enrichment of diGly(K) peptides. As expected, the proportion of missed cleavages was greatly increased for peptides with diGly(K) residue since trypsin cleavage is prevented by diGly(K) remnants [183]. Furthermore, it was not surprising that a mean of about 58 % of ubiquitinated peptides based on peptide area quantification originated from ubiquitin itself. From the remaining 42 % of ubiquitinated peptides, viral peptides made up to 34 % while only 8 % originated from the host or contaminants. It is therefore likely that ubiquitin is derived from viral proteins rather than host proteins. The ubiquitin-like proteins ISG15 and NEDD8 also lead to diGly(K) remnants after trypsin digestion [183], but since these peptides together made up less than 0.2 % of all peptide areas, diGly(K) residues were considered to be ubiquitin-specific. Additionally, protein concentrations calculated by TPA were about 0.01-0.05 µmol/g protein for ISG15 and about 0.002-0.003 µmol/g protein for NEDD8 comparing to 0.52-1.23 µmol/g protein for ubiquitin in non-diGly(K) enriched virions.

All possible seven ubiquitin linkages were identified in all five CPXV strains, except K33, which was not identified in the CPXV Hei strain. Quantitative approximation of lysine linkages using peptide areas of linkage-specific ubiquitin peptides revealed K48 as the most abundant ubiquitin linkage in CPXV IMV particles with a mean of 53 % of all ubiquitin linkages. K63 was identified as the second most abundant linkage with a mean portion of 33 % in CPXV mature virions. K11 and K6 represented about 8 % and 4.5 %, respectively, while K27 and K29-linkages represented less than 1 % of total ubiquitin linkages (**Figure 3.15**).

The number of viral ubiquitination sites ranged from 247 in CPXV BR to 668 in CPXV HumGri, which were assigned to 86 to 148 viral proteins. Furthermore, the number of ubiquitination sites correlated with the ubiquitin amount in non-diGly-enriched virus particles (**Table 3.6**), indicating strain-specific differences in the CPXV IMV ubiquitinome.

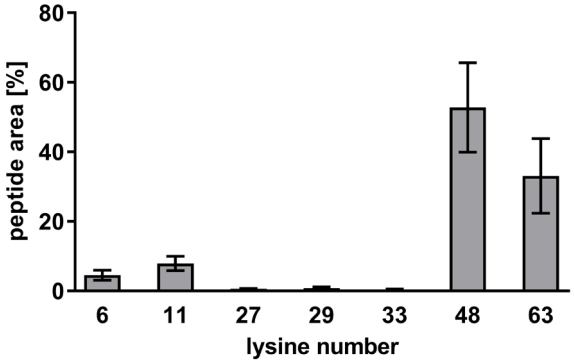

Figure 3.15. Quantification of ubiquitin linkages in CPXV IMV particles. Ubiquitin linkages were quantitatively approximated using peptide areas of linkage-specific ubiquitin peptides. Error bars indicate mean ± standard deviation of five CPXV strains in % of total ubiquitin diGly(K) peptide area.

Table 3.6. Ubiquitin amount, viral ubiquitination sites and associated viral proteins.

CPXV strain	Ubiquitin [µmol/g protein][a]	Number of viral diGly(K) sites	Number of viral diGly(K) proteins
BR	0.52	247	86
Kre	0.57	403	117
Hei	0.52	476	127
Ber	0.61	487	131
Gri	1.23	668	148

[a] Amount in non-diGly(K)-enriched virion preparations calculated by total protein approach (TPA) [180]

The conserved CPXV mature viron ubiquitinome

The identification of conserved ubiquitination sites among the five analyzed CPXV strains was of major interest since these sites might be functionally more important than non-conserved ones. In total 137 conserved ubiquitination sites were identified, considering also homologous lysine residues of proteins with sequence difference between strains (**Table 3.7** and **Table S3**). These sites were assigned to 54 CPXV proteins, all belonging to the conserved CPXV mature virion proteome except A36R [88]. Assuming 152 viral proteins in CPXV mature virion particles [88], it was shown that at least 35 % of CPXV mature virion proteins are ubiquitinated at conserved lysine residues. Another eleven viral proteins contained ubiquitination sites in all five CPXV strains, but no conserved lysine residues were identified (**Table S4**).

More than half of the 54 viral proteins with conserved ubiquitination sites contained one or two diGly(K) sites, while other proteins showed up to ten ubiquitination sites (**Figure 3.16A**). As expected, proteins with conserved diGly(K) sites tended to be essential for virus replication (59.5 %) and conserved in OPV (70.4 %). In addition, most viral proteins with conserved ubiquitination sites belonged to the function host-virus interaction and transcription, but also proteins belonging to the core were identified (**Figure 3.16B**).

Table 3.7. CPXV mature virion proteins with conserved ubiquitination sites.

Protein CPXV[a]	Gene VACV[b]	DiGly(K) sites[c]	Protein description
A11	129	10	Major core protein 4a precursor
A14	132	2	Virion membrane protein
A17	136	1	Virion membrane protein
A19	138	1	Transcript termination protein
A1	119	1	Viral late gene transcription factor 2
A23	142	1	DNA Holliday junction resolvase
A24	143	4	Intermediate transcription factor 3 large subunit
A25	144	1	DNA-directed RNA polymerase 133 kDa polypeptide
A26	148	5	A-type inclusion protein
A28	150	1	14 kDa cell fusion protein
A30	152	1	DNA-directed RNA polymerase 35 kDa subunit
A35	157	1	EEV glycoprotein
A36	158	1	Inhibitor of MHC class II antigen presentation
A44	167	6	Profilin
A4	122	6	Major core protein 4b
A50	173	1	Uncharacterized protein
A52	175	1	Uncharacterized protein
A53	176	1	DNA ligase
A6	124	1	DNA-directed RNA polymerase 19 kDa subunit
A7	125	7	Uncharacterized protein
A8	126	1	Early transcription factor 82 kDa subunit
B2	184	1	Putative uncharacterized protein
B4	187	1	EEV type-I membrane glycoprotein
C17	025	1	Complement control protein
C3	199	2	Uncharacterized protein
C8	013	2	Interleukin 18-binding protein
D12	002	3	TNF alpha receptor-like protein
E13	118	6	Scaffold protein
E5	110	2	Primase D5/uncoating factor
F3	059	1	Double-stranded RNA-binding protein
F4	060	1	DNA-directed RNA polymerase 30 kDa polypeptide
F6	062	2	Uncharacterized protein
F8	064	2	Membrane protein, ass. with IV/IMV and core
G13	052	3	Envelope protein
G17	056	3	LB phosphoprotein
H10	087	1	Myristoylated protein
H1	078	6	Metalloendopeptidase
H2	079	2	Entry/fusion complex component protein
H3	080	1	Late transcription elongation factor
H4	081	3	Glutaredoxin-2
H5	082	1	Putative nuclease
H8	085	5	Assembly protein
J1	099	6	Tyr/ser protein phosphatase
J3	101	5	IMV heparin-binding surface protein
L1	070	6	Telomere-binding protein
L7	076	1	Viral core cysteine proteinase
M1	032	2	Interferon antagonist
N1	088	1	Myristylated IMV virion protein
N3	090	1	IMV protein
N4	091	6	Core protein VP8
O1	095	1	Cap-specific mRNA (nucleoside-2'-O-)-methyltransferase
O4	098	1	DNA-directed RNA polymerase 147 kDa polypeptide
Q1	028	2	Inhibitor of TNF-R and TLR signaling
S1	093	2	Virion protein

[a] According to CPXV GRI-90
[b] According to VACV WR
[c] Number of conserved ubiquitination sites in five analyzed CPXV strains

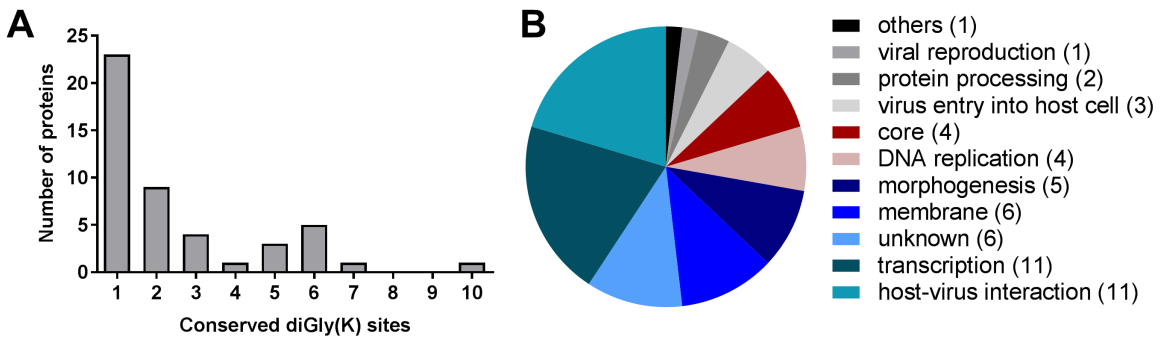

Figure 3.16. CPXV proteins with conserved ubiquitination sites grouped by number and function. Ubiquitination sites identified in all five analyzed CPXV strains were considered as conserved and (**A**) grouped by number of diGly(K) sites or (**B**) by function. Numbers in parenthesis represent numbers of associated proteins.

In the following, ubiquitinated CPXV core proteins are depicted in more detail, because their identification was a major objective of the analysis. Although viral proteins of the core are not defined in detail, they are known to include A11, A4, A5, N4 and A7 [184-186]. These proteins, except A7, are also found at high copy numbers comparable to those of membrane proteins in CPXV mature virions suggesting a structural role [88]. The A7 protein is assigned to unknown function since the function has not been elucidated yet. But A7 and N4 are known to locate inside the core, while A11, A4 and A5 are part of the outer core structure making them likely targets for ubiquitination according to the hypothesis [184,186]. The major core protein A11 contained the greatest number of ubiquitination sites among all proteins identified with ten conserved diGly(K) sites and a mean of 20 diGly(K) sites considering also non-conserved sites. Additionally, the major core protein A4 contained six conserved diGly(K) sites ranking third-highest in the number of conserved ubiquitination sites. The A5 protein was not grouped to the proteins with conserved ubiquitin sites because no site could be detected in the CPXV BR strain, but all other CPXV strains showed at least one ubiquitination site in the A5 protein. Although N4 and A7 are not part of the outer core structure, they contained six and seven conserved ubiquitination sites, respectively, demonstrating that ubiquitination of core proteins is not restricted to the outer part of the core. This data clearly confirmed the extensive ubiquitination of CPXV major core proteins. Consistent with the prevalent K48-ubiquitin linkage found in CPXV virions this supported the hypothesis of proteasomally degraded core proteins which was analyzed in 3.2.3.

3.2.3. UPS-dependent degradation of viral proteins early in infection

As multiple ubiquitination sites in CPXV core proteins were elucidated, the next aim was to show their proteasome-dependent degradation. For this purpose, an MS-based quantitative analysis of ubiquitinated peptides in CPXV-infected HeLa cells in the presence or absence of MG-132 early in infection was done. Control and inhibitor-treated samples were prepared in triplicate, which clustered together in hierarchical clustering and PCA (**Figure 3.17A,B**). Statistical analysis revealed significant abundance differences of ubiquitinated peptides in cells with with non-inhibited versus inhibited proteasome. These peptides belonged to 54 different viral proteins, whereby most viral peptides were stabilized in the presence of proteasome inhibitor (**Figure 3.17C**). Stabilization of proteins as a result of proteasome inhibition implies that these proteins are degraded by an active proteasome. Controversially, one peptide of the viral RhoA signaling inhibitor G11 protein was identified to be degraded by the proteasome while two peptides of G11 where identified as not being degraded. Peptides of all other viral proteins showed clear tendencies for either degradation or not. Functional categorization of CPXV proteins degraded by the proteasome early in infection revealed mostly proteins of unknown function (37 %), followed by proteins associated with host-virus interaction (26 %), transcription (16 %) and DNA replication (11 %) while the residual proteins (10 %) had diverse functions. Although proteins with the functional annotation host-virus interaction and transcription were also abundant among CPXV proteins with conserved ubiquitination sites, only few correlations between viral proteins degraded by the proteasome and conserved ubiquitination sites were observed.

According to the hypothesis, ubiquitinated peptides of CPXV major structural core proteins were expected to accumulate upon proteasome inhibition, but surprisingly the opposite was observed. Major core proteins A11 and A4 were unchanged or even less ubiquitinated when the proteasome was inhibited disproving their direct proteasomal degradation upon core release into the cytoplasm. The core protein A5 was not identified in this experiment which is consistent with the fact that no ubiquitination sites on A5 were identified in the virion ubiquitinome analysis of CPXV BR strain that was used in this experiment.

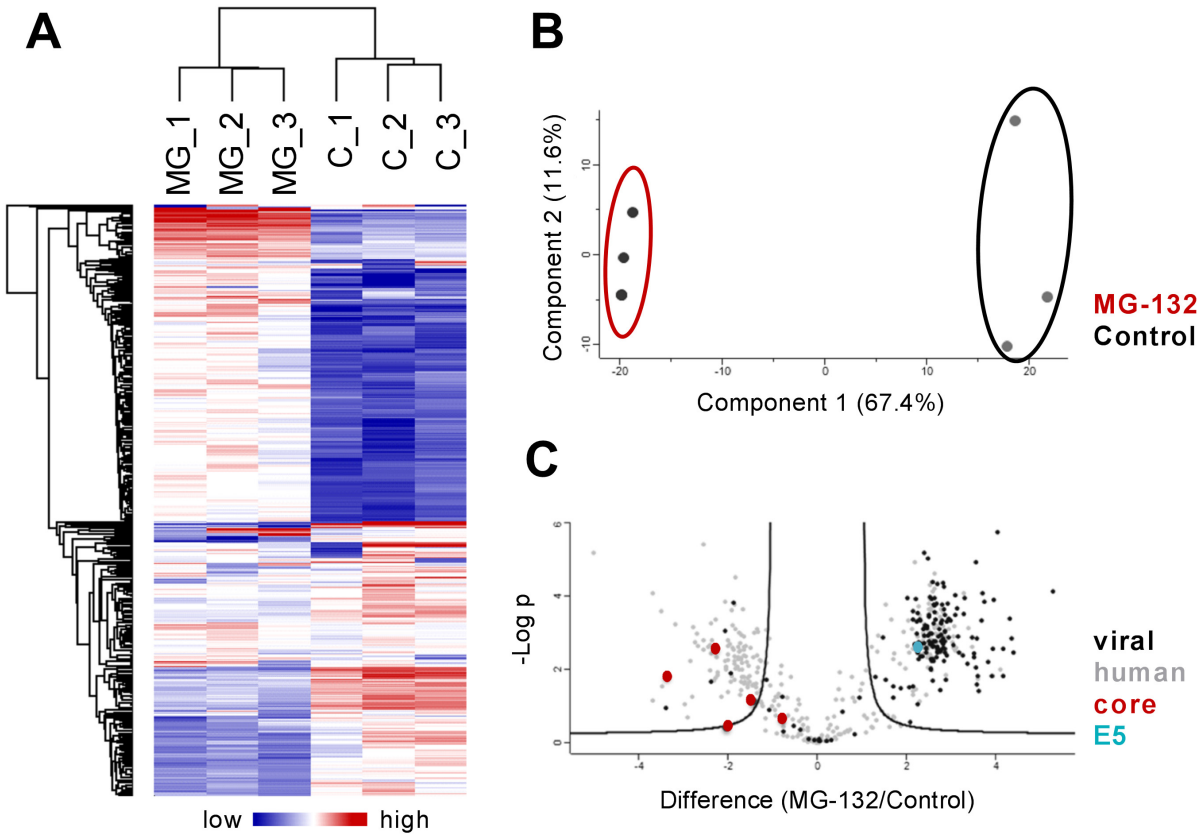

Figure 3.17. Proteasome-dependent degradation of ubiquitinated peptides early in infection. HeLa cells were infected in triplicate with CPXV BR at an MOI of 50 in the presence or absence of 10 µM MG-132. After 2 h p.i. ubiquitinated peptides were analyzed by MS. Plots show normalized ubiquitinated peptide areas. (**A**) Hierarchical cluster analysis reveals ubiquitinated peptides which are more abundant upon proteasome inhibition (samples MG_1-3) compared to cells with non-inhibited proteasome (samples C_1-3), indicating their proteasomal degradation. (**B**) Inhibitor-treated samples (red) can clearly be separated from control samples (black) using principal component analysis. (**C**) Volcano plot showing significant differences (t-test, 5 % permutation-based FDR) in the amount of ubiquitinated peptides. Most viral peptides (black) are degraded in a proteasome-dependent manner, but not the major core proteins A11 and A4 (red). E5: uncoating factor.

Result summary: Role of ubiquitination in CPXV infection

- Proteasome inhibition impairs CPXV core uncoating
- ➔ Ubiquitin is essential for CPXV replication
- Conserved CPXV ubiquitinome: 137 sites in 54 viral proteins identified
- Structural core proteins are highly ubiquitinated, but not proteasomally degraded

3.3. Transcript incorporation in CPXV IMV particles

To test the hypothesis of transcript incorporation in CPXV virions, a protocol using NGS was established. To minimize transcripts outside of virions, IMV particles were highly purified by CsCl gradient centrifugation. Purity and integrity of virions derived from the protocol had been previously confirmed by negative staining TEM (**Figure 3.18**).

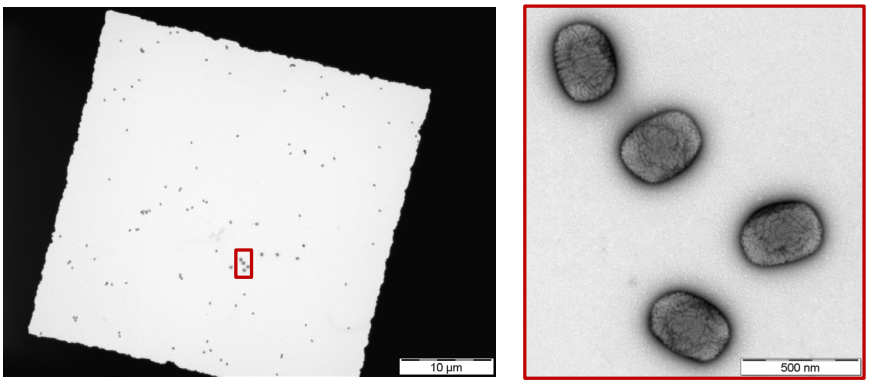

Figure 3.18. Analysis of virion purity and integrity by electron microscopy. Exemplary pictures of CsCl-purified CPXV BR stock (HEp-2-adapted). No protein clouds were detectable outside of virions and particles appeared fully intact.

Possible residual RNA outside of virus particles was digested with RNase in a first step, which was confirmed by spike-in standard during method establishment as described in section 2.10.8. Furthermore, it was confirmed by spike-in standard that the DNase digestion step after RNA extraction did not result in RNA loss.

Transcripts outside of virus particles may also be ribosome-associated rather than free ones. Although ribosomes may also be incorporated in virus particles, ribosome-associated transcripts outside of virions may be less accessible to RNase and hence a protease digestion was tested prior to RNase digestion. Additionally, the RNase digestion was omitted to estimate digestion efficiency and amount of transcripts outside of virions. In principle three protocols were compared:

(I) RNase digestion,
(II) no RNase digestion,
(III) protease and RNase digestion prior to RNA extraction.

Control samples containing buffer without virus particles were carried along during the whole sample preparation, including virion purification, to exclude contaminant RNA. The three mentioned protocols were applied for the analysis of transcripts incorporated in CPXV BR adapted to HEp-2 or Rat-2 cells to elucidate possible adaptation-related transcript incorporation.

As co-purification of ribosomes could not be excluded, the ribosomal content in purified CPXV IMV preparations was approximated on proteome level using TPA [179,180]. The cytoplasmic 80S ribosome is composed of 80 proteins [187] from which 48 were quantified with LFQ in CsCl purified CPXV stocks. After calculation of these 48 ribosomal protein concentrations separately for each single protein, concentrations were averaged over the mean resulting in an 80S ribosomal content of 2.9 and 3.1 nmol/g total protein in HEp-2- and Rat-2-adapted CPXV preparations, respectively. For comparison, ubiquitin was determined to be present at 273 and 810 nmol/g total protein. Moreover, assuming a protein content of 50 μg/10^8 IMV virions (empirical value) the number of 80S ribosomes per virus particle was estimated to be about 870 and 930 in the two CPXV BR preparations. To evaluate the calculated ribosome amounts, the number of virus particles per cell and the number of ribosomes present in a single cell were considered. Poxviruses produce between 10^3 and 10^4 virus particles per cell [188]. With about 3.3×10^6 ribosomes present in a single HeLa cell (uninfected) [189] and the fact that ribosome expression is not increased during poxvirus infection [190] this resulted in an average of 330 to 3,300 ribosomes per virus particle. As the calculated ribosome number of about 900 ribosomes per virus particle is exactly in that range, it can be stated that CsCl-purified CPXV preparations still contained large amounts of ribosomes. Not only proteins belonging to the 80S cytoplasmic ribosome, but also proteins of the 55S mitochondrial (mt) ribosome were found in the virus preparations, but at lesser extend and only quantifiably in the HEp-2-adapted CPXV sample with about 0.15 nmol/g. Nevertheless, it remained unclear whether ribosomal proteins identified in purified CPXV preparations originate from intact ribosomes in the preparations or were separate proteins that arise during cell lysis, resulting in their co-purification.

Data overview

Samples showed a maximum coverage of the virus genome of up to 118,673. In contrast, controls showed only a maximum coverage of up to 188. This observation was conclusive, since control samples contained buffer without virus particles. Instead, controls displayed a considerable number of host reads. As some virus genes may share homology to host genes, multiple mapping of reads to the host and the virus genome was analyzed. A maximum of nine reads was identified which mapped to both the viral and the according host genome (**Table 3.8**). Therefore, multiple mapping reads were considered to be negligible.

Table 3.8. Overview of reads mapping to virus and host genome.

Sample	Protocol[a]	Viral reads	Host reads	Mean genome coverage[b]	Maximum coverage[c]	Multiple mapping[d]
CPXV BR,	I	3.3E+05	6.4E+05	201.4	25,172	4
HEp-2	II	1.0E+05	1.1E+06	49.9	7,134	4
adapted	III	2.6E+05	5.7E+05	141.6	17,081	1
CPXV BR,	I	8.4E+05	4.7E+04	489.3	118,673	0
Rat-2	II	6.7E+05	3.6E+05	578.6	114,124	1
adapted	III	6.3E+05	1.4E+05	504.7	106,390	0
Control	I	7.1E+03	4.1E+05	3.6	188	2
HEp-2	II	1.5E+03	2.6E+05	0.6	51	0
adapted	III	6.5E+03	2.8E+05	2.7	121	9
Control	I	5.5E+02	9.2E+03	0.4	51	0
Rat-2	II	8.3E+02	3.4E+04	0.6	118	1
adapted	III	5.4E+02	2.4E+04	0.4	79	0

[a] I: RNase digestion; II: no RNase digestion; III: protease and RNase digestion
[b] Across viral genome
[c] Of viral genome
[d] Reads mapping to virus and host genome

Up to about 4,500 and 2,600 genes were identified in HEp-2- and Rat-2-adapted virions, respectively, including viral and host genes. However, most genes displayed very low read counts. Hence, to define a gene as a transcript hit, the cutoff for each sample was set in a way that hits included the top 90 % of normalized read counts (**Figure 3.19**). This resulted in seven to 27 transcripts in HEp-2-adapted CPXV and 10 to 22 transcripts in Rat-2-adapted CPXV (**Table 3.9**).

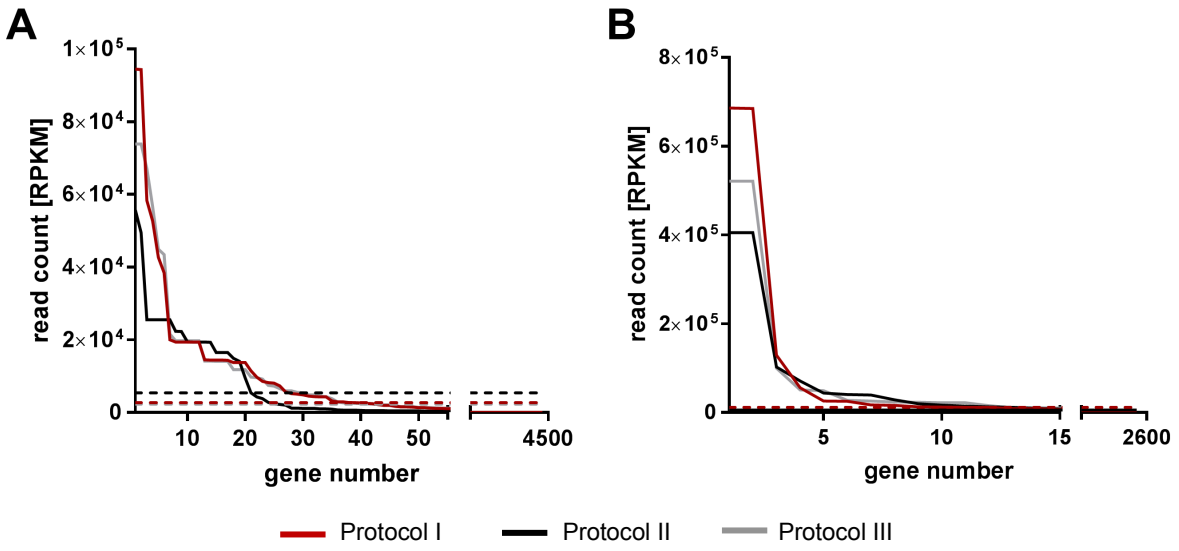

Figure 3.19. Read distribution in samples analyzed for virion-incorporated transcripts. Highly pure CPXV IMV particles adapted to (**A**) HEp-2 or (**B**) Rat-2 cells were analyzed for transcripts by next-generation sequencing. Reads mapping to the virus and the host (human or rat) were sorted by read count (RPKM: reads per kilobase million). The cutoff was set in a way that transcript reads contained the top 90 % of all reads in each sample. Three different protocols were applied for sample preparation: I: RNase digestion, II: no RNase digestion, III: protease and RNase digestion. Dashed lines: cutoff.

Table 3.9. Viral and host transcripts identified in CPXV ranked by normalized read count.

Rank	HEp_I	HEp_II	HEp_III	Rat_I	Rat_II	Rat_III
1	D5L/I1R	18S rRNA	D5L/I1R	D5L/I1R	D5L/I1R	D5L/I1R
2	18S rRNA	28S rRNA	18S rRNA	B8R	mt 12S rRNA	B8R
3	28S rRNA	mt 12S rRNA	28S rRNA	B13R	18S rRNA	18S rRNA
4	B8R	mt 16S rRNA	mt 16S rRNA	C14L	B8R	B13R
5	mt 16S rRNA	D5L/I1R	B8R	C10L	mt 16S rRNA	mt 12S rRNA
6	C10L	C10L	mt 12S rRNA	J5R	B13R	C10L
7	mt 12S rRNA	B8R	C10L	D1L/I5R	002/228[a]	C14L
8	D10L		D10L	18S rRNA	C10L	mt 16S rRNA
9	F3L		002/228[a]	M1L	J5R	J5R
10	D1L/I5R		F3L	A36R	C14L	D1L/I5R
11	002/228[a]		C8L		D1L/I5R	002/228[a]
12	C8L		D1L/I5R		ND1	D10L
13	B13R		C14L		28S rRNA	M1L
14	C14L		B13R		COX3	ND1
15	J5R		C6L		D10L	A36R
16	F4L		F4L		ATP6	C8L
17	C6L		D6L		COX1	COX3
18	D6L		MIR6087		B2R	F3L
19	A36R		J5R		M1L	P2L
20	A34R		A36R		F3L	
21	MIR6087		A34R		C8L	
22	P2L		P2L		A36R	
23	A47R		C13L			
24	B12R		M1L			
25			B10R			
26			A47R			
27			D8L			

I: RNase digestion, II: no RNase digestion, III: protease and RNase digestion
Redundant genes were summarized. Grey: host transcripts; red: ribosomal RNA (mt: mitochondrial)
Viral gene names (non-colored) according to CPXV GRI-90
[a] Gene name according to CPXV BR (no homologous gene in CPXV GRI-90)

Influence of RNase and protease digestion

RNase digestion was performed to remove RNA outside of virions. Hence, transcripts outside of virions should display higher read counts when the RNase digestion is omitted. Generally, omitting the RNase digestion resulted in higher ranking of rRNA, indicating rRNA outside of virions. Cytoplasmic rRNA from human and rat cannot be distinguished, because of sequence identity. In contrast, mt rRNA displays only 79 % identity for 12S and 16S rRNA among human and rat (analyzed by comparing sequences with BLAST). Hence, rat mt rRNA amounts should not be influenced by contaminating human rRNA. Rat mtRNA clealy decreased in rank upon RNase digestion demonstrating mtRNA outside of virions. In the Rat-2-adapted virus preparation using protocol I no mt rRNA was even identified above the cutoff. Summarized, exclusively host transcripts increased in rank upon omitting RNase digestion, while no viral transcript increased in rank (**Table 3.9**). This indicated that viral transcripts are incorporated in virus particles rather than associated outside.

Protease digestion possibly increases ribosome-associated transcript accessibility to RNase digestion outside of virons. Hence, ribosome-associated transcripts outside of virions should decrease in rank compared to sample preparation without prior protease treatment (protocol I) or even be no longer identified as transcript. However, transcript identifications with protease digestion included all identifications of transcripts without protease digestion or even more identifications. The only exception was B12R in HEp-2-adapted CPXV (**Table 3.9**).

3.3.1. Incorporation of viral transcripts

At first sight, the viral genome coverage of each sample showed conspicuous coverage peaks. Additionally, viral genome alignments frequently contained sequences without any aligned reads, verifying the absence of viral genome contamination in preparations (**Figure 3.20**).

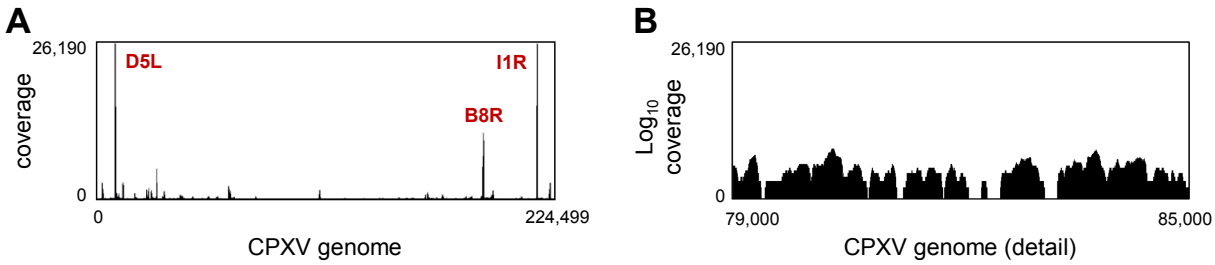

Figure 3.20. Exemplary transcript coverage over CPXV genome. Transcripts were analyzed in highly pure CPXV IMV particles using NGS. (**A**) Multiple genes show exceptionally high coverage (red: genes with highest coverage), (**B**) while some regions displayed no mapping reads at all. Coverage is shown exemplary for HEp-2 protocol I, but the coverage distribution was similar for all samples.

Sequences with increased coverage mapped remarkably well to viral CDS. Moreover, the coverage increase was not restricted to annotated CDS but was also found before and after the respective CDS. This observation made sense in that transcripts were analyzed whose sequence may generally differ from the translated protein sequence (CDS) as a result of untranslated regions at the 3' and 5' ends.

Transcripts identified in at least two sample preparations were considered for further analysis, resulting in 18 and 13 viral transcripts in HEp-2- and Rat-2-adapted virions, respectively. Moreover, twelve viral transcript identifications were shared in CPXV particles adapted to either human or rat cells (**Table 3.10**). The D5L/I1R gene, located in one copy at each end of the genome, displayed by far the highest coverage followed by the B8R gene (**Figure 3.20**). This was observed in all samples independent of the host. However, the rank of some viral genes differed in human and rat-adapted virions, e.g. B8R ranked third-highest in Rat-2-adapted virons, while it ranked at the top eight or ten in HEp-2-adapted virions (**Table 3.9**).

Table 3.10. Viral transcripts identified in CPXV IMV particles.

Gene	Description[a]	Function	Host[b]	Expression[c]
none	Uncharacterized protein	Unknown	H/R	Unknown
D5L/I1R	Inhibitor host DNA-PK[d]	Immune evasion	H/R	Unknown
D6L	Uncharacterized protein	Unknown	H	Unknown
D10L	Uncharacterized protein	Unknown	H/R	Unknown
C6L	Uncharacterized protein	Unknown	H	Early
C8L	Interleukin 18-binding	Immune evasion	H/R	Early
C10L	Uncharacterized protein	Unknown	H/R	Early
C14L	Uncharacterized protein	Unknown	H/R	Early
P2L	Uncharacterized protein	Unknown	H	Early
M1L	IFN antagonist, host range	Immune evasion	R	Early
F3L	dsRNA-binding, host range	Immune evasion	H/R	Early
F4L	DNA-directed RNA pol 30 kDa	Transcription	H	Early
J5R	Viral late transcription factor 4	Transcription	H/R	Early
A34	EEV glycoprotein	Entry	H	Early
A36R	Inhibitor MHC class II antigen presentation	Immune evasion	H/R	Early
A47R	3β-Hydroxysteroid-dehydrogenase/ Δ^{5-4}-isomerase	Immune evasion	H	Early
B8R	Uncharacterized protein	Unknown	H/R	Intermediate
B13R	Inhibitor of host NF-κB	Immune evasion	H/R	Early
D1L/I5R	Secreted chemokine-binding	Immune evasion	H/R	Early

[a] According to UniProt
[b] H: HEp-2; R:Rat-2
[c] According to [119]
[d] According to [191]

Most identified viral transcripts were of unknown function, but interestingly seven transcripts encoded proteins with immunomodulatory function, including two host range proteins. Furthermore, six transcripts were identified exclusively in HEp-2-adapted virions, while one was exclusively identified in Rat-2-adapted virions, which was the IFN-antagonistic host range protein M1 (**Table 3.10**).

Moreover, all identified transcripts, except B8R, belonged to the early class of viral genes. Early OPV promoters have been predicted to contain the consensus promotor sequence AAAA---TGAAAA---A [192]. Moreover, OPV early genes contain the general functional terminator sequence NTTTTTNT [193]. Most OPV transcripts contain a single termination signal. However, some transcripts may contain multiple termination signals, which may also be skipped as a result of secondary structures [192]. Transcript reads were expected to localize between promoter and terminator sequence. The read distribution, however, was not expected to be completely uniform over transcript length due to method-induced bias, e.g. it is known that non-random binding of random hexamer primers used for cDNA amplification prior to sequencing leads to depleted read counts at the 5' and 3' end [194].

Early viral promoter sequences have been predicted for VACV [192] and were found in nine of the viral transcripts identified. These transcripts included the CDS C8L, C10L, M1L, F3L, F4L,

J5R, A34R, A36R and D1L/I5R. Also terminator sequences were identified near these transcript 3' ends. Hence, these genes were used to verify the presence of intact transcripts. The observed coverage fitted remarkably well to the predicted transcript size limited by promoter and terminator sequence. Moreover, coverage distributions showed the expected read depletion at the ends, but, mostly also a tendency to 3' bias, meaning higher coverage towards the mRNA 3' end (**Figure 3.21**).

In **Figure 3.21** the coverage of F3L, F4L, A34R, D1L and CDS 228 is exemplary shown. The coverage of adjacent F3L and F4L showed a clear decrease in between both sequences, indicating separate transcripts. This was underlined by separate promoter and terminator sequences for each transcript. In contrast, D1L/I5R and CDS 228 did not show any coverage decrease in between transcripts, but rather a continuously increased coverage. The promoter of CDS 228 is not predicted [192] and a termination sequence in between both transcripts was absent, suggesting a continuous transcription of both CDS.

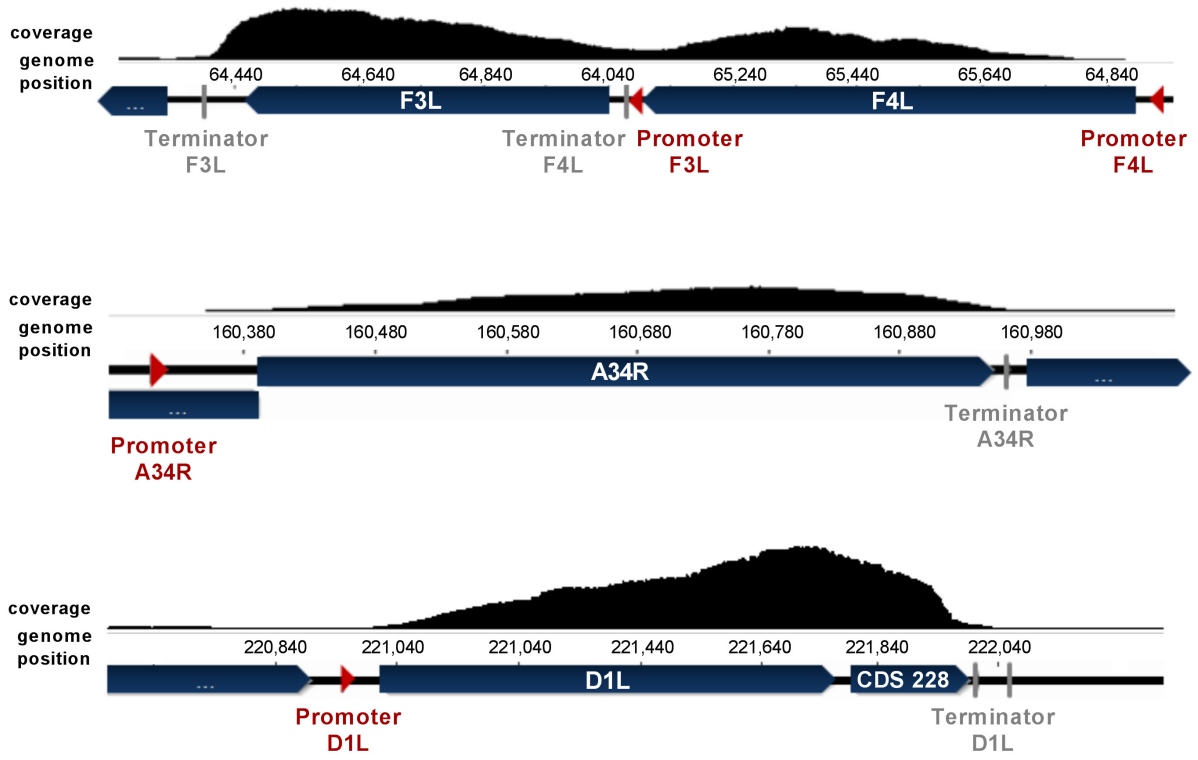

Figure 3.21. Coverage of viral transcripts between predicted promoter and terminator sequence. The coverage of genes clearly correlates with the predicted promoter [192] and terminator [193] sequences. Pictures exemplary show the coverage in the HEp-2-adapted CPXV preparation using protocol I.

3.3.2. Incorporation of host transcripts

The highest amounts of host transcripts in the samples were cytoplasmic 18 and 28S rRNA, but also large amounts of mt 12 and 16S rRNA were found in virion preparations (**Table 3.9**). Furthermore, mt transcripts were identified in Rat-2 samples (ND1, COX1, COX3 and ATP6). In HEp-2 samples these mt transcripts ranked also rather high, but, however, were not included in the cutoff. The identification of mt transcripts may indicate that whole mtDNA or even polycistronic mtRNA was purified during sample preparation. As tRNA genes are distributed throughout the mtDNA one would expect to identify according reads. However, only few tRNA reads were identified, although tRNAs were annotated in the databases. Hence, it could be excluded that whole mtDNA or even polycistronic mtRNA was purified.

HEp-2 samples contained a transcript encoding a predicted microRNA (miRNA 6087) of unknown function. However, as this miRNA was also identified as high-ranking in the control samples, it was considered to be a contaminant rather than a virus-incorporated transcript.

Result summary: transcript incorporation in CPXV particles

Viral:

- Identification of full-length viral transcripts
- Transcripts mostly of immunomodulatory function or uncharacterized
- Highest incorporation rates of D5L/I1R
  (D5L/I1R: inhibitor of host cytoplasmic DNA sensing)

Host:

- Ribosomal RNA (cytoplasmic and mitochondrial)

3.4. Analysis of a heterogeneous CPXV population

3.4.1. NGS-based analysis of a heterogeneous CPXV population during passaging

To analyze the hypothesis of selection of pre-existing variants as CPXV adaptation mechanism, a heterogeneous virus population was simulated. Although multiple mutations during passaging of a CPXV crust were detected that point to a selection of variants, this mechanism can only be elucidated if pre-existing genomic variants are known. Therefore, five CPXV strains were mixed at equal PFU and passaged in duplicates in HEp-2 and Rat-2 cells and the strain ratio of the non-passaged and passaged mix was determined by NGS. Prior to NGS results, the plaque morphology of the original strains without mixing was compared to the non-passaged and passaged virus mix. All CPXV strains showed homogeneous intra-strain plaque morphology, while the virus mix displayed clearly different plaque morphologies, representing those of individual strains (**Figure S3**). Note that one replicate could only be passaged four times in Rat-2 cells, because virus amounts were too low for infection of the next passage.

NGS results were analyzed by least ordinary square method (see section 2.11.2). Mixing five CPXV strains equally, one would expect a portion of about 20 % of each strain in the mix. However, strain portions ranged from about 9 % up to about 29 % in the non-passaged mix (**Table 3.11**). This discrepancy to the hypothetical mix ratio may result at least partially from mixing of PFU, which does not resemble the number of virions, but the number of infectious particles.

Table 3.11. CPXV strain ratios in a simulated heterogeneous virus population.

	BR	Ber	Kre	Hei	Gri
CPXV Mix[a]	25.5	24.7	12.4	8.8	28.6
HEp-2, P5_I	37.6	31.3	13.8	16.2	1.2
HEp-2, P5_II	35.8	32.5	13.8	16.4	1.6
Difference HEp-2[b]	11.2	7.2	1.4	7.5	27.2
Rat-2, P5	31.3	41.2	14.9	11.6	1.1
Rat-2, P4	33.6	39.1	14.3	12.2	0.8
Difference Rat-2[b]	7.9	15.5	2.2	3.1	27.7

[a] Mix of 5 CPXV strains (equal PFU); P: passage number
[b] Difference between mix and mean of passages

Strain ratios of passaged replicates were reproducible and also the replicate passaged only four times in Rat-2 cells did not differ in the strain portions from the replicate passaged one more time. This indicated that changes in the strain mix ratio appeared prior to the fifth passage. Differences between HEp-2 and Rat-2-passaged ratios were overall low (< 5 % mean difference), except the Ber strain, which was more prevalent after passaging in Rat-2 than in HEp-2 cells. The portion of virus strains changed in a range between 1.4 % and 15.5 % during passaging, except the Gri strain, which changed by more than 27 % during passaging in both cell lines. Notably, the CPXV

Gri strain nearly disappeared during passaging in both cell lines, although it started with the highest ratio in the initial mix (**Table 3.11**). The disappearance of the Gri strain during passaging was further investigated using RTCA.

3.4.2. Real-time cell analysis of different CPXV strains

The five CPXV strains used for the simulation of a heterogeneous CPXV population were analyzed by RTCA to elucidate strain-specific differences. Therefore, HEp-2 and Rat-2 cells were infected at low (0.1), medium (1) and high (5) MOI. The order of cell detachment was reproducible for each cell line independently of the MOI, except Rat-2 cells at high MOI. Strikingly, the slowest cell detachment was observed using the Gri strain, independent of the MOI and cell line (**Figure 3.22**).

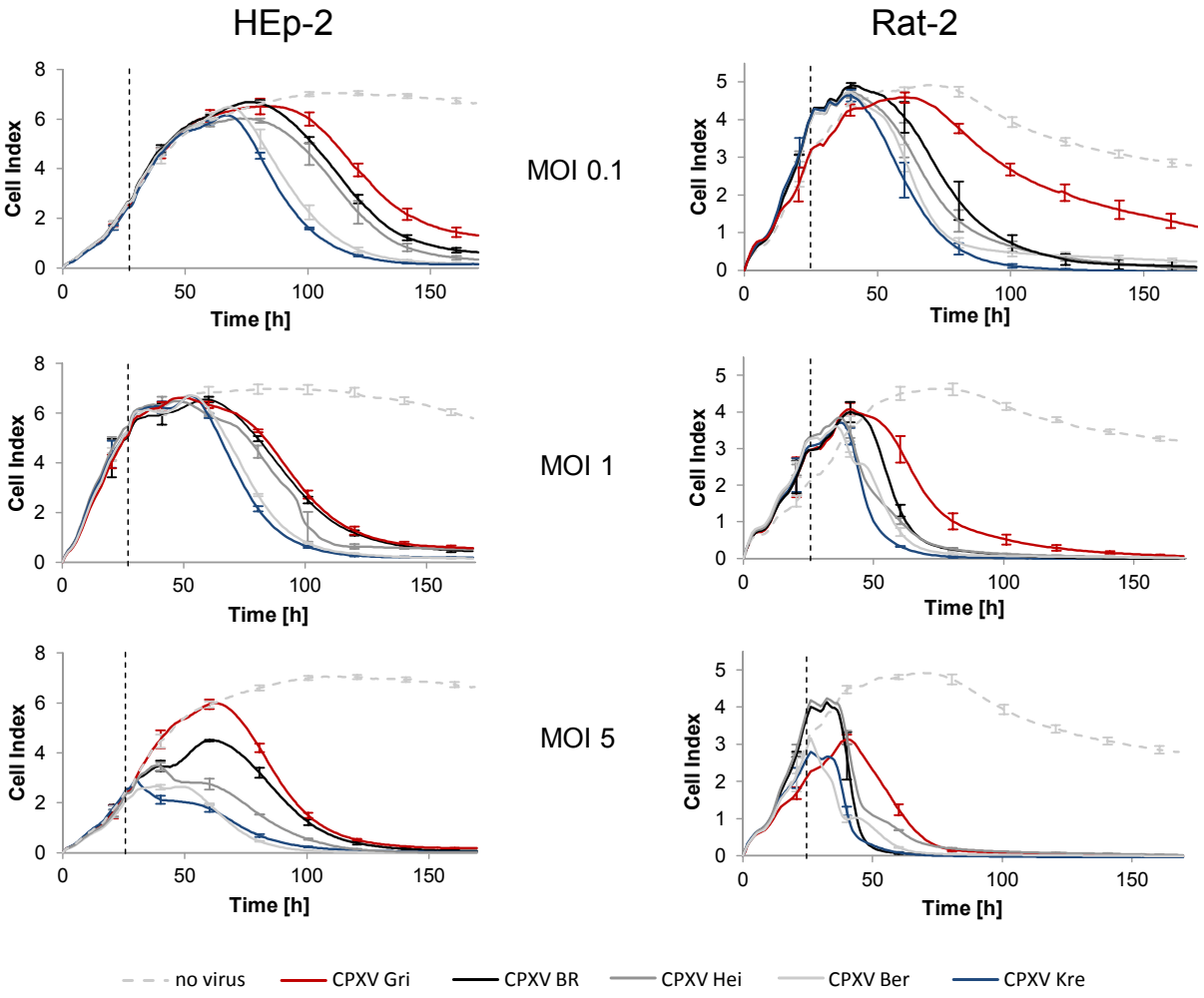

Figure 3.22. Real-time cell analysis of five different CPXV strains. HEp-2 or Rat-2 cells were seeded in 96-well E-plates and the cell adherence was monitored using the xCELLigence RTCA system. After about 24 h cells were infected with five different CPXV strains (Kre, Hei, BR, Ber and Gri) at different MOIs, as indicated by the vertical dashed line. Error bars indicate mean ± standard deviation of one experiment performed at least in triplicate.

Since cell adherence correlates with cell viability, a decreasing CI may be interpreted as cell death. Hence, the results indicated more viable cells upon infection with the Gri strain compared to the other four strains, what correlated with the near disappearance of CPXV Gri in a heterogeneous virus population. This may be due to an overall slower entry of the Gri strain, a slower replication or an overall lesser virulence, resulting from strain-specific sequence differences.

3.4.3. Sequence differences in the CPXV GRI strain

Decreasing amounts of CPXV Gri during passaging in a strain mix and slower cell death associated with CPXV Gri infection may result from strain-specific proteomic sequence differences. Hence, amino acid sequences of CPXV Br, Ber, Kre and Hei were compared to Gri using the Gene Heatmap Plugin in Geneious. CDS 003-012 and CDS 222-227 were not included in the analysis because of partially incomplete sequence information at the ends of the viral genomes. From 206 compared CDS, seven showed at least 5 % amino acid difference between the Gri strain and all other strains (**Table 3.12**). Besides four uncharacterized proteins (B10, C14, C2 and Q2), these proteins included one protein associated with immune evasion (Q1), one virion membrane protein (A10) and, moreover, one protein of the entry-fusion complex (A29). As A29 is essential for poxvirus entry [195], it may by hypothesized that the entry of the CPXV GRI strain is altered compared to the other CPXV strains leading to the observed strain-specific differences.

Table 3.12. Protein differences in CPXV Gri.[a]

Protein name	Description
A10	Virion membrane protein
A29	Envelope protein
B10	Uncharacterized protein
C14	Uncharacterized protein
C2	Uncharacterized protein
Q1	Inhibitor of TNF-R and TLR signaling
Q2	Uncharacterized, Alpha-amanitin target

[a] Proteins with at least 5 % amino acid difference between CPXV Gri and CPXV Hei, Kre, Ber and BR

Result summary: passaging of a heterogeneous CPXV population

- Selection of pre-existing variants confirmed as potential CPXV adaptation mechanism
- Disappearance of CPXV Gri strain during passaging
  - correlates with slower cell death of CPXV Gri-infected cells
  - possibly results from altered viral entry due to sequence differences in A29 (A29: viral protein of the entry-fusion complex)

4. Discussion

Cell culture passaging is the gold standard for virus isolation and propagation in research, diagnostics and vaccine production [6,14]. VACV was the first virus grown *in vitro* [11] and its adaptation to cell culture has already been observed in the 1960s reporting initially poor virus growth that improved during passaging [17,196]. At that time the observed adaptation was thought to result from a selection of pre-existing genomic variants [196]. However, by now it is known that this is only one possible adaptation mechanism of OPV. There are diverse studies verifying the adaptive potential of poxviruses in cell culture on genomic level by *de novo* mutations and gene expansion. However, these studies used already cell culture-adapted viruses like VACV [34], extensive cell culture passaging, e.g. more than 500 passages for modified vaccinia virus Ankara (MVA) [197], or applied artificial selection pressure to distinct genes by knockdown of complementary genes [57]. Therefore, prior to the conducted study, it remained elusive how OPV particles adapt to cell culture right after isolation from a natural host without selective pressure by gene knockout. As for research purposes commonly less than five passages are used to isolate and propagate the virus for further analyses, these first passages are of special interest. It is known that extensive cell culture passaging leads to altered or even attenuated viruses, like MVA [197], but changes of virus particles during early passages have been hardly investigated.

In the present study, modern -omics techniques were applied to analyze the adaptation of CPXV in cell culture during the first five passages, resulting in the first ever comparative proteome analysis of *in vivo* isolated virus particles before and after propagation in cell lines. Moreover, methods were established to analyze ubiquitination sites in virion proteins and ubiquitinated proteins during infection, providing the groundwork to elucidate the role of ubiquitin for poxvirus adaptation. Additionally, the hypothesis of transcript incorporation in poxvirus particles and the selection of pre-existing variants were analyzed. In the following, proteins are named according to CPXV GRI-90, although the cited studies might refer to VACV homologs.

4.1. Changes of CPXV identified by *in vitro* characteristics

Poxvirus adaptation in cell culture may be primarily observed by differences in CPE or virus yield. These changes may be detected by standard methods, e.g. plaque assay or qPCR, which are commonly performed during virus isolation in cell culture.

In this study, CPXV particles were isolated from a rat crust and passaged five times in a human and a rat cell line. Passaging resulted in increased viral fitness in human cells, but not in rat cells (**Figure 3.2**), suggesting an adaptation of CPXV to human cells. As rat cells are closer related to the host organism from which CPXV were isolated, a lesser degree of adaptation to these cells seems plausible. Although CPE appearance did not change during passaging in both cell lines, a

CPE was visible two days earlier in rat cells compared to human cells (**Figure 3.1**). Additionally, an overall lesser degree of rat cell adherence compared to human cells was observed in RTCA (**Figure 3.3**), which may be partially responsible for the faster detachment of rat cells. However, passaged virions did not differ in infection kinetics. As infection kinetics based on measurement of cell attachment to the surface, it makes sense that results agree with CPE observation, which revealed no differences. However, inhomogeneous courses of the non-passaged crust isolate were observed in infection kinetics, what is discussed in section 4.4. Taken together, from the standard virus isolation perspective **using CPE observation and yield determination one would infer an adaptation of CPXV IMV particles during passaging in human, but not in rat cells**.

4.2. Genomic adaptation of CPXV in cell culture

Genomic adaptation of OPV may occur by *de novo* mutations, CNV [57] or recombination events [143]. Furthermore, one may argue that DNA modifications may lead to poxvirus adaptation. But as poxvirus DNA is not methylated [198], DNA modification as a mechanism underlying adaptation can be excluded. CNV was not detected during passaging of CPXV particles in HEp-2 and Rat-2 cells. Moreover, recombination events could not be detected since low variant frequencies made it unfeasible to distinguish between *de novo* mutations and recombination events. Although minor variants, including *de novo* mutations, were identified at low frequencies during passaging in both cell lines, **the present study confirms the overall CPXV genome stability during cell culture passaging**.

Most minor variants were identified in virions passaged in both cell lines. Although mutations identified in both cell lines were for the most part not detected in the same passage, this indicated **a common underlying cell-type independent mechanism, which may temporally differ among cell lines** (**Figure 3.5**).

Concerning the analysis of minor variants, it should be noted, however, that errors can occur during sequencing, which may result in false positive variant identification:

- The most frequently observed errors in Illumina sequencing are substitutions [199] with base-call error rates of about 0.1-0.01 [200]. These tend to accumulate at the end of the read, because residual chemicals accumulate during the sequencing process.
- Strand bias of base-call errors may be observed, meaning sequencing errors occurring only in reads in a single direction [201]. Base-call errors are of major concern when working with low coverage [202], which was not the case in the conducted experiment. Moreover, strand bias in the variant analysis was controlled by p-value.
- Systematic errors have been observed among different Illumina platforms, showing reproducible motif error sites, which are hypothesized to result from modified ddNTPs, especially ddGTP, and the engineered Pol used for sequencing [201,202].

- Bias may be also introduced prior to sequencing by PCR amplification and transposome-based fragmentation [201,203].

With two exceptions, variants were not detected in every passage. Some variants were only identified in a single passage, while others appeared in multiple passages (**Figure 3.5**). The latter observation may be due to low frequencies (< 5 %), which may be in some passages below the cutoff of 1 % variant frequency. In contrast, the missing of variants with higher frequencies (up to about 17 %) in some passages cannot be explained therewith. These may result from an artificial selection process during passaging, because very limited virus amounts (only a few µL) were used for infection of a new passage. Nevertheless, as variants re-emerge during passaging, it may be concluded that **the appearance of minor variants during CPXV passaging is a rather frequent event**.

Strikingly, variants were primarily found in tandem repeats. These so-called microsatellites can be found throughout the whole poxvirus genome making up about 24 % of the sequence [204]. Early stop mutations were found to be accumulated in chordopoxvirus microsatellites, leading to the hypothesis of microsatellite hypervariability as a major source of poxvirus genome variability and hence as a source of poxvirus adaptation [204]. In this study it is shown for the first time that **hypervariability in microsatellites presumably is a CPXV adaptation mechanism in cell culture**.

4.2.1 Mutations in transcription-related genes

CDS-localized mutations were preferably found in transcription-related genes, indicating major importance (**Table 3.2**). This seems conclusive, because poxviruses replicate in the cytoplasm of the host cell, and hence need to encode their own transcription machinery, which may adapt to the host. However, variant frequencies of transcription-associated genes were rather low (≤ 3 %), except a single substitution in the A25R gene, which displayed up to 11.4 % variant frequency in virions passaged in human cells (**Table 3.3**). This Lys90Thr substitution in the RNA Pol gene A25R was the only variant accumulating in frequency during passaging. The OPV DNA-directed RNA Pol is composed of eight subunits, which partially display similarity to the eukaryotic Pol [205,206]. Also the second largest subunit encoded by A25R displays homology to the eukaryotic RNA Pol [148]. Mutations in the A25R gene during OPV cell culture passaging have already been described in the literature [133,141,207], as explained in the following.

A25R mutations have been associated with isatin-β-thiosemicarbazone (IBT) resistance or reduced IBT sensitivity [141,207-209]. IBT treatment leads to an abortive infection, presumably by increasing RNA processivity by either inhibiting transcription termination or stimulating elongation, but the detailed mechanism is still unknown [141,210].

Cone [133] and Brennan and colleagues [141] observed VACV A25R mutations in cell culture while applying selective pressure to different Protein kinase R (PKR) inhibitors. PKR is an IFN-stimulated gene (ISG) and functions as antiviral sensor protein of the host cell which detects viral dsRNA leading to phosphorylation of the eukaryotic translation initiation factor eIF2α which in turn leads to translational shutdown. Although poxviruses are DNA viruses and, hence, do not replicate via dsRNA intermediate, dsRNA is a known pathogen-associated molecular pattern (PAMP) that has also been detected in poxvirus [211] and other DNA virus-infected cells [212]. DsRNA during poxvirus infection originates from complementary viral gene products activating PKR [213]. Hence, it is no surprise that poxviruses, like diverse other DNA viruses, encode PKR antagonists [214]. Established CPXV PKR antagonists are the proteins M3 and F3 [215,216]. It has been reported that passaging of a F3L knockout mutant leads to gene expansion of M3L which goes along with an adaptive mutation in the A25R gene. Although this mutation reduced dsRNA level, it however also activated PKR [133]. Furthermore, it has been shown that introduction of a rhesus CMV-derived PKR antagonist (rhtrs1) in a M3L/F3L double-knockout strain leads to either gene expansion of rhtrs1 or to mutations in A25R or A36R gene, both of which improving replication during cell culture passaging [141].

In the present study no gene expansions during CPXV passaging were detected, possibly because no artificial selection pressure was applied. Anyway, the literature data suggests that mutations in the A25R gene are related to transcription elongation and PKR antagonism [210]. Hence, the accumulation of the Lys90Thr variant during passaging of a CPXV crust isolate in cell culture may be related to altered transcription, although the detected mutation does not agree with mutations reported in the literature [133,141,207,209]. Nevertheless, it can be stated that **the OPV RNA Pol second largest subunit is a major target of mutations**. It has been shown that ubiquitination of a lysine residue at an unknown position in the second largest RNA Pol subunit in eukaryotes alters the subunit composition of the RNA Pol holoenzyme [217]. This additionally underlines the hypothesis that **the Lys90Thr substitution in A25 may be related to transcriptional activity of the RNA Pol**. In the analysis of the conserved CPXV IMV ubiquitinome in this study up to twelve ubiquitination sites were identified in A25. However, no modification was identified at K90, which does not exclude the ubiquitination at this position.

It may be speculated whether the Lys90Thr variant, observed at the highest frequency in the fifth passage in human cells, may be responsible for increased viral fitness in this passage. One may argue that this mutation was also observed in rat passaged virions, which did not show increased viral fitness. However, frequency in rat passaged virions was lower, and effects may also be host-dependent. Additionally, another mutation in a gene associated with transcription elongation was identified exclusively in the fifth passage in human cells. This gene encodes the positive late

transcription elongation factor H3 [218]. Hence, **the increased viral fitness during passaging in human cells may be a combination of A25 and H3 mutations**.

4.2.2. Mutations in the ATI gene

The largest number of variants was identified in the A26L gene encoding the A-type inclusion protein (**Table 3.2**). Minor variants with up to 5 % frequency were detected in the crust and in the passaged virions. A-type inclusion bodies (ATIs) are proteinaceous cytoplasmic inclusions which are suspected to protect IMV particles from the environment, e.g. UV light [219]. ATIs consist of the A26 protein and are found in some, but not all, OPV, e.g. VACV and VARV encode a truncated ati gene while the CPXV Hei strain used in this study encodes a full-length ati gene. Additionally to the A26 protein, the A27 (p4c) protein is necessary to direct IMV particles into ATIs [220]. From the genome sequence it can be deduced that the used CPXV strain encodes a truncated version of the A27 protein and hence is not capable of embedding IMVs in ATIs. However, deletion of the ati gene in a CPXV strain encoding also a full-length A27 was reported to result in enhanced virulence in mice [221]. Moreover, both the A26 and A27 protein have been shown to contribute to the strain-specificity of IMV host cell entry [222]. VACV strains encoding both genes necessary for ATI formation enter the host cell via endocytosis, while knockout of either gene results in activation of the plasma fusion entry pathway [222]. Therefore, mutations in the A26 gene may play a role in the entry process of virions, but no detailed mechanism is known. However, **as variant frequencies of A26L mutations did not increase during passaging, an adaptive role of A26 seems unlikely**.

4.3. Adaptation of the CPXV mature virion proteome in cell culture

Apart from minor variants, CPXV genomes were remarkably stable during passaging, suggesting adaptation may take place on proteome rather than on genome level. Hence, global proteomic changes of CPXV IMV particles during passaging were analyzed. This analysis revealed a single viral protein that changed in an adaptation-associated manner in both cell lines (**Figure 3.8A**), while 15 and eight proteins were exclusively altered in virions passaged in human and rat cells, respectively (**Figure 3.8B,C**). **For the first time, it could be shown that poxvirus adaptation takes place on virion proteome level.** Viral proteins that changed upon switch from crust to cell culture and, moreover, changes of viral and host proteins during passaging were identified. Viral proteins displaying adaptation-associated changes can be functionally categorized into proteins associated with attachment/entry, immune evasion and proteins with other functions (**Table 3.4**), which is discussed in the following.

4.3.1. Adaptation of cell attachment and entry

OPV enter the host cell either by fusion with the plasma membrane or internalization by endocytosis [222]. OPV entry has been shown to differ in a species- and strain-specific manner and cell culture passaging has been suggested to contribute to the entry adaptation process [222-224]. Moreover, strain-specific differences in the attachment of VACV have been reported [224]. Therefore, viral proteins involved in attachment and cell entry represent possible targets of adaptation. During CPXV crust passaging in different cell lines, the abundance of a single membrane-associated viral protein (G13) changed in a cell line-independent manner (**Figure 3.8A**). Two membrane-associated proteins (E8 and E13) changed upon the first passage in human cells and, additionally, the amount of the membrane-associated A34 protein changed during passaging in HEp-2 cells (**Figure 3.8C**). Moreover, the amount of membrane-associated B4 protein increased upon passaging in rat cells (**Figure 3.8B**). These abundance changes suggest an extensive adaptation of CPXV membrane proteins during cell culture passaging.

G13 is the most abundant viral envelope component in EEV particles and target of the anti-poxvirus drug ST-246 [225]. Although purified IMV particles were analyzed and the co-purification of EEV particles seemed unlikely, because of their unstable outer membrane [226], it has been shown that EEV proteins, like A34, G13 and B4, can be detected even in highly pure CPXV IMV preparations [88]. G13 plays a role in wrapping of IMV to produce EEV particles [225]. Moreover, G13-knockout mutants result in severe attenuation in mice [227]. In cell culture, deletion of G13 has been shown to result in smaller plaque size [227]. However, the role of increased G13 amounts in IMV particles passaged in HEp-2 and Rat-2 cells remains elusive.

Interestingly, changes in A34 and B4 protein amounts were detected during cell culture passaging. A34 in combination with A37 is required to repulse superinfecting virions. The A34/A37 complex localizes on the surface of infected cells and induces actin tail formation upon contact with new virions containing the B4 protein, which repels virions to uninfected cells (**Figure 4.1**) [228,229]. This mechanism allows a four times faster virus spread than the replication cycle would permit. Moreover, an early expression of A34 and A37 is required for effective virus spread and normal plaque formation cell culture [228].

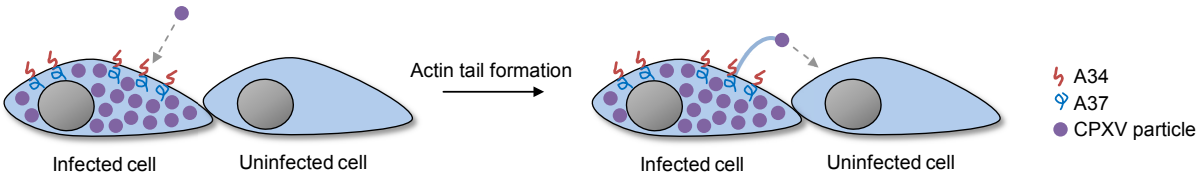

Figure 4.1. Prevention of superinfection by actin tail formation. Contact of new virions with the A34/A37 complex at the surface of infected cells induces actin tail formation, repelling virions towards uninfected cells. Modified from [228].

Increased amounts of B4 and A34 in passaged virions may indicate an enhanced capacity for repulsing virions from already infected cells. Incorporation of these proteins in virus particles would enable a repulsion of virions right after infection, even before early viral protein expression. While A34 amounts increased in virions during passaging in HEp-2 cells, B4 amounts increased in virions passaged in rat cells upon infection of the first passage. This hypothesis may be underlined by the observation of an increased plaque size during passaging (**Figure 4.2**). However, as an increase in plaque size was observed in both cell lines, it may be hypothesized that **increased virus spread may be a general mechanism underlying CPXV adaptation in cell culture**.

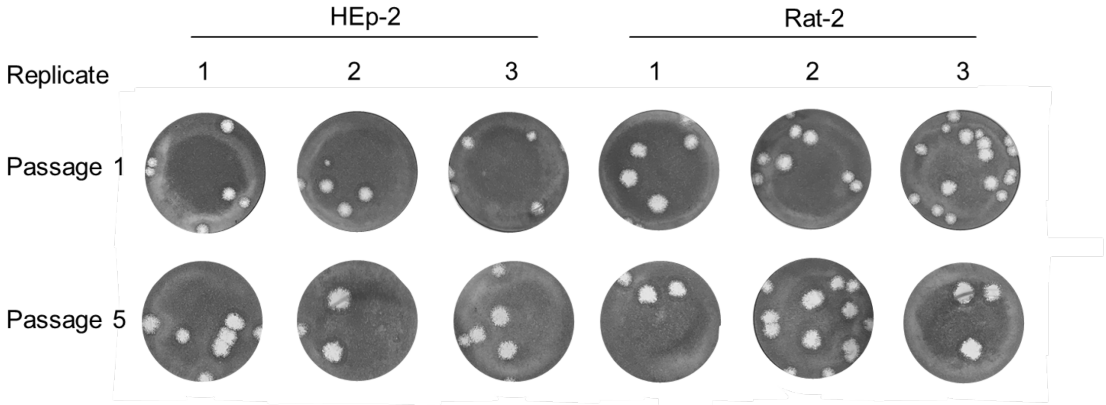

Figure 4.2 Increase of plaque size during passaging of CPXV isolated from a rat crust.

Controversially, the fifths passage in xCELLigence-based RTCA did not show any differences compared to the other passages. As the system measures cell adherence, which depends on CPE, one would expect to observe changes upon faster cell spread. Nevertheless, the difference between plaque assay and RTCA is that using plaque assay secondary infections are prevented by addition of CMC. This is not the case during RTCA. Here, virus particles can diffuse through the medium and infect cells far away in the well, which may compensate the virus repulsion during plaque assay.

Furthermore, ubiquitination sites were identified in three viral membrane proteins (**Table 3.5**). The amount of ubiquitinated IMV membrane protein E8 increased upon passaging in HEp-2 cells in an adaptation-associated manner (**Figure 3.11A**), which correlated with a general increase of E8 in HEp-2-passaged virions (**Figure 3.8C**). These results suggest that **adaptation of CPXV in cell culture may take place on ubiquitinome level.** However, only seven ubiquitination sites in virus proteins were detected in the passaging experiment. Because of limited sample material it was not feasible to perform an enrichment of ubiquitinated peptides. Thus, to verify that ubiquitin is a major poxvirus modification, the ubiquitinome of the CPXV IMV virion was analyzed, which is discussed in section 4.6. In the context of membrane protein ubiquitination, six membrane-associated CPXV mature virion proteins were identified that contain conserved ubiquitination sites (**Figure 3.16B**), underlining the importance of OPV membrane protein ubiquitination.

4.3.2. Adaptation of viral immunomodulatory proteins

Upon viral infection, pathogen-associated molecular patterns are recognized by cellular pattern-recognition receptors, like toll-like receptors (TLRs), which are part of the innate immune system. Recognition activates transcription factors, e.g. NF-κB and interferon regulatory factors (IRFs) leading to expression of antiviral gene products such as type I IFNs, pro-inflammatory cytokines and chemokines. These in turn induce the inflammation response [230]. As shown in **Table 1.1**, CPXV are remarkably complex viruses, encoding diverse proteins to evade the host immune system. Immunomodulatory proteins that changed during CPXV passaging can be grouped into different pathways which they interfere with, as explained in the following.

Inhibition of NF-κB activation

NF-κB is a key transcription factor during inflammation, whose activation is prevented by diverse poxvirus proteins [231]. The CPXV Q1 protein inhibits NF-κB and IRF-3 activation, although the mechanism remains unclear [232,233]. Hence, Q1 is considered to be an inhibitor of TLR signaling. Moreover, proinflammatory cytokine secretion from primary monocytes is inhibited in the presence of Q1 [234], and Q1 deletion results in attenuation in mice, demonstrating Q1 is a poxvirus virulence factor [235]. While in Rat-2-passaged virions Q1 amounts increased upon the first passage, Q1 amounts were continuously increasing during passaging in HEp-2 cells (**Figure 3.8B,C**). Hence, it may be hypothesized that increased amounts of Q1 reduce NF-κB activation *in vitro*. Furthermore, in the passaging experiment, Q1 ubiquitination at lysine number 70 was identified. This site was confirmed to be a conserved ubiquitination site among different CPXV strains indicating a conserved function. The amount of ubiquitinated Q1 changed during cell culture passaging in HEp-2-passaged virions in an adaptation-associated manner. Therefore, **CPXV mature virion adaptation presumably takes place by changes in protein composition and, moreover, by changes in the amount of ubiquitinated proteins**.

Adaptation to the IFN pathway

Type I IFN induction represents the first line of antiviral host defense and viruses of diverse families have developed strategies to evade these mechanisms [236]. CPXV encode diverse proteins to evade the type I IFN antiviral system. Briefly, these viral proteins include a soluble type I IFN receptor (B17), a protein inhibiting IFN signal transduction (J1) and multiple proteins antagonizing IFN-stimulated genes (C13, F3, M1, M3).

The amount of B17 in HEp-2-passaged virus particles continuously increased during passaging while amounts in Rat-2-passaged virions remained unchanged (**Figure 3.8C**). The soluble IFN-α/β receptor B17 possesses a remarkably broad capacity of binding and inhibiting type I IFN from different species, e.g. human, rat, mouse, bovine and rabbit [237]. While VACV encoding B17 is able to suppress IFN-α in mice, infection with a B17 deficient strain induces type I

interferon antiviral response [238]. Knockout of the type I IFN receptor in mice has been shown to result in drastically increased VACV replication [239] demonstrating that suppression of type I IFN is crucial for OPV infection *in vivo*. Additionally, replication of a VACV B17 knockout mutant is reduced in cell culture in the presence of IFN, showing that B17 is also advantageous for OPV replication *in vitro* [240]. Hence, it may be hypothesized that increased amounts of viral IFN-antagonizing protein B17 represent an adaptation to IFN in cell culture.

Besides viral proteins antagonizing the type I IFN pathway, CPXV encode the B7 protein, which specifically blocks the type II IFN pathway activated by IFN-γ. As part of the innate immune response, IFN-γ is primarily secreted from natural killer and natural killer T cells [241]. B7 is a soluble IFN-γ receptor which is able to bind and inhibit human, rat and bovine IFN-γ [242]. Passaging of a CPXV crust isolate in rat cells resulted in a decrease of virion-associated B7 amounts (**Figure 3.8B**). In contrast, B7 amounts virions passaged in human cells did not change in an adaptation-related manner. The HEp-2 and Rat-2 cell lines used in the present study are IFN-competent, meaning that they produce IFNs upon infection [243-245]. Hence, **it may be hypothesized that altered amounts of viral IFN-antagonizing proteins represent an adaptation of OPV to IFN in cell culture**.

Adaptation to inflammation

Inflammation may be induced by the complement cascade or proinflammatory cytokines like CC chemokines. C17 is a complement-binding protein, which increased continuously during passaging in human cells (**Figure 3.8C**). It is a virulence factor *in vivo* which interferes with innate and adaptive immune system components [246,247]. However, the role of C17 in cell culture remains elusive. Like C17, D1/I5 amounts increased in virions during passaging in human cells. The D1/I5 protein is a chemokine-binding protein, which is secreted from infected cells to inhibit CC chemokine-mediated immune cell activation [248]. Moreover, it is a virulence factor *in vivo* [249].

Summarized, four immunomodulatory proteins, which are virulence factors *in vivo* (B17, C17, D1/I5 and Q1), increased in abundance in virons passaged in human cells (**Figure 4.3**). OPV IMV particles seem proteomically rather dynamic, as indicated by numerous viral proteins that significantly changed during passaging. However, most of these proteins were not correlated with hypothesized adaptation-associated courses and, hence, do not represent a stable adaptation. Observed adaptation-associated changes may represent a specific adaptation process to cell culture, but they may also represent a rather general adaptation program of OPV. The latter hypothesis implies that observed changes may not necessarily be advantageous in cell culture, e.g. immune cells are absent and hence adaptation to the inflammation response is not conclusive. However, from the evolutionary point of view, viruses adapt *in vivo*. Therefore, it makes sense

that **CPXV adaptation is presumably organized in a way that will enhance replication *in vivo***. Nevertheless, as *in vivo* virulence factors have also been shown to enhance virulence *in vitro*, adaptation of these factors may be beneficial for CPXV replication in cell culture.

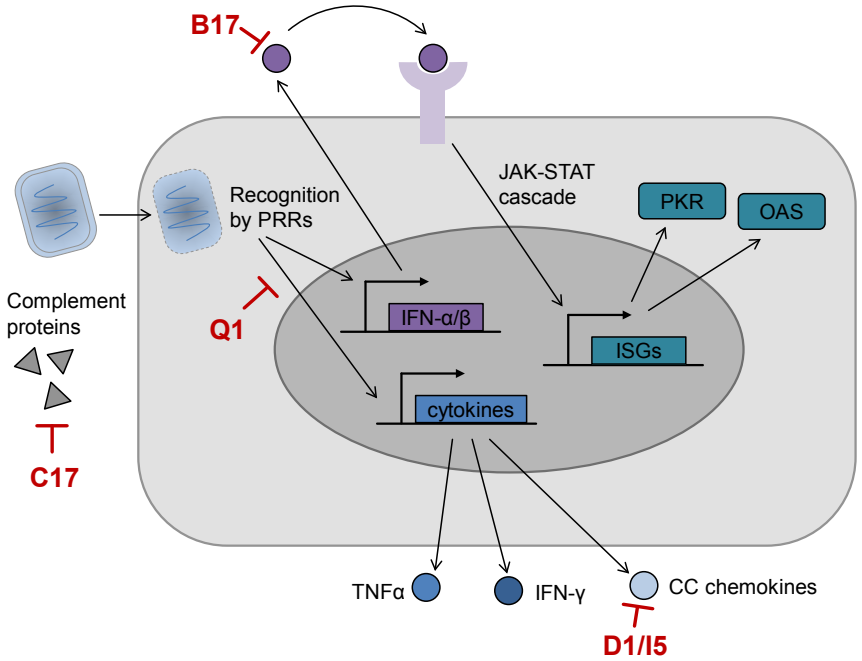

Figure 4.3. Adaptation of CPXV immune modulators during passaging in HEp-2 cells. Simplified presentation showing CPXV immune modulatory proteins with significantly increasing amounts during passaging in HEp-2 cells. PRR: pattern recognition receptor; IFN: Interferon; ISG: Interferon-stimulated gene; PKR: protein kinase R; OAS: 2′-5′ oligoadenylate synthetase; TNF: Tumor necrosis factor

4.3.3. Adaptation of viral proteins associated with other functions

Besides viral proteins proteins associated with attachment/entry and immune evasion, proteins associated with other functions changed in cell culture-passaged virions:

- The A48 protein encodes a protein with partial sequence homology to the superoxide dismutase. However, no A48 enzymatic superoxide dismutase activity could be detected, because the protein lacks residues, which are important for the according catalytic activity. As A48 does influence neither replication nor virulence [250], the role of this protein during poxvirus cell culture adaptation remains elusive.
- The viral DNA ligase A53 increased in amounts upon passaging in human cells, and also during passaging in rat cells a continuous increase of A53 was observed (**Figure 3.8 B,C**). A53 recruits a host factor, the cellular topoisomerase II to viral replication sites during infection [251]. Although topoisomerase II was identified in purified virions, amounts did not change in an adaption-associated manner.
- As described in section 1.3.4, CPXV encode diverse proteins involved in DNA repair. Among those proteins, the dUTPase G2 minimizes dUTP incorporation in DNA, converting dUTP to dUMP [252]. Upon passaging in human cells, G2 amounts decreased in virions, coinciding with the fact that G2 deletion does not impact replication *in vitro* [252].

- The oxidoreductase H4 increased during passaging in HEp-2 cells (**Figure 3.8C**). OPV encode their own disulfide bond formation machinery, which is composed of F10, A3 and H4. H4, also known as poxvirus glutaredoxin-2, is the last protein among these three enzymes acting in a cascade-like manner [253]. H4 is known to catalyze the disulfide bonds in viral membrane proteins and, moreover, is suspected to catalyze disulfide bonds in core and LB proteins [254]. Poxviruses encode two glutaredoxin proteins, H4 and R2. While R2 is non-essential for virus replication, H4 plays an essential role during virion assembly [255,256]. Hence, increased amounts of H4 may indicate an enhanced capacity for disulfide bond formation. However, there is no literature available supporting this hypothesis.

4.3.4. Incorporation of host proteins

The incorporation of host proteins in virions is a possible adaptation mechanism. VACV EEV particles have been reported to incorporate host complement control proteins [33,34], but also cytoskeletal proteins and chaperones [257]. Host protein expression is nearly shut down during poxvirus infection by shutting down host mRNA expression. Seven hours p.i. 80-90 % of all mRNAs in VACV-infected cells were found to be of viral origin [258]. Nevertheless, multiple host proteins are associated with a role during OPV infection and may be constantly expressed, differentially regulated or redistributed during infection (**Table 4.1**).

Table 4.1. Host proteins playing a role during OPV infection.

Host protein(s)	Description	Reference
Dinucleotide dehydrogenase 4	Mitochondrial protein involved in ATP generation	[259]
Cyclooxygenase-2	Mitochondrial protein involved in ATP generation	[259]
Heat shock protein 90	Involved in virus growth, associates with VF	[260]
Topoisomerase II	Recruited to VF	[251]
Ubiquitin	Recruited to VF	[132]
Translation initiation complex	Recruited to VF	[261]
Ras GTPase-activating protein-binding protein 1	Involved in transcription of intermediate genes	[114]
Caprin-1	Involved in transcription of intermediate genes	[114]
Heterogeneous nuclear ribonucleoprotein A2/B1	Involved in late viral promoter activation	[115]
RNA binding motif protein 3	Involved in late viral promoter activation	[116]

VF: virus factories

All of the host proteins shown in **Table 4.1**, except Dinucleotide dehydrogenase 4 (ND4) and Cyclooxygenase-2 (COX-2), were identified in the present study.

Because LC-MS/MS is a highly sensitive analytical approach, it is clear that many contaminating proteins are identified, as demonstrated by 3,453 identified host proteins. The number of protein identifications depends on the degree of virion purification. As IMV particles were purified by sucrose gradient centrifugation, they still contain considerable protein amounts associated outside

of virions [91]. Further purification by CsCl gradient was not feasible, because in previous experiments performed for the present study, CsCl purification of IMVs from rat crust resulted in insufficient virion amounts for proteome analysis. To discriminate between contaminant and virion-associated host proteins an enrichment analysis may be done as by Doellinger and colleagues [88]. An enrichment analysis in the present study was not feasible, since no reference values of HEp-2 and Rat-2 protein expression were available. Nevertheless, most host proteins that changed during passaging in an adaptation-related manner in the present experiment (**Figure 3.10**) have been already identified in highly pure OPV IMV preparations [88]. Doellinger and colleagues calculated enrichment values to distinguish between virion-associated host proteins and contaminants [88], which are used to filter the host proteins of the present study for virion-association, resulting in the proteins shown in **Table 4.2**.

Table 4.2. CPXV IMV-associated host proteins that change during passaging.

Gene name	Description	Enrichment IMV[a]
HEp-2		
PFN-1	Profilin-1	35.1
PGK1	Phosphoglycerate kinase 1	12.9
ARF1	ADP-ribosylation factor 1	12.8
PDCD6	Programmed cell death protein 6	7.2
XRCC5	*X-ray repair cross-complementing protein 5*	*6.6*
PRDX6	Peroxiredoxin-6	4.3
ATIC	*Bifunctional purine biosynthesis protein*	*3.7*
ACP1	Acid phosphatase 1	3.3
HSPA8	Heat shock cognate 71 kDa protein	2.4
CAD	*CAD protein*	*2.4*
EIF3B	*Eukaryotic translation initiation factor 3 subunit*	*2.1*
MPG	DNA-3-methyladenine glycosylase	2.0
Rat-2		
Sqstm1	Sequestosome-1	8.3
Dstn	Destrin	7.6
Itpa	*Inosine triphosphate pyrophosphatase*	*4.6*
Phb2	Prohibitin-2	3.4
Psmc5	*26S protease regulatory subunit 8*	*3.4*
Eif3b	*Eukaryotic translation initiation factor 3 subunit B*	*2.1*
Dnajc7	DnaJ homolog subfamily C member 7	2.1
Rab6a	Ras-related protein Rab-6A	2.0

[a] iBAQ ratio OPV IMV/HepG2 ≥ 2 according to [88]
Proteins increasing in amounts during passaging are indicated by italics.

Among the host proteins that were considered to be virion-associated (**Table 4.2**), **EIF3B is the only host protein that changed in an adaptation-associated manner in both cell lines**. EIF3B is the RNA-binding component of the eukaryotic translation initiation factor 3 and part of the

translation initiation complex, which is recruited to VF during OPV infection [261]. Hence, eIF3B may be incorporated in IMV particles during assembly in VF, but its adaptive role for CPXV remains elusive.

Apart from EIF3B, which changed during passaging in both cell lines, eleven proteins changed exclusively in HEp-2-passaged virions (**Table 4.2**). Some of these proteins can be associated with viral infection:

- Virion-incorporated cellular Profilin decreased in amounts during passaging in human cells. OPV encode a viral Profilin protein A44, but in contrast to cellular Profilin, which modulates actin dynamics, poxvirus Profilin rather influences polyphosphoinositides metabolism [262]. One may speculate whether viral Profilin amounts may increase, since cellular Profilin amounts decrease. However, this was not the case.
- ARF1 is involved in the formation of Golgi-coated vesicles. During poxvirus infection, IMV particles are wrapped with trans-Golgi membranes to form IEV particles, but the role of ARF1 for poxvirus infection is unknown [263].
- XRCC5, also known as Ku80, is part of a large cellular DNA repair complex, which functions as pattern recognition receptor for DNA viruses, activating innate immune response. Poxviruses encode a Ku80 antagonistic protein (D5L/I1R), which blocks binding of the Ku80-complex to DNA [191]. Interestingly, increased Ku80 amounts in CPXV particles passaged in human cells correlate with increased viral DNA amounts (**Figure 3.2** and **Figure 3.10**).
- HSPA8, also known as HSC70, is a heat shock protein involved in protein import into the nucleus, mitochondria and the ER, but also plays a role in virus infection, e.g. it interacts with virus proteins, for example Influenza virus protein M1 [264]. However, the role of HSPA8 for OPV infection remains elusive.

The seven host proteins changing exclusively in Rat-2-passaged virions have not been associated with OPV infection in the literature. However, interestingly, a regulatory subunit of the proteasome (Psmc5) increased in abundance during passaging. Although multiple proteasomal subunits have been identified in highly pure CPXV preparations [88] the localization of the proteasome during OPV infection has not been analyzed yet. It has been reported, for example, that proteasomal subunits relocalize during CMV infection and partially are recruited to viral replication centers [265].

Besides the mentioned host proteins, which changed in abundance during passaging, ubiquitin is a host factor, which is essential for OPV [127,128], as discussed in section 4.6. Hence, the incorporation of ubiquitin and ubiquitin-related proteins in CPXV particles may be important. Although the amount of virion-associated ubiquitin changed during cell culture passaging (**Figure 3.11**), no adaptation-associated course was identified. However, the amount of K48-

linked polyubiquitin decreased in virions passaged in human cells, indicating an adaptation. Furthermore, apart from ubiquitin, the conjugation of OPV proteins with SUMO has been reported [266,267]. Biological functions of SUMOylation are diverse including localization, interaction and also proteasomal degradation of target proteins [268]. The amount of SUMO2 decreased during passaging in human cells, but not in an adaptation-associated course.

Technical limitations of shotgun proteomics

Although multiple adaptation-related changes of virus and host proteins were identified during passaging, technical limitations of the applied shotgun proteome analysis combined with LFQ have also to be considered. In shotgun proteome analysis, peptides are analyzed in a data-dependent manner, meaning that the most intense peptides are selected for fragmentation. This in turn means that peptides may be not identified, because they are absent, or because they are present at low abundance, and hence not subjected to fragmentation. Although identifications are transferred across runs by the MBR algorithm implemented in MaxQuant, missing LFQ values are frequently observed. These are replaced from normal distribution, assuming low abundance. Therefore, the absence of a protein from a passage cannot be stated by this experimental design. Moreover, due to the diverse nature, some peptides show higher variation than others [269], e.g. three injections from the same sample results in varying peak areas of the same peptide. Replicates and statistics are therefore of major importance. This implies further that from some proteins smaller variations are detectable than from others. Hence, if statistics reveals no significant change, this may be also due to inherent variation and small fold changes. Benchmarking the MaxLFQ algorithm with E.coli proteins spiked into HeLa lysate has shown that all truly changing proteins can be detected at a ratio ≥ 3. Lowering the ratio to 1.6 still resulted in the identification of 50 % of truly changing proteins at a fixed FDR [177], demonstrating that even small fold changes are detectable with LFQ. Although no fold changes were calculated in the present study, but rather the difference in relation to the mean protein content across samples was calculated, these changes ranged generally between two and four fold, suggesting that all truly changing proteins may be identified. Finally, differences may also be introduced during sample preparation, because, in contrast to other relative quantification methods like stable isotope labeling by amino acids in cell culture (SILAC), samples are prepared and measured completely separate for LFQ.

4.4. CPXV adaptation by selection of pre-existing variants

Selection of pre-existing variants from a heterogeneous virus population is considered to be the main mechanisms underlying RNA virus adaptation [270]. Because of their comparably low mutation rates, DNA viruses are expected to adapt by other mechanisms [271]. However, there are some results indicating that CPXV undergo a selection process during cell culture propagation.

Using RTCA-based infection kinetics, courses of the crust resembling those of passaged virus were detected, but also courses showing significantly faster cell death than passaged virus (**Figure 3.3**). Since gradient purified virions were used for this experiment, the effect of residual factors originating from the rat crust should be negligible. If residual factors were responsible for faster death of cells infected with virus isolated from the crust this is expected to be observed in every replicate. From these results it can be hypothesized that the crust isolate contained a heterogeneous virus population and cell culture passaging may lead to a selection of pre-existing variants. This hypothesis was confirmed by passaging of a simulated heterogeneous population, which clearly demonstrates that distinct genomic variants, simulated by different strains, are selected during cell culture passaging (**Table 3.11**). It has to be noted that genetic recombination was not considered in this analysis.

Differences between virions leading to different courses of the crust in RTCA were of special interest, but virus amounts in the 96-well E-plate used in xCELLigence experiments were too low to purify virions for further genomic or proteomic analysis. Therefore, to analyze the genome sequence of viruses leading to the diverse infection kinetics of the virions from the crust the AmpliSeq technology was applied (data not shown). This technology uses a set of multiple hundreds of primers to amplify a target sequence, in this case the CPXV genome, from crude samples like cell lysates, followed by NGS analysis of amplicons. However, sequence information from NGS was not sufficient to construct whole CPXV genome sequences, likely because the provided primers were originally designed for another CPXV strain (RatKre), which is genomically different from the used Hei strain. Anyway, the A→C transversion at position 269 in the A25R gene leading to Lys90Thr mutation was not identified by AmpliSeq technology. By designing specific primers it may be possible to analyze the whole CPXV genome sequence from xCELLigence supernatants. Finally, because the observed Lys90Thr mutation was already detected in the crust, the **selection of pre-existing variants is presumably a mechanism of CPXV adaptation in cell culture.**

4.5. Transcript incorporation as CPXV adaptation mechanism

Transcripts have been shown to be incorporated in virions of dsDNA viruses like CMV [37-39], Herpes simplex virus 1 (HSV-1) [40] and Mimivirus [41]. While only viral transcripts have been detected in Mimivirus particles [41,42], CMV and HSV-1 particles were also reported to contain host transcripts [37-40]. Intact virion-packaged transcripts are released upon entry into the host cell, enabling the rapid expression of according proteins [38,40]. The incorporation of mRNA in virus particles appears to occur in proportion to the intracellular concentration during virus assembly [37,39]. Moreover, it has been shown for CMV that transcript incorporation is independent of sequence-specific cis-acting packaging elements as present e.g. in retroviruses [39]. Instead, transcript packaging into virions may rather be mediated by nonspecific interactions of mRNA with virion proteins [272]. The biological function of virion-incorporated transcripts has been hardly investigated so far. Nevertheless, interestingly, mRNA encoding a secreted viral chemokine receptor, which binds and inhibits RANTES chemokine, was identified in CMV virions [39,273], suggesting immunomodulatory advantages mediated by virion-incorporated transcripts. Although transcript incorporation is presumably an undirected process, virion-packaged mRNA may be regulated by mRNA levels during virus assembly, as suggested by Terhune and colleagues [39]. In that way transcript incorporation may also contribute to virus adaptation and, hence, was analyzed in the present study.

Ribosomal RNA identified in CPXV IMV particles

Since rRNA is the most abundant RNA species in the cell representing 80-90 % of total RNA [274], it was no surprise to detect large rRNA amounts in all samples (**Table 3.9**). Ribosomal RNA is likely already contained in virion preparations as indicated by the identification of ribosomal proteins in proteome analysis of the purified virus stocks. However, rRNA and possibly other contaminating RNA may also be introduced during sample preparation. It should be noted that amplification prior to NGS may result in massive amounts of even the smallest contaminations. This may be underlined by the observation that controls were also dominated by rRNA, which did not result from cross-contamination since no rat mt rRNA was detected in rat controls. Moreover, if cross-contamination were an issue, one would expect to identify also viral transcripts with high abundance in the control, which was not the case.

RNase digestion was not able to remove rRNA, indicating either an incomplete digestion, virion-incorporated rRNA or rRNA introduced during later sample preparation steps. Incomplete digestion may be ruled out since RNase digestion efficiency was verified by high amounts of RNA spike-in during method establishment. Incorporation of rRNA in virus particles may be explained by proximity of ribosomes and mitochondria to VF during infection [275]. Taken together, detected rRNA in CPXV IMV particles is presumably a mix of rRNA contained in virions, associated outside of virions as well as introduced during sample preparation. However,

rat mt rRNA amounts indicate that **viron-incorporated rRNA makes up the largest portion of rRNA identified in highly purified CPXV IMV preparations**.

Protease digestion prior to RNase digestion did not led to the expected depletion of transcript identifications. This may be explained by non-ribosome-associated transcripts or incomplete digestion of ribosomes. Additionally, transcripts are possibly digested by RNase although they are ribosome-bound, because only small parts of the transcript are covered by ribosomes. This may be supported by the fact that RNase digestion of ribosome-bound transcripts is the technique underlying ribosome profiling resulting in small fragments of about 30-31 bp, which are protected by ribosomes during digestion [276].

Apart from rRNA and mt transcripts, exclusively viral transcripts were identified in CPXV particles. **Viral transcripts were not digested by RNase, indicating their incorporation in virions rather than association outside of virus particles.** The distinct distribution of reads between promoter and terminator sequences strongly suggests the presence of intact transcripts. (**Figure 3.22**). Moreover, reads were frequently biased towards the 3' end of the transcript, which is generally observed in cDNA synthesis with oligo(dT) primers [194]. Controversially, random hexamer primers were used in the present study, which rather tend to induce 5' bias [277]. However, bias may also be introduced as a result of mRNA secondary structure, which may lead to interruption of reverse transcription during cDNA synthesis and early termination [278]. Another conceivable hypothesis for the higher coverages of the transcripts' 3'-ends may be the presence of transcripts, which are partially degraded at the 5'end, leading to lower 5' coverage. OPV encode two decapping enzymes, which remove the 5' cap resulting in degradation of viral and host mRNA presumably by the host 5'-3' mRNA exonuclease Xrn1 [279]. Decapping promotes translational shutdown of host mRNA and controls dsRNA levels arising from viral transcripts [280].

Function of CPXV-incorporated transcripts

Most identified viral transcripts encoded proteins of unknown function, while the largest number of transcripts with known function was associated with immune evasion (**Table 3.10**). From seven transcripts encoding immunomodulatory proteins, five were identified in both HEp-2 and Rat-2-passaged virions. Notably, the D5/I1-encoding transcript was identified in extraordinary high amounts in all samples (**Figure 3.21**). D1/I5 inactivates the DNA-dependent protein kinase, which is a cellular DNA sensor in the cytoplasm. Moreover, D1/I5 is a virulence factor *in vivo* [191].

Immunomodulatory genes are generally expressed early during infection in order to prevent the antiviral response of the host [119,281]. Out of 15 transcripts with known expression, 14 were expressed early during infection (**Table 3.10**). It has been shown that OPVs express an immediate-early class of genes including 35 genes in VACV, which are expressed already 0.5-1 h p.i. [282]. Strikingly, nine transcripts identified in CPXV IMV particles belong to this immediate-

early class, including C14L, P2L, M1L, F3L, F4L, A34R, A36R, A47R and B13R. The incorporation of transcripts in virus particles may, at least partially, explain their immediate-early expression.

Assarsson and colleagues [282] showed that the immediate-early class of genes is expressed highest during infection, exceeding even viral late gene expression up to 24 h p.i.. Therefore, immediate-early transcripts are presumably most abundant during CPXV particle assembly. This suggests that **incorporation of transcripts in CPXV particles may be an undirected process occurring in proportion to the intracellular concentration**, as described for CMV [39]. In addition, poxviruses effectively shut down host mRNA expression [283], which explains the lack of host transcripts other than rRNA in CPXV IMV particles.

Furthermore, differences of transcript identifications in HEp-2 and Rat-2-adapted CPXV IMV particles were observed. The absence of a transcript in HEp-2 or Rat-2-adapted CPXV in **Table 3.10** does not mean the absence of any transcript of the corresponding gene, but may result from a transcript amount below the cutoff. It should be noted further that due to a lack of biological replicates the conclusions about an adaptation-related incorporation is limited. Nevertheless, if transcript incorporation is proportional to mRNA concentration in the cell, as indicated by the identification of mostly transcripts, which are highly abundant during infection, it seems likely that **altered mRNA level resulting from adaptation may lead to altered transcript incorporation in virions**.

4.6. Ubiquitin is a major poxvirus modification

Ubiquitin is essential for VACV replication [127,128]. This also applies to CPXV as proven in the present study. Results of the present study and studies in the literature (as described in section 1.3.3) indicate that the proteasomal degradation of structural core proteins is the mechanism underlying OPV uncoating (**Figure 1.7**). To prove this hypothesis, a method was established to analyze the CPXV IMV ubiquitinome, by which 137 conserved ubiquitination sites in 54 virion proteins could be identified (**Table 3.7**), verifying that ubiquitin is a major poxvirus modification. According to the hypothesis it was shown that CPXV particles contain large amounts of K48-linked polyubiquitin and core proteins are extensively ubiquitinated. Nevertheless, core proteins are not degraded by the proteasome upon infection. Instead, another class of viral proteins seems interesting in this context. Using siRNA screening Kilcher and colleagues identified 15 viral candidate genes that impaired intermediate but not early VACV gene expression [113]. From these 15 candidate genes four reduced the number of prereplication sites, meaning precursor sites of viral DNA replication [284], more than 40 %. Strikingly, all these four proteins were found to be stabilized by proteasome inhibition in the present study. These proteins included the serine/threonine-protein kinase B1, the putative nuclease H5, the ssDNA-binding phosphoprotein

L3 as well as the Primase E5. Kilcher and colleagues finally identified the E5 protein as the genome uncoating factor whose depletion leads to the accumulation of cores in the cytoplasm [113]. Moreover, they suggested a proteasomal regulation of E5 [113]. Hence, the results suggest that the proteasome-dependent degradation of proteins associated with the formation of pre-replication sites, especially the uncoating factor E5, is a prerequisite for CPXV genome uncoating. This data demonstrates that ubiquitin is of major biological relevance for CPXV infection. Therefore, it seems conclusive that ubiquitin is also relevant for CPXV adaptation. This is underlined by the fact that not only the amount of virion-associated ubiquitin changed during cell culture passaging, but also the amount of various ubiquitinated viral proteins. As described in section 4.2 and 4.3, viral proteins associated with transcription, membrane/entry and immunomodulation are of special interest in the context of adaptation. Hence, they are discussed in the following:

Transcription

Five of the eight CPXV Pol subunits contain conserved ubiquitination sites including O4 (147 kDa), A25 (132 kDa), A30 (35 kDa), F4 (30 kDa) and A6 (19 kDa). The eukaryotic Pol II is known to become K63-polyubiquitinated following DNA damage, for example, and Pol ubiquitination is a mechanism of transcriptional regulation in eukaryotes [285-287]. Considering the given homology between the eukaryotic and the OPV Pol, **it is likely that CPXV transcription is regulated by ubiquitination**.

Besides subunits of the CPXV Pol itself, viral transcription factors of all three classes contain ubiquitination sites. These include the A8 protein, a subunit of the early transcription factor, the A24 protein, an intermediate transcription factor subunit, and A1, a viral late transcription factor. Eukaryotic transcription factors seem to be activated and also tagged for degradation by ubiquitination [288,289], but no mechanism has been described for OPV yet.

Membrane/Entry

Two membrane proteins (A14 and A17) and two EEV glycoproteins (A35 and B4) contain conserved ubiquitination sites. Furthermore, the scaffold protein E13 and the H2 protein belonging to the entry/fusion complex are ubiquitinated. Furthermore, three CPXV proteins associated with entry into the host cell were identified to be ubiquitinated. These proteins include the cell fusion protein A28, the IMV heparin-binding surface protein J3 and the myristoylated protein H10, **indicating that ubiqutitination may be involved in CPXV entry**.

Immunomodulation

Six proteins associated with viral immune evasion contain conserved ubiquitination sites, including the inhibitor of antigen presentation A36, the complement control protein C17, the IL-18-binding protein C8, the inhibitor of TNF-R and TLR signaling Q1 and the two host range

factors F3 and M1. Of those proteins, F3 is known to be ubiquitinated but distinct lysine residues have not been identified before [267]. Also, Q1 has been shown to be ubiquitinated at all six possible lysine residues [233]. In this study two conserved ubiquitination sites in the CPXV Q1 protein at positions 70 and 78 were identified.

Identifying up to 668 ubiquitination sites in a single CPXV strain raised the question of a primary structure ubiquitination motif. Therefore, the amino acid sequence around ubiquitinated lysine residues (+/- eight amino acids) was compared to the non-ubiquitinated lysine background using motif-x [155]. However, this did not lead to any results. Also, the sequence logo analysis implemented in Perseus revealed no primary amino acid motif for ubiquitination. Therefore, it may be concluded that **ubiquitination site specificity of CPXV mature virion proteins is independent of a distinct amino acid motif near the ubiquitinated lysine residue**. It is not fully understood what determines ubiquitination site specificity, but recently it was suggested that proteins destined for the proteasome contain three factors, which are referred to as tripartite degron architecture [290]. These consist of a primary peptide motif recognized by an E3-ubiquitin ligase (degron), target lysine site(s) for ubiquitination and a disordered degradation initiation site. From the proposed model it becomes clear that the degron can be distant from the target ubiquitination site, which could explain why no ubiquitination motif around the lysine residue was identified.

Besides ubiquitination as a major known PTM in OPV, phosphorylation of VACV mature virion proteins has been studied with MS [35,36]. Recently, 396 unique phosphorylation sites among 83 VACV proteins were identified [36]. Strikingly, about 70 % of CPXV proteins with conserved ubiquitination sites were identified to contain phosphorylation sites in homologous VACV proteins. This correlation may be important since cross-talk between phosphorylation and ubiquitination has been described, e.g. the regulation of proteasomal degradation by phosphorylation [290]. Interestingly, the data from Ngo and colleagous [36] reveals the largest number of phosphorylation sites in VACV core proteins A11 and A4 with 17 and 34 unique phosphorylation sites, respectively, indicating that core proteins are packaged in a phosphorylated state in mature virions. Although Ngo and colleagues [36] did not state the presence of phosphorylation motifs in VACV proteins, they observed the presence of phosphorylation clusters, which were also found in major core proteins A11 and A4. Since it is known that phosphorylation motifs, so-called phosphodegrons, can serve as recognition signals for E3 ligases [291] and that phosphorylation can change accessibility of degrons [290], it can be hypothesized that OPV proteins may contain similar phosphorylation motifs representing binding signals for ubiquitin ligases or regulating degron accessibility. Finally, it remains to be elucidated, whether a host or the poxvirus-encoded p28-like ubiquitin ligase [131] catalyzes ubiquitination of poxvirus proteins.

4.7. Which is the major mechanism of OPV adaptation in cell culture?

In the present study the adaptation of CPXV in cell culture was analyzed in an unprecedented depth. The elucidated mechanisms may also apply to other OPV, e.g. VACV or VARV. It could be shown that OPV adaptation takes place on various levels, including genomic and proteomic changes, selection of pre-existing variants and possibly transcript incorporation (**Table 4.3**). Although each of these mechanisms apparently applies to CPXV adaptation in cell culture, the question arises which mechanism may be the major driving force for CPXV adaptation?

Table 4.3. Result overview of analyzed CPXV adaptation mechanisms in cell culture.

Adaptation mechanism	Details	First analysis[a]	True for CPXV[b]
Genomic changes	*De novo* mutations	x	✓
	Copy number variation	x	(x)
Proteomic changes	Viral protein composition	✓	✓
	Associated host proteins	✓	✓
	PTMs (Ubiquitin)	✓	✓
Selection of pre-existing variants	Heterogeneous virus population	x	✓
Transcript incorporation	mRNA incorporation	✓	✓

[a] Mechanism analyzed for the first time in present study
[b] Proven for CPXV adaptation in cell culture
✓:true; x: false; (x): not detected, but shown for VACV before

Generally, changes in the amount of virus proteins during cell culture propagation may result from either increased expression of these proteins or higher incorporation rates in virus particles. Increased protein amounts may be regulated on transcription or translation level. Interestingly, viral genome changes were mainly detected in transcription-related genes. The Lys90Thr mutation in the A25 RNA Pol subunit may be related to transcription processivity, which in turn may alter viral protein amounts resulting in increased incorporation rates. As poxvirus transcription rates are not controlled by enhancer elements [282], they exclusively rely on the RNA Pol transcription efficiency, which in turn is likely regulated by ubiquitination as discussed in section 4.6. If ubiquitination of virus proteins is, at least partially, catalyzed by a host ubiquitin ligase, it seems likely that modification changes may directly occur as a result of host change, because ubiquitination may differ from host to host. Although ubiquitination in different hosts was not investigated, the methods established in this study can be used to answer this question.

Finally, another possible mechanism of virus adaptation may be also the incorporation of metabolites and small molecules in virus particles. Although there are studies investigating the metabolome of infected cells, the incorporation of metabolites in any virus particles has not been investigated yet [292,293].

4.8. Summary

CPXV adaptation in cell culture is most likely explained by two major mechanisms:

1. **Upon infection of the first passage, PTMs, like ubiquitination, change.**
2. **Minor variants permanently arise during virus replication, mainly in transcription-associated genes.**

Both mechanisms may lead to altered transcription, resulting in proteomic difference, which in turn may alter the proteome composition of virions. The first mechanism applies to host changes, explaining differences observed between the crust and the first passage. In contrast, the second mechanism explains differences observed during further passaging. Additionally, as a combination of both mechanisms, mutations may result in amino acid changes, which lead to altered PTM sites (**Figure 4.4**).

The results of the present study do not only expand the knowledge of OPV adaptation mechanisms, but also lead to a novel understanding of DNA virus adaptation in general. As demonstrated, DNA virus particles change during passaging in cell culture, even at a low number of passages.

This work leads to the following novel hypothesis about OPV adaptation mechanisms *in vivo*:

1. **Proteomic changes are a major driving force of OPV adaptation.**
2. **Host switch of OPV is enabled by changes in PTMs, e.g. ubiquitination.**
3. **Transcript incorporation in virons may contribute to OPV adaptation.**

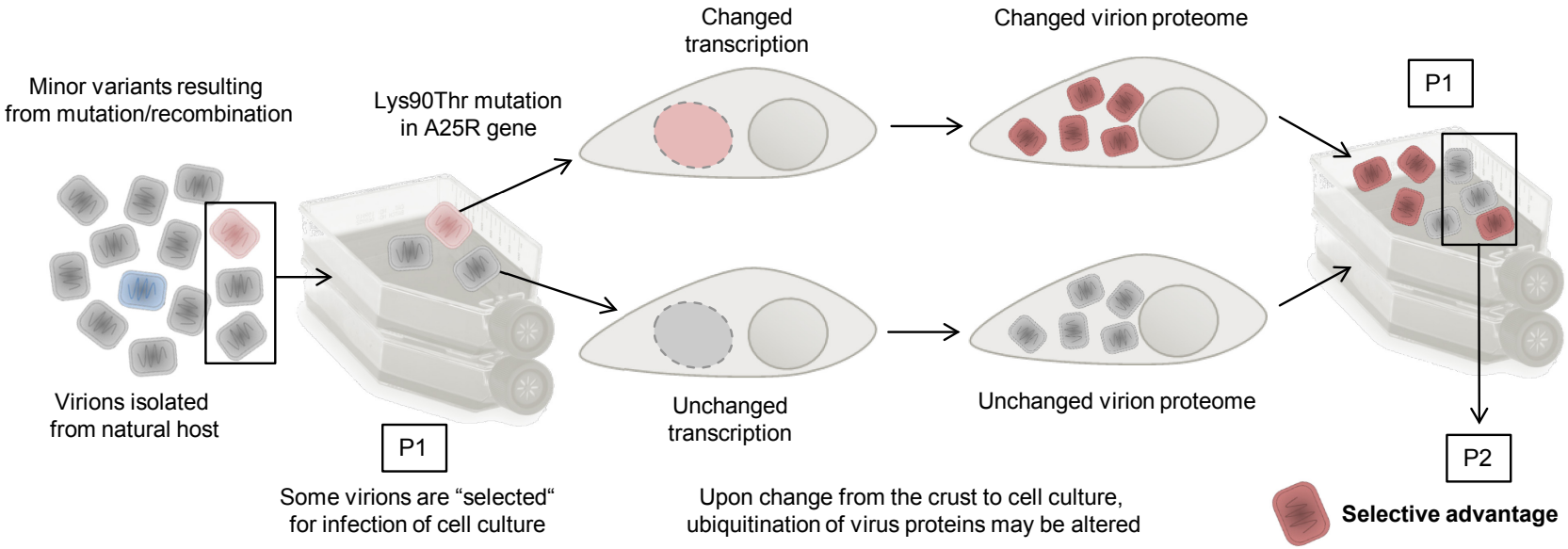

Figure 4.4. Hypothetical model of CPXV adaptation in cell culture. Mutation and ubiquitination changes are hypothesized to result in altered transcription, which in turn leads to an altered virion proteome composition, resulting in a selective advantage of distinct virions. P1: first passage; P2: second passage.

4.9. Outlook

Generally, changes of DNA virus particles during cell culture passaging may become noticeable in the amount of virus yield, but they may also be inconspicuous in analysis of *in vitro* characteristic. To date, it is not common to state the passage number of the virus used for analysis. It may be indispensable to propagate viruses in cell culture prior to analysis. However, depending on the research question, the pitfalls should be kept in mind, for example when investigating pathogenic mechanisms that rely on *in vivo* experiments or distinct outbreaks. **To enable a better evaluation of conclusions drawn from virological experiments using cell culture-passaged viruses, the virus origin, passage number and cell type used for propagation have to be stated**.

The results and methods established in this study provide the groundwork for further detailed investigation of OPV adaptation. Amongst others, further experiments may include:

1. Testing the hypothesis of altered CPXV transcription by A25R mutations by comparing the transcriptome and proteome of cells infected with a wild type and a Lys90Thr variant.

2. Analyzing the incorporation of host proteins in CPXV particles by infection of SILAC-labeled cells.

3. Elucidating the ubiquitin ligase responsible for ubiquitination of CPXV proteins by comparing the ubiquitinome of a CPXV strain encoding the viral ubiquitin ligase p28 to a p28 knockout mutant.

4. Testing the hypothesis of a phosphorylation motif for ubiquitination site specificity by a correlated ubiquitinome-phosphoproteome analysis.

5. Analyzing changes of ubiquitination during infection, e.g. by analyzing the ubiquitinome of CPXV-infected cells at different time points during infection.

6. Analyzing global ubiquitinome changes of poxvirus IMV particles upon host change.

7. Analyzing the role of E5 for CPXV uncoating, e.g. by identifying E5 interaction partner.

8. Verifying the presence of intact mRNA in CPXV particles by qPCR.

References

1. Froissart, R.; Roze, D.; Uzest, M.; Galibert, L.; Blanc, S.; Michalakis, Y. Recombination every day: Abundant recombination in a virus during a single multi-cellular host infection. *PLOS Biol* **2005**, *3*, e89.
2. Klempner, M.S.; Shapiro, D.S. Crossing the species barrier--one small step to man, one giant leap to mankind. *N Engl J Med* **2004**, *350*, 1171-1172.
3. Fenner, F. Fenner's veterinary virology. Vol 4. Elsevier/Academic Press: London, **2011**, 108.
4. Milian, E.; Kamen, A.A. Current and emerging cell culture manufacturing technologies for influenza vaccines. *Biomed Res Int* **2015**, *2015*, 504831.
5. Genzel, Y. Designing cell lines for viral vaccine production: Where do we stand? *Biotechnol J* **2015**, *10*, 728-740.
6. Leland, D.S.; Ginocchio, C.C. Role of cell culture for virus detection in the age of technology. *Clin Microbiol Rev* **2007**, *20*, 49-78.
7. Mohan, C.M.; Dey, S.; Kumanan, K.; Manohar, B.M.; Nainar, A.M. Adaptation of a velogenic newcastle disease virus to vero cells: Assessing the molecular changes before and after adaptation. *Vet Res Commun* **2007**, *31*, 371-383.
8. Nikolay, A.; Castilho, L.R.; Reichl, U.; Genzel, Y. Propagation of brazilian zika virus strains in static and suspension cultures using vero and bhk cells. *Vaccine* **2017**.
9. McAuley, A.J.; Beasley, D.W. Propagation and titration of west nile virus on vero cells. *Methods Mol Biol* **2016**, *1435*, 19-27.
10. Coleman, C.M.; Frieman, M.B. Growth and quantification of mers-cov infection. *Curr Protoc Microbiol* **2015**, *37*, 15E 12 11-19.
11. Steinhardt, E.; Israeli, C.; Lambert, R.A. Studies on the cultivation of the virus of vaccinia. *J Infect Dis* **1913**, *13*, 294-300.
12. Enders, J.F.; Weller, T.H.; Robbins, F.C. Cultivation of the lansing strain of poliomyelitis virus in cultures of various human embryonic tissues. *Science* **1949**, *109*, 85-87.
13. Jones, H.W., Jr. Record of the first physician to see henrietta lacks at the johns hopkins hospital: History of the beginning of the hela cell line. *Am J Obstet Gynecol* **1997**, *176*, S227-228.
14. Hematian, A.; Sadeghifard, N.; Mohebi, R.; Taherikalani, M.; Nasrolahi, A.; Amraei, M.; Ghafourian, S. Traditional and modern cell culture in virus diagnosis. *Osong Public Health Res Perspect* **2016**, *7*, 77-82.
15. Hill, M. Cell culture at https://cellbiology.med.unsw.edu.au/cellbiology/index.php/Group_4_Project_-_Cell_Culture (access date **30.05.2017**).
16. Koprowski, H.; Lennette, E.H. Effect of in vitro cultivation on the pathogenicity of west nile virus. *J Bacteriol* **1946**, *51*, 617.
17. Randall, C.C.; Ryden, F.W. Adaptation of vaccinia virus to earle's l-cells with prolonged noninfectious period. *Proc Soc Exp Biol Med* **1960**, *103*, 723-725.
18. Lundkvist, A.; Cheng, Y.; Sjolander, K.B.; Niklasson, B.; Vaheri, A.; Plyusnin, A. Cell culture adaptation of puumala hantavirus changes the infectivity for its natural reservoir, clethrionomys glareolus, and leads to accumulation of mutants with altered genomic RNA S segment. *J Virol* **1997**, *71*, 9515-9523.
19. Bankamp, B.; Fontana, J.M.; Bellini, W.J.; Rota, P.A. Adaptation to cell culture induces functional differences in measles virus proteins. *Virol J* **2008**, *5*, 129.
20. Mohapatra, J.K.; Pandey, L.K.; Rai, D.K.; Das, B.; Rodriguez, L.L.; Rout, M.; Subramaniam, S.; Sanyal, A.; Rieder, E.; Pattnaik, B. Cell culture adaptation mutations in foot-and-mouth disease virus serotype a capsid proteins: Implications for receptor interactions. *J Gen Virol* **2015**, *96*, 553-564.
21. Wang, W.D.; Lee, G.C.; Kim, Y.Y.; Lee, C.H. A comparison between low- and high-passage strains of human cytomegalovirus. *J Microbiol Biotechnol* **2016**, *26*, 1800-1807.
22. Aravind, S.; Kamble, N.M.; Gaikwad, S.S.; Shukla, S.K.; Dey, S.; Mohan, C.M. Adaptation and growth kinetics study of an indian isolate of virulent duck enteritis virus in vero cells. *Microb Pathog* **2015**, *78*, 14-19.

23. Mandl, C.W.; Kroschewski, H.; Allison, S.L.; Kofler, R.; Holzmann, H.; Meixner, T.; Heinz, F.X. Adaptation of tick-borne encephalitis virus to BHK-21 cells results in the formation of multiple heparan sulfate binding sites in the envelope protein and attenuation in vivo. *J Virol* **2001**, *75*, 5627-5637.
24. McKnight, K.L.; Simpson, D.A.; Lin, S.C.; Knott, T.A.; Polo, J.M.; Pence, D.F.; Johannsen, D.B.; Heidner, H.W.; Davis, N.L.; Johnston, R.E. Deduced consensus sequence of sindbis virus strain AR339: Mutations contained in laboratory strains which affect cell culture and in vivo phenotypes. *J Virol* **1996**, *70*, 1981-1989.
25. Bankamp, B.; Hodge, G.; McChesney, M.B.; Bellini, W.J.; Rota, P.A. Genetic changes that affect the virulence of measles virus in a rhesus macaque model. *Virology* **2008**, *373*, 39-50.
26. Louz, D.; Bergmans, H.E.; Loos, B.P.; Hoeben, R.C. Cross-species transfer of viruses: Implications for the use of viral vectors in biomedical research, gene therapy and as live-virus vaccines. *J Gene Med* **2005**, *7*, 1263-1274.
27. Sinzger, C.; Schmidt, K.; Knapp, J.; Kahl, M.; Beck, R.; Waldman, J.; Hebart, H.; Einsele, H.; Jahn, G. Modification of human cytomegalovirus tropism through propagation in vitro is associated with changes in the viral genome. *J Gen Virol* **1999**, *80 (Pt 11)*, 2867-2877.
28. Sanjuan, R.; Nebot, M.R.; Chirico, N.; Mansky, L.M.; Belshaw, R. Viral mutation rates. *J Virol* **2010**, *84*, 9733-9748.
29. Lauring, A.S.; Andino, R. Quasispecies theory and the behavior of rna viruses. *PLoS Pathog* **2010**, *6*, e1001005.
30. Qin, L.; Evans, D.H. Genome scale patterns of recombination between coinfecting vaccinia viruses. *J Virol* **2014**, *88*, 5277-5286.
31. Aubertin, A.M.; McAuslan, B.R. Virus-associated nucleases: Evidence for endonuclease and exonuclease activity in rabbitpox and vaccinia viruses. *J Virol* **1972**, *9*, 554-556.
32. Modrow, S., Falke, D., Truyen, U., Schätzl, H. . Molekulare virologie. Vol 3. Spektrum Akademischer Verlag: Heidelberg, **2010**, 610-634.
33. Krauss, O.; Hollinshead, R.; Hollinshead, M.; Smith, G.L. An investigation of incorporation of cellular antigens into vaccinia virus particles. *J Gen Virol* **2002**, *83*, 2347-2359.
34. Vanderplasschen, A.; Mathew, E.; Hollinshead, M.; Sim, R.B.; Smith, G.L. Extracellular enveloped vaccinia virus is resistant to complement because of incorporation of host complement control proteins into its envelope. *Proc Natl Acad Sci U S A* **1998**, *95*, 7544-7549.
35. Matson, J.; Chou, W.; Ngo, T.; Gershon, P.D. Static and dynamic protein phosphorylation in the vaccinia virion. *Virology* **2014**, *452-453*, 310-323.
36. Ngo, T.; Mirzakhanyan, Y.; Moussatche, N.; Gershon, P.D. Protein primary structure of the vaccinia virion at increased resolution. *J Virol* **2016**, *90*, 9905-9919.
37. Greijer, A.E.; Dekkers, C.A.; Middeldorp, J.M. Human cytomegalovirus virions differentially incorporate viral and host cell rna during the assembly process. *J Virol* **2000**, *74*, 9078-9082.
38. Bresnahan, W.A.; Shenk, T. A subset of viral transcripts packaged within human cytomegalovirus particles. *Science* **2000**, *288*, 2373-2376.
39. Terhune, S.S.; Schroer, J.; Shenk, T. Rnas are packaged into human cytomegalovirus virions in proportion to their intracellular concentration. *J Virol* **2004**, *78*, 10390-10398.
40. Sciortino, M.T.; Suzuki, M.; Taddeo, B.; Roizman, B. RNAs extracted from herpes simplex virus 1 virions: Apparent selectivity of viral but not cellular RNAs packaged in virions. *J Virol* **2001**, *75*, 8105-8116.
41. Raoult, D.; Audic, S.; Robert, C.; Abergel, C.; Renesto, P.; Ogata, H.; La Scola, B.; Suzan, M.; Claverie, J.M. The 1.2-megabase genome sequence of mimivirus. *Science* **2004**, *306*, 1344-1350.
42. Suzan-Monti, M.; La Scola, B.; Raoult, D. Genomic and evolutionary aspects of mimivirus. *Virus Res* **2006**, *117*, 145-155.
43. Hudu, S.A.; Alshrari, A.S.; Syahida, A.; Sekawi, Z. Cell culture, technology: Enhancing the culture of diagnosing human diseases. *J Clin Diagn Res* **2016**, *10*, DE01-05.
44. Shendure, J.; Ji, H. Next-generation DNA sequencing. *Nat Biotechnol* **2008**, *26*, 1135-1145.
45. International Human Genome Sequencing, C. Finishing the euchromatic sequence of the human genome. *Nature* **2004**, *431*, 931-945.
46. Fox, E.J.; Reid-Bayliss, K.S.; Emond, M.J.; Loeb, L.A. Accuracy of next generation sequencing platforms. *Next Gener Seq Appl* **2014**, *1*.

47. Katta, M.A.; Khan, A.W.; Doddamani, D.; Thudi, M.; Varshney, R.K. NGS-QCbox and raspberry for parallel, automated and rapid quality control analysis of large-scale next generation sequencing (Illumina) data. *PLoS One* **2015**, *10*, e0139868.
48. Metzker, M.L. Sequencing technologies - the next generation. *Nat Rev Genet* **2010**, *11*, 31-46.
49. Liu, L.; Li, Y.; Li, S.; Hu, N.; He, Y.; Pong, R.; Lin, D.; Lu, L.; Law, M. Comparison of next-generation sequencing systems. *J Biomed Biotechnol* **2012**, *2012*, 251364.
50. Goodwin, S.; McPherson, J.D.; McCombie, W.R. Coming of age: Ten years of next-generation sequencing technologies. *Nat Rev Genet* **2016**, *17*, 333-351.
51. Park, S.T.; Kim, J. Trends in next-generation sequencing and a new era for whole genome sequencing. *Int Neurourol J* **2016**, *20*, S76-83.
52. Illumina sequencing platforms at https://www.illumina.com/systems/sequencing-platforms.html (access date **22.06.2017**).
53. Radford, A.D.; Chapman, D.; Dixon, L.; Chantrey, J.; Darby, A.C.; Hall, N. Application of next-generation sequencing technologies in virology. *J Gen Virol* **2012**, *93*, 1853-1868.
54. Capobianchi, M.R.; Giombini, E.; Rozera, G. Next-generation sequencing technology in clinical virology. *Clin Microbiol Infect* **2013**, *19*, 15-22..
55. Isakov, O.; Borderia, A.V.; Golan, D.; Hamenahem, A.; Celniker, G.; Yoffe, L.; Blanc, H.; Vignuzzi, M.; Shomron, N. Deep sequencing analysis of viral infection and evolution allows rapid and detailed characterization of viral mutant spectrum. *Bioinformatics* **2015**, *31*, 2141-2150.
56. Andino, R.; Domingo, E. Viral quasispecies. *Virology* **2015**, *479-480*, 46-51.
57. Elde, N.C.; Child, S.J.; Eickbush, M.T.; Kitzman, J.O.; Rogers, K.S.; Shendure, J.; Geballe, A.P.; Malik, H.S. Poxviruses deploy genomic accordions to adapt rapidly against host antiviral defenses. *Cell* **2012**, *150*, 831-841.
58. Wei, H.; Audet, J.; Wong, G.; He, S.; Huang, X.; Cutts, T.; Theriault, S.; Xu, B.; Kobinger, G.; Qiu, X. Deep-sequencing of marburg virus genome during sequential mouse passaging and cell-culture adaptation reveals extensive changes over time. *Sci Rep* **2017**, *7*, 3390.
59. Wilkins, M.R.; Sanchez, J.C.; Gooley, A.A.; Appel, R.D.; Humphery-Smith, I.; Hochstrasser, D.F.; Williams, K.L. Progress with proteome projects: Why all proteins expressed by a genome should be identified and how to do it. *Biotechnol Genet Eng Rev* **1996**, *13*, 19-50.
60. Han, X.; Aslanian, A.; Yates, J.R., 3rd. Mass spectrometry for proteomics. *Curr Opin Chem Biol* **2008**, *12*, 483-490.
61. Bennike, T.; Birkelund, S.; Stensballe, A.; Andersen, V. Biomarkers in inflammatory bowel diseases: Current status and proteomics identification strategies. *World J Gastroenterol* **2014**, *20*, 3231-3244.
62. Naryzhny, S.N.; Zgoda, V.G.; Maynskova, M.A.; Ronzhina, N.L.; Belyakova, N.V.; Legina, O.K.; Archakov, A.I. [Experimental estimation of proteome size for cells and human plasma]. *Biomed Khim* **2015**, *61*, 279-285.
63. Smith, L.M.; Kelleher, N.L.; Consortium for Top Down, P. Proteoform: A single term describing protein complexity. *Nat Methods* **2013**, *10*, 186-187.
64. Ponomarenko, E.A.; Poverennaya, E.V.; Ilgisonis, E.V.; Pyatnitskiy, M.A.; Kopylov, A.T.; Zgoda, V.G.; Lisitsa, A.V.; Archakov, A.I. The size of the human proteome: The width and depth. *Int J Anal Chem* **2016**, *2016*, 7436849.
65. Patterson, S.D.; Aebersold, R.H. Proteomics: The first decade and beyond. *Nat Genet* **2003**, *33 Suppl*, 311-323.
66. Aebersold, R.; Mann, M. Mass-spectrometric exploration of proteome structure and function. *Nature* **2016**, *537*, 347-355.
67. Klose, J. Protein mapping by combined isoelectric focusing and electrophoresis of mouse tissues. A novel approach to testing for induced point mutations in mammals. *Humangenetik* **1975**, *26*, 231-243.
68. O'Farrell, P.H. High resolution two-dimensional electrophoresis of proteins. *J Biol Chem* **1975**, *250*, 4007-4021.
69. Yates, J.R. A century of mass spectrometry: From atoms to proteomes. *Nature Methods* **2011**, *8*, 633-637.

70. Tanaka, K.; Waki, H.; Ido, Y.; Akita, S.; Yoshida, Y.; Yoshida, T.; Matsuo, T. Protein and polymer analyses up to m/z 100 000 by laser ionization time-of-flight mass spectrometry. *Rapid Commun Mass Spectrom* **1988**, *2*, 151-153.
71. Whitehouse, C.M.; Dreyer, R.N.; Yamashita, M.; Fenn, J.B. Electrospray interface for liquid chromatographs and mass spectrometers. *Anal Chem* **1985**, *57*, 675-679.
72. Aebersold, R.; Mann, M. Mass spectrometry-based proteomics. *Nature* **2003**, *422*, 198-207.
73. Futrell, J.H.M., C.D. . Tandem mass spectrometer for the study of ion-molecule reactions. *Rev. Sci. Instrum.* **1966**, *37*, 1521–1526.
74. Henzel, W.J.; Billeci, T.M.; Stults, J.T.; Wong, S.C.; Grimley, C.; Watanabe, C. Identifying proteins from two-dimensional gels by molecular mass searching of peptide fragments in protein sequence databases. *Proc Natl Acad Sci U S A* **1993**, *90*, 5011-5015.
75. Wilm, M.; Shevchenko, A.; Houthaeve, T.; Breit, S.; Schweigerer, L.; Fotsis, T.; Mann, M. Femtomole sequencing of proteins from polyacrylamide gels by nano-electrospray mass spectrometry. *Nature* **1996**, *379*, 466-469.
76. Scigelova, M.; Makarov, A. Orbitrap mass analyzer--overview and applications in proteomics. *Proteomics* **2006**, *6 Suppl 2*, 16-21.
77. Eliuk, S.; Makarov, A. Evolution of orbitrap mass spectrometry instrumentation. *Annu Rev Anal Chem (Palo Alto Calif)* **2015**, *8*, 61-80.
78. Usaite, R.; Wohlschlegel, J.; Venable, J.D.; Park, S.K.; Nielsen, J.; Olsson, L.; Yates Iii, J.R. Characterization of global yeast quantitative proteome data generated from the wild-type and glucose repression saccharomyces cerevisiae strains: The comparison of two quantitative methods. *J Proteome Res* **2008**, *7*, 266-275.
79. Nagaraj, N.; Wisniewski, J.R.; Geiger, T.; Cox, J.; Kircher, M.; Kelso, J.; Paabo, S.; Mann, M. Deep proteome and transcriptome mapping of a human cancer cell line. *Mol Syst Biol* **2011**, *7*, 548.
80. Kim, M.S.; Pinto, S.M.; Getnet, D.; Nirujogi, R.S.; Manda, S.S.; Chaerkady, R.; Madugundu, A.K.; Kelkar, D.S.; Isserlin, R.; Jain, S.*, et al.* A draft map of the human proteome. *Nature* **2014**, *509*, 575-581.
81. Wilhelm, M.; Schlegl, J.; Hahne, H.; Gholami, A.M.; Lieberenz, M.; Savitski, M.M.; Ziegler, E.; Butzmann, L.; Gessulat, S.; Marx, H.*, et al.* Mass-spectrometry-based draft of the human proteome. *Nature* **2014**, *509*, 582-587.
82. Cristea, I.M.; Graham, D. Virology meets proteomics. *Proteomics* **2015**, *15*, 1941-1942.
83. Lind, S.B.; Artemenko, K.A.; Pettersson, U. Proteome analysis of adenovirus using mass spectrometry. *Methods Mol Biol* **2014**, *1089*, 25-44.
84. Leroy, B.; Gillet, L.; Vanderplasschen, A.; Wattiez, R. Structural proteomics of herpesviruses. *Viruses* **2016**, *8*.
85. Buscher, N.; Paulus, C.; Nevels, M.; Tenzer, S.; Plachter, B. The proteome of human cytomegalovirus virions and dense bodies is conserved across different strains. *Med Microbiol Immunol* **2015**, *204*, 285-293.
86. Dent, S.D.; Xia, D.; Wastling, J.M.; Neuman, B.W.; Britton, P.; Maier, H.J. The proteome of the infectious bronchitis virus Beau-R virion. *Journal of General Virology* **2015**, *96*, 3499-3506.
87. Fischer, M.G.; Kelly, I.; Foster, L.J.; Suttle, C.A. The virion of Cafeteria roenbergensis virus (CroV) contains a complex suite of proteins for transcription and DNA repair. *Virology* **2014**, *466-467*, 82-94.
88. Doellinger, J.; Schaade, L.; Nitsche, A. Comparison of the cowpox virus and vaccinia virus mature virion proteome: Analysis of the species- and strain-specific proteome. *PLoS One* **2015**, *10*, e0141527.
89. Chung, C.S.; Chen, C.H.; Ho, M.Y.; Huang, C.Y.; Liao, C.L.; Chang, W. Vaccinia virus proteome: Identification of proteins in vaccinia virus intracellular mature virion particles. *J Virol* **2006**, *80*, 2127-2140.
90. Resch, W.; Hixson, K.K.; Moore, R.J.; Lipton, M.S.; Moss, B. Protein composition of the vaccinia virus mature virion. *Virology* **2007**, *358*, 233-247.
91. Wunschel, D.; Tulman, E.; Engelmann, H.; Clowers, B.H.; Geary, S.; Robinson, A.; Liao, X. Forensic proteomics of poxvirus production. *Analyst* **2013**, *138*, 6385-6397.
92. Roth, G.A.; Fee, E. Images of health. Smallpox: The first vaccine. *Am J Public Health* **2011**, *101*, 1217.

93. Smith, G.L.; McFadden, G. Smallpox: Anything to declare? *Nat Rev Immunol* **2002**, *2*, 521-527.
94. Babkin, I.V.; Babkina, I.N. The origin of the variola virus. *Viruses* **2015**, *7*, 1100-1112.
95. Hughes, A.L.; Irausquin, S.; Friedman, R. The evolutionary biology of poxviruses. *Infect Genet Evol* **2010**, *10*, 50-59.
96. Essbauer, S.; Pfeffer, M.; Meyer, H. Zoonotic poxviruses. *Vet Microbiol* **2010**, *140*, 229-236.
97. Morand, A.; Delaigue, S.; Morand, J.J. Review of poxvirus: Emergence of monkeypox. *Med Sante Trop* **2017**, *27*, 29-39.
98. Lewis-Jones, S. Zoonotic poxvirus infections in humans. *Curr Opin Infect Dis* **2004**, *17*, 81-89.
99. Shchelkunov, S.N. An increasing danger of zoonotic orthopoxvirus infections. *PLoS Pathog* **2013**, *9*, e1003756.
100. Alzhanova, D.; Fruh, K. Modulation of the host immune response by cowpox virus. *Microbes Infect* **2010**, *12*, 900-909.
101. Werden, S.J.; Rahman, M.M.; McFadden, G. Poxvirus host range genes. *Adv Virus Res* **2008**, *71*, 135-171.
102. Hoffmann, D.; Franke, A.; Jenckel, M.; Tamosiunaite, A.; Schluckebier, J.; Granzow, H.; Hoffmann, B.; Fischer, S.; Ulrich, R.G.; Hoper, D.*, et al.* Out of the reservoir: Phenotypic and genotypic characterization of a novel cowpox virus isolated from a common vole. *J Virol* **2015**, *89*, 10959-10969.
103. Zaba, R.; Jalowska, M.; Kowalczyk, M.J.; Bowszyc-Dmochowska, M.; Adamski, Z.; Szkaradkiewicz, A. Cowpox virus infection in a child after contact with a domestic cat: A case report. *New Microbiol* **2017**, *40*, 148-150.
104. Becker, C.; Kurth, A.; Hessler, F.; Kramp, H.; Gokel, M.; Hoffmann, R.; Kuczka, A.; Nitsche, A. Cowpox virus infection in pet rat owners: Not always immediately recognized. *Dtsch Arztebl Int* **2009**, *106*, 329-334.
105. Nitsche, A., Kurth, A. Cowpox in zoo animals at https://veteriankey.com/cowpox-in-zoo-animals/ (access date **02.06.2017**).
106. Vorou, R.M.; Papavassiliou, V.G.; Pierroutsakos, I.N. Cowpox virus infection: An emerging health threat. *Curr Opin Infect Dis* **2008**, *21*, 153-156.
107. Pelkonen, P.M.; Tarvainen, K.; Hynninen, A.; Kallio, E.R.; Henttonen, K.; Palva, A.; Vaheri, A.; Vapalahti, O. Cowpox with severe generalized eruption, Finland. *Emerg Infect Dis* **2003**, *9*, 1458-1461.
108. Gronemeyer, L.L.; Baltzer, A.; Broekaert, S.; Schrick, L.; Moller, L.; Nitsche, A.; Mossner, R.; Schon, M.P.; Buhl, T. Generalised cowpox virus infection. *Lancet* **2017**.
109. Czerny, C.P.; Eis-Hubinger, A.M.; Mayr, A.; Schneweis, K.E.; Pfeiff, B. Animal poxviruses transmitted from cat to man: Current event with lethal end. *Zentralbl Veterinarmed B* **1991**, *38*, 421-431.
110. Pauli, G.; Blumel, J.; Burger, R.; Drosten, C.; Groner, A.; Gurtler, L.; Heiden, M.; Hildebrandt, M.; Jansen, B.; Montag-Lessing, T.*, et al.* Orthopox viruses: Infections in humans. *Transfus Med Hemother* **2010**, *37*, 351-364.
111. Baxby, D.; Bennett, M.; Getty, B. Human cowpox 1969-93: A review based on 54 cases. *Br J Dermatol* **1994**, *131*, 598-607.
112. Van Vliet, K.; Mohamed, M.R.; Zhang, L.; Villa, N.Y.; Werden, S.J.; Liu, J.; McFadden, G. Poxvirus proteomics and virus-host protein interactions. *Microbiol Mol Biol Rev* **2009**, *73*, 730-749.
113. Kilcher, S.; Schmidt, F.I.; Schneider, C.; Kopf, M.; Helenius, A.; Mercer, J. siRNA screen of early poxvirus genes identifies the AAA+ ATPase D5 as the virus genome-uncoating factor. *Cell Host Microbe* **2014**, *15*, 103-112.
114. Katsafanas, G.C.; Moss, B. Vaccinia virus intermediate stage transcription is complemented by Ras-GTPase-activating protein SH3 domain-binding protein (G3BP) and cytoplasmic activation/proliferation-associated protein (p137) individually or as a heterodimer. *J Biol Chem* **2004**, *279*, 52210-52217.
115. Dellis, S.; Strickland, K.C.; McCrary, W.J.; Patel, A.; Stocum, E.; Wright, C.F. Protein interactions among the vaccinia virus late transcription factors. *Virology* **2004**, *329*, 328-336. interactions among the vaccinia virus late transcription factors. *Virology* **2004**, *329*, 328-336.
116. Wright, C.F.; Oswald, B.W.; Dellis, S. Vaccinia virus late transcription is activated in vitro by cellular heterogeneous nuclear ribonucleoproteins. *J Biol Chem* **2001**, *276*, 40680-40686.

117. Schramm, B.; Locker, J.K. Cytoplasmic organization of poxvirus DNA replication. *Traffic* **2005**, *6*, 839-846.
118. Moss, B. Poxvirus DNA replication. *Cold Spring Harb Perspect Biol* **2013**, *5*.
119. Yang, Z.; Reynolds, S.E.; Martens, C.A.; Bruno, D.P.; Porcella, S.F.; Moss, B. Expression profiling of the intermediate and late stages of poxvirus replication. *J Virol* **2011**, *85*, 9899-9908.
120. Smith, G.L.; Law, M. The exit of vaccinia virus from infected cells. *Virus Res* **2004**, *106*, 189-197.
121. Manes, N.P.; Estep, R.D.; Mottaz, H.M.; Moore, R.J.; Clauss, T.R.; Monroe, M.E.; Du, X.; Adkins, J.N.; Wong, S.W.; Smith, R.D. Comparative proteomics of human monkeypox and vaccinia intracellular mature and extracellular enveloped virions. *J Proteome Res* **2008**, *7*, 960-968.
122. Yoder, J.D.; Chen, T.S.; Gagnier, C.R.; Vemulapalli, S.; Maier, C.S.; Hruby, D.E. Pox proteomics: Mass spectrometry analysis and identification of vaccinia virion proteins. *Virol J* **2006**, *3*, 10.
123. Doellinger, J. Dissertation: Proteomanalysen der Virus-Wirt-Wechselwirkung von Kuhpockenviren at the Robert Koch Institute, ZBS 1, **2014**.
124. Calistri, A.; Munegato, D.; Carli, I.; Parolin, C.; Palu, G. The ubiquitin-conjugating system: Multiple roles in viral replication and infection. *Cells* **2014**, *3*, 386-417.
125. Lopez, T.; Silva-Ayala, D.; Lopez, S.; Arias, C.F. Replication of the rotavirus genome requires an active ubiquitin-proteasome system. *J Virol* **2011**, *85*, 11964-11971.
126. Raaben, M.; Posthuma, C.C.; Verheije, M.H.; te Lintelo, E.G.; Kikkert, M.; Drijfhout, J.W.; Snijder, E.J.; Rottier, P.J.; de Haan, C.A. The ubiquitin-proteasome system plays an important role during various stages of the coronavirus infection cycle. *J Virol* **2010**, *84*, 7869-7879.
127. Satheshkumar, P.S.; Anton, L.C.; Sanz, P.; Moss, B. Inhibition of the ubiquitin-proteasome system prevents vaccinia virus DNA replication and expression of intermediate and late genes. *J Virol* **2009**, *83*, 2469-2479.
128. Teale, A.; Campbell, S.; Van Buuren, N.; Magee, W.C.; Watmough, K.; Couturier, B.; Shipclark, R.; Barry, M. Orthopoxviruses require a functional ubiquitin-proteasome system for productive replication. *J Virol* **2009**, *83*, 2099-2108.
129. Mercer, J.; Snijder, B.; Sacher, R.; Burkard, C.; Bleck, C.K.; Stahlberg, H.; Pelkmans, L.; Helenius, A. RNAi screening reveals proteasome- and cullin3-dependent stages in vaccinia virus infection. *Cell Rep* **2012**, *2*, 1036-1047.
130. Barry, M.; van Buuren, N.; Burles, K.; Mottet, K.; Wang, Q.; Teale, A. Poxvirus exploitation of the ubiquitin-proteasome system. *Viruses* **2010**, *2*, 2356-2380.
131. Huang, J.; Huang, Q.; Zhou, X.; Shen, M.M.; Yen, A.; Yu, S.X.; Dong, G.; Qu, K.; Huang, P.; Anderson, E.M.*, et al.* The poxvirus p28 virulence factor is an E3 ubiquitin ligase. *J Biol Chem* **2004**, *279*, 54110-54116.
132. Nerenberg, B.T.; Taylor, J.; Bartee, E.; Gouveia, K.; Barry, M.; Fruh, K. The poxviral ring protein p28 is a ubiquitin ligase that targets ubiquitin to viral replication factories. *J Virol* **2005**, *79*, 597-601.
133. Cone, K.R.; Kronenberg, Z.N.; Yandell, M.; Elde, N.C. Emergence of a viral RNA polymerase variant during gene copy number amplification promotes rapid evolution of vaccinia virus. *J Virol* **2017**, *91*.
134. Modrow, S., Falke, D, Truyen, U, Schätzl, H. Molekulare Virologie. 3. Auflage. Springer Spektrum Verlag: Heidelberg, **2010,** 610-634.
135. Culyba, M.J.; Minkah, N.; Hwang, Y.; Benhamou, O.M.; Bushman, F.D. DNA branch nuclease activity of vaccinia A22 resolvase. *J Biol Chem* **2007**, *282*, 34644-34652.
136. Eckert, D.; Williams, O.; Meseda, C.A.; Merchlinsky, M. Vaccinia virus nicking-joining enzyme is encoded by K4L (VACWR035). *J Virol* **2005**, *79*, 15084-15090.
137. Stuart, D.T.; Upton, C.; Higman, M.A.; Niles, E.G.; McFadden, G. A poxvirus-encoded uracil DNA glycosylase is essential for virus viability. *J Virol* **1993**, *67*, 2503-2512.
138. Czarnecki, M.W.; Traktman, P. The vaccinia virus DNA polymerase and its processivity factor. *Virus Res* **2017**.

139. Stanitsa, E.S.; Arps, L.; Traktman, P. Vaccinia virus uracil DNA glycosylase interacts with the A20 protein to form a heterodimeric processivity factor for the viral DNA polymerase. *J Biol Chem* **2006**, *281*, 3439-3451.
140. Domingo, E. Mechanisms of viral emergence. *Vet Res* **2010**, *41*, 38.
141. Brennan, G.; Kitzman, J.O.; Shendure, J.; Geballe, A.P. Experimental evolution identifies vaccinia virus mutations in A24R and A35R that antagonize the protein kinase R pathway and accompany collapse of an extragenic gene amplification. *J Virol* **2015**, *89*, 9986-9997.
142. Hendrickson, R.C.; Wang, C.; Hatcher, E.L.; Lefkowitz, E.J. Orthopoxvirus genome evolution: The role of gene loss. *Viruses* **2010**, *2*, 1933-1967.
143. Fenner, F.; Comben, B.M. [Genetic studies with mammalian poxviruses. I. Demonstration of recombination between two strains of vaccina virus]. *Virology* **1958**, *5*, 530-548.
144. Dumbell, K.R.; Bedson, H.S. The use of ceiling temperature and reactivation in the isolation of pox virus hybrids. *J Hyg (Lond)* **1964**, *62*, 133-140.
145. Strayer, D.S.; Skaletsky, E.; Cabirac, G.F.; Sharp, P.A.; Corbeil, L.B.; Sell, S.; Leibowitz, J.L. Malignant rabbit fibroma virus causes secondary immunosuppression in rabbits. *J Immunol* **1983**, *130*, 399-404.
146. Gammon, D.B.; Evans, D.H. The 3'-to-5' exonuclease activity of vaccinia virus DNA polymerase is essential and plays a role in promoting virus genetic recombination. *J Virol* **2009**, *83*, 4236-4250.
147. McFadden, G.; Murphy, P.M. Host-related immunomodulators encoded by poxviruses and herpesviruses. *Curr Opin Microbiol* **2000**, *3*, 371-378.
148. Patel, D.D.; Pickup, D.J. The second-largest subunit of the poxvirus RNA polymerase is similar to the corresponding subunits of procaryotic and eucaryotic RNA polymerases. *J Virol* **1989**, *63*, 1076-1086.
149. Ahn, B.Y.; Gershon, P.D.; Jones, E.V.; Moss, B. Identification of rpo30, a vaccinia virus RNA polymerase gene with structural similarity to a eucaryotic transcription elongation factor. *Mol Cell Biol* **1990**, *10*, 5433-5441.
150. Schroeder, K.; Nitsche, A. Multicolour, multiplex real-time pcr assay for the detection of human-pathogenic poxviruses. *Mol Cell Probes* **2010**, *24*, 110-113.
151. Wolfel, R.; Paweska, J.T.; Petersen, N.; Grobbelaar, A.A.; Leman, P.A.; Hewson, R.; Georges-Courbot, M.C.; Papa, A.; Gunther, S.; Drosten, C. Virus detection and monitoring of viral load in Crimean-Congo hemorrhagic fever virus patients. *Emerg Infect Dis* **2007**, *13*, 1097-1100.
152. Mahy, B.; van Regenmortel, M. Desk encyclopedia of human and medical virology. 1st edition, Academic Press: **2010**, 670.
153. Langmead, B.; Salzberg, S.L. Fast gapped-read alignment with bowtie 2. *Nat Methods* **2012**, *9*, 357-359.
154. Cox, J.; Mann, M. MaxQuant enables high peptide identification rates, individualized p.p.b.-range mass accuracies and proteome-wide protein quantification. *Nat Biotechnol* **2008**, *26*, 1367-1372.
155. Chou, M.F.; Schwartz, D. Biological sequence motif discovery using motif-x. *Curr Protoc Bioinformatics* **2011**, *Chapter 13*, Unit 13 15-24.
156. Tyanova, S.; Temu, T.; Sinitcyn, P.; Carlson, A.; Hein, M.Y.; Geiger, T.; Mann, M.; Cox, J. The Perseus computational platform for comprehensive analysis of (prote)omics data. *Nat Methods* **2016**, *13*, 731-740.
157. Tausch, S.H.; Renard, B.Y.; Nitsche, A.; Dabrowski, P.W. RAMBO-K: Rapid and sensitive removal of background sequences from next generation sequencing data. *PLoS One* **2015**, *10*, e0137896.
158. Bankevich, A.; Nurk, S.; Antipov, D.; Gurevich, A.A.; Dvorkin, M.; Kulikov, A.S.; Lesin, V.M.; Nikolenko, S.I.; Pham, S.; Prjibelski, A.D.*, et al.* Spades: A new genome assembly algorithm and its applications to single-cell sequencing. *J Comput Biol* **2012**, *19*, 455-477.
159. Szklarczyk, D.; Franceschini, A.; Wyder, S.; Forslund, K.; Heller, D.; Huerta-Cepas, J.; Simonovic, M.; Roth, A.; Santos, A.; Tsafou, K.P.*, et al.* STRING v10: protein-protein interaction networks, integrated over the tree of life. *Nucleic Acids Res* **2015**, *43*, D447-452.
160. Zerbino, D.R.; Birney, E. Velvet: Algorithms for de novo short read assembly using de Bruijn graphs. *Genome Res* **2008**, *18*, 821-829.

161. Wisniewski, J.R.; Gaugaz, F.Z. Fast and sensitive total protein and peptide assays for proteomic analysis. *Anal Chem* **2015**, *87*, 4110-4116.
162. Laue, M. Electron microscopy of viruses. *Methods Cell Biol* **2010**, *96*, 1-20.
163. Earl, P.L.; Moss, B.; Wyatt, L.S.; Carroll, M.W. Generation of recombinant vaccinia viruses. *Curr Protoc Mol Biol* **2001**, *Chapter 16*, Unit16 17.
164. Puppe, A. Dissertation at the Robert Koch Insitute, ZBS 1, **2014**.
165. Bolger, A.M.; Lohse, M.; Usadel, B. Trimmomatic: A flexible trimmer for illumina sequence data. *Bioinformatics* **2014**, *30*, 2114-2120.
166. Andrews, S. Babraham bioinformatics: Fastqc. http://www.bioinformatics.babraham.ac.uk/projects/fastqc/ (access date **16.08.2017**).
167. Kearse, M.; Moir, R.; Wilson, A.; Stones-Havas, S.; Cheung, M.; Sturrock, S.; Buxton, S.; Cooper, A.; Markowitz, S.; Duran, C.*, et al.* Geneious basic: An integrated and extendable desktop software platform for the organization and analysis of sequence data. *Bioinformatics* **2012**, *28*, 1647-1649.
168. Kim, D.; Pertea, G.; Trapnell, C.; Pimentel, H.; Kelley, R.; Salzberg, S.L. TopHat2: Accurate alignment of transcriptomes in the presence of insertions, deletions and gene fusions. *Genome Biol* **2013**, *14*, R36.
169. Liao, Y.; Smyth, G.K.; Shi, W. FeatureCounts: An efficient general purpose program for assigning sequence reads to genomic features. *Bioinformatics* **2014**, *30*, 923-930.
170. Kulak, N.A.; Pichler, G.; Paron, I.; Nagaraj, N.; Mann, M. Minimal, encapsulated proteomic-sample processing applied to copy-number estimation in eukaryotic cells. *Nat Methods* **2014**, *11*, 319-324.
171. Wisniewski, J.R.; Zougman, A.; Nagaraj, N.; Mann, M. Universal sample preparation method for proteome analysis. *Nat Methods* **2009**, *6*, 359-362.
172. Ishihama, Y.; Rappsilber, J.; Mann, M. Modular stop and go extraction tips with stacked disks for parallel and multidimensional peptide fractionation in proteomics. *J Proteome Res* **2006**, *5*, 988-994.
173. Hahne, H.; Pachl, F.; Ruprecht, B.; Maier, S.K.; Klaeger, S.; Helm, D.; Medard, G.; Wilm, M.; Lemeer, S.; Kuster, B. DMSO enhances electrospray response, boosting sensitivity of proteomic experiments. *Nat Methods* **2013**, *10*, 989-991.
174. Strzelecka, D.; Holman, S.W.; Eyers, C.E. Evaluation of dimethyl sulfoxide (DMSO) as a mobile phase additive during top 3 label-free quantitative proteomics. *Int J Mass Spectrom* **2015**, *391*, 157-160.
175. Bielow, C.; Mastrobuoni, G.; Kempa, S. Proteomics quality control: Quality control software for MaxQuant results. *J Proteome Res* **2016**, *15*, 777-787.
176. Cox, J.; Neuhauser, N.; Michalski, A.; Scheltema, R.A.; Olsen, J.V.; Mann, M. Andromeda: A peptide search engine integrated into the maxquant environment. *J Proteome Res* **2011**, *10*, 1794-1805.
177. Cox, J.; Hein, M.Y.; Luber, C.A.; Paron, I.; Nagaraj, N.; Mann, M. Accurate proteome-wide label-free quantification by delayed normalization and maximal peptide ratio extraction, termed MaxLFQ. *Mol Cell Proteomics* **2014**, *13*, 2513-2526.
178. Kall, L.; Canterbury, J.D.; Weston, J.; Noble, W.S.; MacCoss, M.J. Semi-supervised learning for peptide identification from shotgun proteomics datasets. *Nat Methods* **2007**, *4*, 923-925.
179. Wisniewski, J.R.; Ostasiewicz, P.; Dus, K.; Zielinska, D.F.; Gnad, F.; Mann, M. Extensive quantitative remodeling of the proteome between normal colon tissue and adenocarcinoma. *Mol Syst Biol* **2012**, *8*, 611.
180. Wisniewski, J.R.; Rakus, D. Multi-enzyme digestion FASP and the 'Total Protein Approach'-based absolute quantification of the escherichia coli proteome. *J Proteomics* **2014**, *109*, 322-331.
181. Fritsch, A. Master's thesis at the Robert Koch Institute, ZBS 1: The role of the ubiquitin-proteasome system in CPXV infections and the ubiquitinome of CPXV virions. **2017**.
182. Goldberg, A.L. Development of proteasome inhibitors as research tools and cancer drugs. *J Cell Biol* **2012**, *199*, 583-588.
183. Udeshi, N.D.; Mertins, P.; Svinkina, T.; Carr, S.A. Large-scale identification of ubiquitination sites by mass spectrometry. *Nat Protoc* **2013**, *8*, 1950-1960.

184. Pedersen, K.; Snijder, E.J.; Schleich, S.; Roos, N.; Griffiths, G.; Locker, J.K. Characterization of vaccinia virus intracellular cores: Implications for viral uncoating and core structure. *J Virol* **2000**, *74*, 3525-3536.
185. Jensen, O.N.; Houthaeve, T.; Shevchenko, A.; Cudmore, S.; Ashford, T.; Mann, M.; Griffiths, G.; Krijnse Locker, J. Identification of the major membrane and core proteins of vaccinia virus by two-dimensional electrophoresis. *J Virol* **1996**, *70*, 7485-7497.
186. Meng, X.; Embry, A.; Sochia, D.; Xiang, Y. Vaccinia virus A6L encodes a virion core protein required for formation of mature virion. *J Virol* **2007**, *81*, 1433-1443.
187. Khatter, H.; Myasnikov, A.G.; Natchiar, S.K.; Klaholz, B.P. Structure of the human 80S ribosome. *Nature* **2015**, *520*, 640-645.
188. Fenner, F.; McAuslan, R.; Mims, C. The biology of animal viruses. 2nd edition. Academic Press **1974**, 207.
189. Duncan, R.; Hershey, J.W. Identification and quantitation of levels of protein synthesis initiation factors in crude HeLa cell lysates by two-dimensional polyacrylamide gel electrophoresis. *J Biol Chem* **1983**, *258*, 7228-7235.
190. Jefferts, E.R.; Holowczak, J.A. RNA synthesis in vaccinia-infected L cells: Inhibition of ribosome formation and maturation. *Virology* **1971**, *46*, 730-744.
191. Peters, N.E.; Ferguson, B.J.; Mazzon, M.; Fahy, A.S.; Krysztofinska, E.; Arribas-Bosacoma, R.; Pearl, L.H.; Ren, H.; Smith, G.L. A mechanism for the inhibition of DNA-PK-mediated DNA sensing by a virus. *PLoS Pathog* **2013**, *9*, e1003649.
192. Yang, Z.; Bruno, D.P.; Martens, C.A.; Porcella, S.F.; Moss, B. Simultaneous high-resolution analysis of vaccinia virus and host cell transcriptomes by deep RNA sequencing. *Proc Natl Acad Sci U S A* **2010**, *107*, 11513-11518.
193. Yuen, L.; Moss, B. Oligonucleotide sequence signaling transcriptional termination of vaccinia virus early genes. *Proc Natl Acad Sci U S A* **1987**, *84*, 6417-6421.
194. Hansen, K.D.; Brenner, S.E.; Dudoit, S. Biases in Illumina transcriptome sequencing caused by random hexamer priming. *Nucleic Acids Res* **2010**, *38*, e131.
195. Senkevich, T.G.; Ward, B.M.; Moss, B. Vaccinia virus entry into cells is dependent on a virion surface protein encoded by the A28L gene. *J Virol* **2004**, *78*, 2357-2366.
196. Sharp, D.G.; Sadhukhan, P.; Galasso, G.J. Quality changes in vaccinia virus during adaptation to growth in cultures of Earle's L cells. *J Bacteriol* **1964**, *88*, 309-312.
197. Meyer, H.; Sutter, G.; Mayr, A. Mapping of deletions in the genome of the highly attenuated vaccinia virus mva and their influence on virulence. *J Gen Virol* **1991**, *72 (Pt 5)*, 1031-1038.
198. Traktman, P. DNA replication in eukaryotic cells. Chapter 27: Poxvirus DNA replication *Cold Spring Harb Protoc* **1996**, 775-797.
199. Schirmer, M.; Ijaz, U.Z.; D'Amore, R.; Hall, N.; Sloan, W.T.; Quince, C. Insight into biases and sequencing errors for amplicon sequencing with the Illumina MiSeq platform. *Nucleic Acids Res* **2015**, *43*, e37.
200. Lou, D.I.; Hussmann, J.A.; McBee, R.M.; Acevedo, A.; Andino, R.; Press, W.H.; Sawyer, S.L. High-throughput DNA sequencing errors are reduced by orders of magnitude using circle sequencing. *Proc Natl Acad Sci U S A* **2013**, *110*, 19872-19877.
201. Schirmer, M.; D'Amore, R.; Ijaz, U.Z.; Hall, N.; Quince, C. Illumina error profiles: Resolving fine-scale variation in metagenomic sequencing data. *BMC Bioinformatics* **2016**, *17*, 125.
202. Meacham, F.; Boffelli, D.; Dhahbi, J.; Martin, D.I.; Singer, M.; Pachter, L. Identification and correction of systematic error in high-throughput sequence data. *BMC Bioinformatics* **2011**, *12*, 451.
203. Aird, D.; Ross, M.G.; Chen, W.S.; Danielsson, M.; Fennell, T.; Russ, C.; Jaffe, D.B.; Nusbaum, C.; Gnirke, A. Analyzing and minimizing PCR amplification bias in Illumina sequencing libraries. *Genome Biol* **2011**, *12*, R18.
204. Hatcher, E.L.; Wang, C.; Lefkowitz, E.J. Genome variability and gene content in chordopoxviruses: Dependence on microsatellites. *Viruses* **2015**, *7*, 2126-2146.
205. Knutson, B.A.; Broyles, S.S. Expansion of poxvirus RNA polymerase subunits sharing homology with corresponding subunits of RNA polymerase II. *Virus Genes* **2008**, *36*, 307-311.
206. Moss, B.; Ahn, B.Y.; Amegadzie, B.; Gershon, P.D.; Keck, J.G. Cytoplasmic transcription system encoded by vaccinia virus. *J Biol Chem* **1991**, *266*, 1355-1358.

207. Cresawn, S.G.; Prins, C.; Latner, D.R.; Condit, R.C. Mapping and phenotypic analysis of spontaneous isatin-beta-thiosemicarbazone resistant mutants of vaccinia virus. *Virology* **2007**, *363*, 319-332.
208. Condit, R.C.; Easterly, R.; Pacha, R.F.; Fathi, Z.; Meis, R.J. A vaccinia virus isatin-beta-thiosemicarbazone resistance mutation maps in the viral gene encoding the 132-kDa subunit of RNA polymerase. *Virology* **1991**, *185*, 857-861.
209. Prins, C.; Cresawn, S.G.; Condit, R.C. An isatin-beta-thiosemicarbazone-resistant vaccinia virus containing a mutation in the second largest subunit of the viral RNA polymerase is defective in transcription elongation. *J Biol Chem* **2004**, *279*, 44858-44871.
210. Condit, R.C.; Niles, E.G. Regulation of viral transcription elongation and termination during vaccinia virus infection. *Biochim Biophys Acta* **2002**, *1577*, 325-336.
211. Colby, C.; Duesberg, P.H. Double-stranded RNA in vaccinia virus infected cells. *Nature* **1969**, *222*, 940-944.
212. Son, K.N.; Liang, Z.; Lipton, H.L. Double-stranded RNA is detected by immunofluorescence analysis in RNA and DNA virus infections, including those by negative-stranded RNA viruses. *J Virol* **2015**, *89*, 9383-9392.
213. Willis, K.L.; Langland, J.O.; Shisler, J.L. Viral double-stranded RNAs from vaccinia virus early or intermediate gene transcripts possess PKR activating function, resulting in NF-kappaB activation, when the K1 protein is absent or mutated. *J Biol Chem* **2011**, *286*, 7765-7778.
214. Carpentier, K.S.; Geballe, A.P. An evolutionary view of the arms race between protein kinase R and large DNA viruses. *J Virol* **2016**, *90*, 3280-3283.
215. Davies, M.V.; Elroy-Stein, O.; Jagus, R.; Moss, B.; Kaufman, R.J. The vaccinia virus K3L gene product potentiates translation by inhibiting double-stranded-RNA-activated protein kinase and phosphorylation of the alpha subunit of eukaryotic initiation factor 2. *J Virol* **1992**, *66*, 1943-1950.
216. Davies, M.V.; Chang, H.W.; Jacobs, B.L.; Kaufman, R.J. The E3L and K3L vaccinia virus gene products stimulate translation through inhibition of the double-stranded RNA-dependent protein kinase by different mechanisms. *J Virol* **1993**, *67*, 1688-1692.
217. Daulny, A.; Geng, F.; Muratani, M.; Geisinger, J.M.; Salghetti, S.E.; Tansey, W.P. Modulation of RNA polymerase II subunit composition by ubiquitylation. *Proc Natl Acad Sci U S A* **2008**, *105*, 19649-19654.
218. Latner, D.R.; Xiang, Y.; Lewis, J.I.; Condit, J.; Condit, R.C. The vaccinia virus bifunctional gene J3 (nucleoside-2'-o-)-methyltransferase and poly(A) polymerase stimulatory factor is implicated as a positive transcription elongation factor by two genetic approaches. *Virology* **2000**, *269*, 345-355.
219. Howard, A.R.; Moss, B. Formation of orthopoxvirus cytoplasmic A-type inclusion bodies and embedding of virions are dynamic processes requiring microtubules. *J Virol* **2012**, *86*, 5905-5914.
220. McKelvey, T.A.; Andrews, S.C.; Miller, S.E.; Ray, C.A.; Pickup, D.J. Identification of the orthopoxvirus p4c gene, which encodes a structural protein that directs intracellular mature virus particles into A-type inclusions. *J Virol* **2002**, *76*, 11216-11225.
221. Kastenmayer, R.J.; Maruri-Avidal, L.; Americo, J.L.; Earl, P.L.; Weisberg, A.S.; Moss, B. Elimination of A-type inclusion formation enhances cowpox virus replication in mice: Implications for orthopoxvirus evolution. *Virology* **2014**, *452-453*, 59-66.
222. Chang, S.J.; Chang, Y.X.; Izmailyan, R.; Tang, Y.L.; Chang, W. Vaccinia virus A25 and A26 proteins are fusion suppressors for mature virions and determine strain-specific virus entry pathways into HeLa, CHO-K1, and L cells. *J Virol* **2010**, *84*, 8422-8432.
223. Bengali, Z.; Satheshkumar, P.S.; Moss, B. Orthopoxvirus species and strain differences in cell entry. *Virology* **2012**, *433*, 506-512.
224. Bengali, Z.; Townsley, A.C.; Moss, B. Vaccinia virus strain differences in cell attachment and entry. *Virology* **2009**, *389*, 132-140.
225. Husain, M.; Moss, B. Vaccinia virus F13L protein with a conserved phospholipase catalytic motif induces colocalization of the B5R envelope glycoprotein in post-Golgi vesicles. *J Virol* **2001**, *75*, 7528-7542.
226. Bidgood, S.R.; Mercer, J. Cloak and dagger: Alternative immune evasion and modulation strategies of poxviruses. *Viruses* **2015**, *7*, 4800-4825.

227. Vliegen, I.; Yang, G.; Hruby, D.; Jordan, R.; Neyts, J. Deletion of the vaccinia virus F13L gene results in a highly attenuated virus that mounts a protective immune response against subsequent vaccinia virus challenge. *Antiviral Res* **2012**, *93*, 160-166.
228. Doceul, V.; Hollinshead, M.; Breiman, A.; Laval, K.; Smith, G.L. Protein B5 is required on extracellular enveloped vaccinia virus for repulsion of superinfecting virions. *J Gen Virol* **2012**, *93*, 1876-1886.
229. Doceul, V.; Hollinshead, M.; van der Linden, L.; Smith, G.L. Repulsion of superinfecting virions: A mechanism for rapid virus spread. *Science* **2010**, *327*, 873-876.
230. Takeuchi, O.; Akira, S. Pattern recognition receptors and inflammation. *Cell* **2010**, *140*, 805-820.
231. Mohamed, M.R.; McFadden, G. NFkB inhibitors: Strategies from poxviruses. *Cell Cycle* **2009**, *8*, 3125-3132.
232. DiPerna, G.; Stack, J.; Bowie, A.G.; Boyd, A.; Kotwal, G.; Zhang, Z.; Arvikar, S.; Latz, E.; Fitzgerald, K.A.; Marshall, W.L. Poxvirus protein N1L targets the I-kappaB kinase complex, inhibits signaling to NF-kappaB by the tumor necrosis factor superfamily of receptors, and inhibits NF-kappaB and IRF3 signaling by toll-like receptors. *J Biol Chem* **2004**, *279*, 36570-36578.
233. Maluquer de Motes, C.; Schiffner, T.; Sumner, R.P.; Smith, G.L. Vaccinia virus virulence factor N1 can be ubiquitylated on multiple lysine residues. *J Gen Virol* **2014**, *95*, 2038-2049.
234. Zhang, Z.; Abrahams, M.R.; Hunt, L.A.; Suttles, J.; Marshall, W.; Lahiri, D.K.; Kotwal, G.J. The vaccinia virus N1L protein influences cytokine secretion in vitro after infection. *Ann N Y Acad Sci* **2005**, *1056*, 69-86.
235. Bartlett, N.; Symons, J.A.; Tscharke, D.C.; Smith, G.L. The vaccinia virus N1L protein is an intracellular homodimer that promotes virulence. *J Gen Virol* **2002**, *83*, 1965-1976.
236. Schulz, K.S.; Mossman, K.L. Viral evasion strategies in type I IFN signaling - a summary of recent developments. *Front Immunol* **2016**, *7*, 498.
237. Symons, J.A.; Alcami, A.; Smith, G.L. Vaccinia virus encodes a soluble typeI interferon receptor of novel structure and broad species specificity. *Cell* **1995**, *81*, 551-560.
238. Waibler, Z.; Anzaghe, M.; Frenz, T.; Schwantes, A.; Pohlmann, C.; Ludwig, H.; Palomo-Otero, M.; Alcami, A.; Sutter, G.; Kalinke, U. Vaccinia virus-mediated inhibition of type I interferon responses is a multifactorial process involving the soluble type i interferon receptor B18 and intracellular components. *J Virol* **2009**, *83*, 1563-1571.
239. van den Broek, M.F.; Muller, U.; Huang, S.; Zinkernagel, R.M.; Aguet, M. Immune defence in mice lacking type I and/or type II interferon receptors. *Immunol Rev* **1995**, *148*, 5-18.
240. Alcami, A.; Symons, J.A.; Smith, G.L. The vaccinia virus soluble alpha/beta interferon (IFN) receptor binds to the cell surface and protects cells from the antiviral effects of IFN. *J Virol* **2000**, *74*, 11230-11239.
241. Schoenborn, J.R.; Wilson, C.B. Regulation of interferon-gamma during innate and adaptive immune responses. *Adv Immunol* **2007**, *96*, 41-101.
242. Alcami, A.; Smith, G.L. Vaccinia, cowpox, and camelpox viruses encode soluble gamma interferon receptors with novel broad species specificity. *J Virol* **1995**, *69*, 4633-4639.
243. Young, D.F.; Galiano, M.C.; Lemon, K.; Chen, Y.H.; Andrejeva, J.; Duprex, W.P.; Rima, B.K.; Randall, R.E. Mumps virus enders strain is sensitive to interferon (IFN) despite encoding a functional IFN antagonist. *J Gen Virol* **2009**, *90*, 2731-2738.
244. Brzozka, K.; Finke, S.; Conzelmann, K.K. Identification of the rabies virus alpha/beta interferon antagonist: Phosphoprotein P interferes with phosphorylation of interferon regulatory factor 3. *J Virol* **2005**, *79*, 7673-7681.
245. Peng, Y.; Lin, F.C.; Verardi, P.H.; Jones, L.A.; Yilma, T.D. Lower levels of gamma interferon expressed by a pseudotyped single-cycle simian immunodeficiency virus enhance immunogenicity in rats. *J Virol* **2009**, *83*, 1592-1601.
246. Isaacs, S.N.; Kotwal, G.J.; Moss, B. Vaccinia virus complement-control protein prevents antibody-dependent complement-enhanced neutralization of infectivity and contributes to virulence. *Proc Natl Acad Sci U S A* **1992**, *89*, 628-632.
247. Girgis, N.M.; Dehaven, B.C.; Xiao, Y.; Alexander, E.; Viner, K.M.; Isaacs, S.N. The vaccinia virus complement control protein modulates adaptive immune responses during infection. *J Virol* **2011**, *85*, 2547-2556.

248. Alcami, A.; Symons, J.A.; Collins, P.D.; Williams, T.J.; Smith, G.L. Blockade of chemokine activity by a soluble chemokine binding protein from vaccinia virus. *J Immunol* **1998**, *160*, 624-633.
249. Reading, P.C.; Symons, J.A.; Smith, G.L. A soluble chemokine-binding protein from vaccinia virus reduces virus virulence and the inflammatory response to infection. *Journal of Immunology* **2003**, *170*, 1435-1442.
250. Almazan, F.; Tscharke, D.C.; Smith, G.L. The vaccinia virus superoxide dismutase-like protein (A45R) is a virion component that is nonessential for virus replication. *J Virol* **2001**, *75*, 7018-7029.
251. Lin, Y.C.; Li, J.; Irwin, C.R.; Jenkins, H.; DeLange, L.; Evans, D.H. Vaccinia virus DNA ligase recruits cellular topoisomerase II to sites of viral replication and assembly. *J Virol* **2008**, *82*, 5922-5932.
252. Prichard, M.N.; Kern, E.R.; Quenelle, D.C.; Keith, K.A.; Moyer, R.W.; Turner, P.C. Vaccinia virus lacking the deoxyuridine triphosphatase gene (F2L) replicates well in vitro and in vivo, but is hypersensitive to the antiviral drug (n)-methanocarbathymidine. *Virol J* **2008**, *5*, 39.
253. Senkevich, T.G.; White, C.L.; Koonin, E.V.; Moss, B. Complete pathway for protein disulfide bond formation encoded by poxviruses. *Proc Natl Acad Sci U S A* **2002**, *99*, 6667-6672.
254. Schmidt, F.I.; Bleck, C.K.; Reh, L.; Novy, K.; Wollscheid, B.; Helenius, A.; Stahlberg, H.; Mercer, J. Vaccinia virus entry is followed by core activation and proteasome-mediated release of the immunomodulatory effector VH1 from lateral bodies. *Cell Rep* **2013**, *4*, 464-476.
255. White, C.L.; Senkevich, T.G.; Moss, B. Vaccinia virus G4L glutaredoxin is an essential intermediate of a cytoplasmic disulfide bond pathway required for virion assembly. *J Virol* **2002**, *76*, 467-472.
256. White, C.L.; Weisberg, A.S.; Moss, B. A glutaredoxin, encoded by the G4L gene of vaccinia virus, is essential for virion morphogenesis. *J Virol* **2000**, *74*, 9175-9183.
257. Castro, A.P.; Carvalho, T.M.; Moussatche, N.; Damaso, C.R. Redistribution of cyclophilin a to viral factories during vaccinia virus infection and its incorporation into mature particles. *J Virol* **2003**, *77*, 9052-9068.
258. Boone, R.F.; Moss, B. Sequence complexity and relative abundance of vaccinia virus mRNA's synthesized in vivo and in vitro. *J Virol* **1978**, *26*, 554-569.
259. Chang, C.W.; Li, H.C.; Hsu, C.F.; Chang, C.Y.; Lo, S.Y. Increased ATP generation in the host cell is required for efficient vaccinia virus production. *J Biomed Sci* **2009**, *16*, 80.
260. Hung, J.J.; Chung, C.S.; Chang, W. Molecular chaperone HSP90 is important for vaccinia virus growth in cells. *J Virol* **2002**, *76*, 1379-1390.
261. Liem, J.; Liu, J. Stress beyond translation: Poxviruses and more. *Viruses* **2016**, *8*.
262. Machesky, L.M.; Cole, N.B.; Moss, B.; Pollard, T.D. Vaccinia virus expresses a novel profilin with a higher affinity for polyphosphoinositides than actin. *Biochemistry* **1994**, *33*, 10815-10824.
263. Husain, M.; Moss, B. Similarities in the induction of post-Golgi vesicles by the vaccinia virus F13L protein and phospholipase d. *J Virol* **2002**, *76*, 7777-7789.
264. Stricher, F.; Macri, C.; Ruff, M.; Muller, S. HSPA8/hsc70 chaperone protein: Structure, function, and chemical targeting. *Autophagy* **2013**, *9*, 1937-1954.
265. Tran, K.; Mahr, J.A.; Spector, D.H. Proteasome subunits relocalize during human cytomegalovirus infection, and proteasome activity is necessary for efficient viral gene transcription. *J Virol* **2010**, *84*, 3079-3093.
266. Palacios, S.; Perez, L.H.; Welsch, S.; Schleich, S.; Chmielarska, K.; Melchior, F.; Locker, J.K. Quantitative SUMO-1 modification of a vaccinia virus protein is required for its specific localization and prevents its self-association. *Mol Biol Cell* **2005**, *16*, 2822-2835.
267. Gonzalez-Santamaria, J.; Campagna, M.; Garcia, M.A.; Marcos-Villar, L.; Gonzalez, D.; Gallego, P.; Lopitz-Otsoa, F.; Guerra, S.; Rodriguez, M.S.; Esteban, M.*, et al.* Regulation of vaccinia virus E3 protein by small ubiquitin-like modifier proteins. *Journal of Virology* **2011**, *85*, 12890-12900.
268. Miteva, M.; Keusekotten, K.; Hofmann, K.; Praefcke, G.J.; Dohmen, R.J. Sumoylation as a signal for polyubiquitylation and proteasomal degradation. *Subcell Biochem* **2010**, *54*, 195-214.
269. Lai, X.; Wang, L.; Witzmann, F.A. Issues and applications in label-free quantitative mass spectrometry. *Int J Proteomics* **2013**, *2013*, 756039.

270. Elena, S.F.; Sanjuan, R. Adaptive value of high mutation rates of RNA viruses: Separating causes from consequences. *J Virol* **2005**, *79*, 11555-11558.
271. Sanjuan, R.; Domingo-Calap, P. Mechanisms of viral mutation. *Cell Mol Life Sci* **2016**, *73*, 4433-4448.
272. Sciortino, M.T.; Taddeo, B.; Poon, A.P.; Mastino, A.; Roizman, B. Of the three tegument proteins that package mRNA in herpes simplex virions, one (VP22) transports the mRNA to uninfected cells for expression prior to viral infection. *Proc Natl Acad Sci U S A* **2002**, *99*, 8318-8323.
273. Wang, D.; Bresnahan, W.; Shenk, T. Human cytomegalovirus encodes a highly specific rantes decoy receptor. *Proc Natl Acad Sci U S A* **2004**, *101*, 16642-16647.
274. Costa, V.; Angelini, C.; De Feis, I.; Ciccodicola, A. Uncovering the complexity of transcriptomes with RNA-seq. *J Biomed Biotechnol* **2010**, *2010*, 853916.
275. Tolonen, N.; Doglio, L.; Schleich, S.; Krijnse Locker, J. Vaccinia virus DNA replication occurs in endoplasmic reticulum-enclosed cytoplasmic mini-nuclei. *Mol Biol Cell* **2001**, *12*, 2031-2046.
276. Jackson, R.; Standart, N. The awesome power of ribosome profiling. *RNA* **2015**, *21*, 652-654.
277. Mortazavi, A.; Williams, B.A.; McCue, K.; Schaeffer, L.; Wold, B. Mapping and quantifying mammalian transcriptomes by RNA-Seq. *Nat Methods* **2008**, *5*, 621-628.
278. Malboeuf, C.M.; Isaacs, S.J.; Tran, N.H.; Kim, B. Thermal effects on reverse transcription: Improvement of accuracy and processivity in cdna synthesis. *Biotechniques* **2001**, *30*, 1074-1078, 1080, 1082, passim.
279. Burgess, H.M.; Mohr, I. Cellular 5'-3' mRNA exonuclease XRN1 controls double-stranded RNA accumulation and anti-viral responses. *Cell Host Microbe* **2015**, *17*, 332-344.
280. Liu, S.W.; Katsafanas, G.C.; Liu, R.K.; Wyatt, L.S.; Moss, B. Poxvirus decapping enzymes enhance virulence by preventing the accumulation of dsrna and the induction of innate antiviral responses. *Cell Host Microbe* **2015**, *17*, 320-331.
281. Rubins, K.H.; Hensley, L.E.; Bell, G.W.; Wang, C.; Lefkowitz, E.J.; Brown, P.O.; Relman, D.A. Comparative analysis of viral gene expression programs during poxvirus infection: A transcriptional map of the vaccinia and monkeypox genomes. *PLoS One* **2008**, *3*, e2628.
282. Assarsson, E.; Greenbaum, J.A.; Sundstrom, M.; Schaffer, L.; Hammond, J.A.; Pasquetto, V.; Oseroff, C.; Hendrickson, R.C.; Lefkowitz, E.J.; Tscharke, D.C.*, et al.* Kinetic analysis of a complete poxvirus transcriptome reveals an immediate-early class of genes. *Proc Natl Acad Sci U S A* **2008**, *105*, 2140-2145.
283. Chou, W.; Ngo, T.; Gershon, P.D. An overview of the vaccinia virus infectome: A survey of the proteins of the poxvirus-infected cell. *J Virol* **2012**, *86*, 1487-1499.
284. Domi, A.; Beaud, G. The punctate sites of accumulation of vaccinia virus early proteins are precursors of sites of viral DNA synthesis. *J Gen Virol* **2000**, *81*, 1231-1235.
285. Conaway, R.C.; Brower, C.S.; Conaway, J.W. Emerging roles of ubiquitin in transcription regulation. *Science* **2002**, *296*, 1254-1258.
286. Harreman, M.; Taschner, M.; Sigurdsson, S.; Anindya, R.; Reid, J.; Somesh, B.; Kong, S.E.; Banks, C.A.; Conaway, R.C.; Conaway, J.W.*, et al.* Distinct ubiquitin ligases act sequentially for RNA polymerase II polyubiquitylation. *Proc Natl Acad Sci U S A* **2009**, *106*, 20705-20710.
287. Lee, K.B.; Sharp, P.A. Transcription-dependent polyubiquitination of RNA polymerase II requires lysine 63 of ubiquitin. *Biochemistry* **2004**, *43*, 15223-15229.
288. Thomas, D.; Tyers, M. Transcriptional regulation: Kamikaze activators. *Curr Biol* **2000**, *10*, R341-343.
289. Salghetti, S.E.; Caudy, A.A.; Chenoweth, J.G.; Tansey, W.P. Regulation of transcriptional activation domain function by ubiquitin. *Science* **2001**, *293*, 1651-1653.
290. Guharoy, M.; Bhowmick, P.; Sallam, M.; Tompa, P. Tripartite degrons confer diversity and specificity on regulated protein degradation in the ubiquitin-proteasome system. *Nat Commun* **2016**, *7*, 10239.
291. Hunter, T. The age of crosstalk: Phosphorylation, ubiquitination, and beyond. *Mol Cell* **2007**, *28*, 730-738.
292. Sun, H.; Zhang, A.; Yan, G.; Piao, C.; Li, W.; Sun, C.; Wu, X.; Li, X.; Chen, Y.; Wang, X. Metabolomic analysis of key regulatory metabolites in hepatitis c virus-infected tree shrews. *Mol Cell Proteomics* **2013**, *12*, 710-719.

293. Birungi, G.; Chen, S.M.; Loy, B.P.; Ng, M.L.; Li, S.F. Metabolomics approach for investigation of effects of dengue virus infection using the EA.hy926 cell line. *J Proteome Res* **2010**, *9*, 6523-6534.
294. Vizcaino, J.A.; Csordas, A.; Del-Toro, N.; Dianes, J.A.; Griss, J.; Lavidas, I.; Mayer, G.; Perez-Riverol, Y.; Reisinger, F.; Ternent, T.*, et al.* 2016 update of the PRIDE database and its related tools. *Nucleic Acids Res* **2016**, *44*, 11033.

Supplements

The MS proteomics data have been deposited to the ProteomeXchange Consortium via the PRIDE [294] partner repository with the dataset identifier PXD007567 (passaging experiment) and PXD006426 (ubiquitination experiment). Genomic sequence files are available from the NCBI Sequence Read Archive under the BioProject ID 399073 (passaging experiment) and PRJNA401971 (transcripts in CPXV IMV experiment).

Supplementary Figures

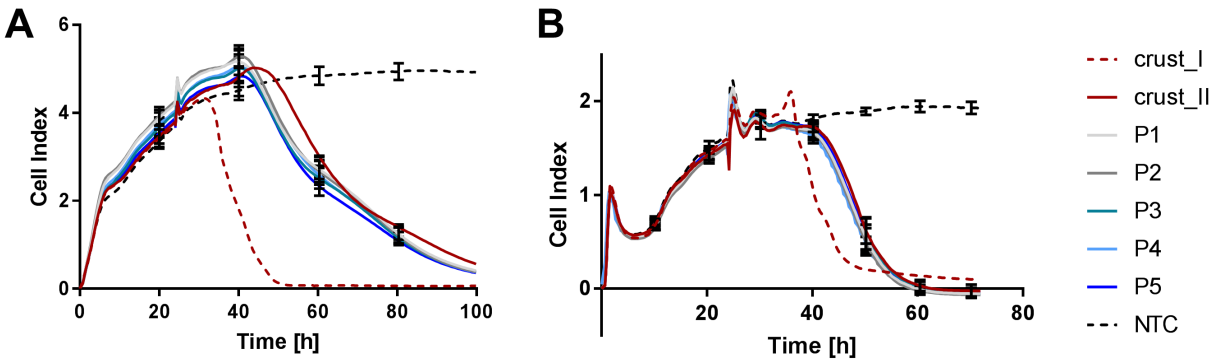

Figure S1. Real-time cell analysis of passaged and non-passaged CPXV. Repetition of the experiment. (**A**) HEp-2 or (**B**) Rat-2 cells were infected with passaged or non-passaged CPXV 24 h after seeding. Shown are mean values ± standard deviation of three biological replicates of passaged virions and four (HEp-2) or five (Rat-2) technical replicates non-passaged virions. In each cell line a single replicate of the non-passaged virions shows faster cell detachment (crust_I).

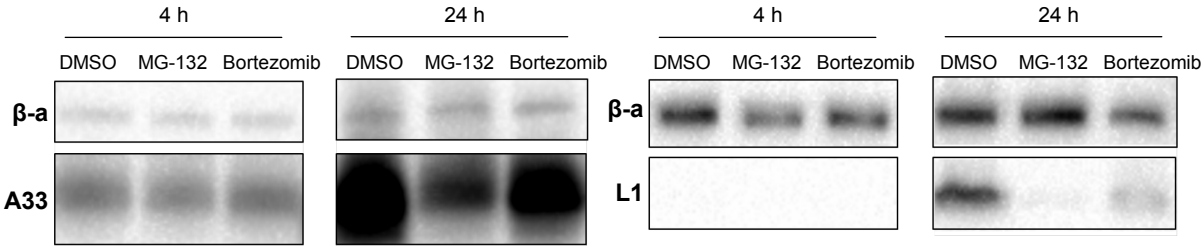

Figure S2. Western Blot of CPXV protein expression upon proteasome inhibition. HeLa cells were infected with CPXV BR at an MOI of 1 in the presence or absence of 10 µM MG-132, 1 µM Bortezomib or 1 % DMSO (control). At 4 and 24 h p.i. cells were harvested and Western blotted with anti-A33 (early/late) and anti-L1 (late). β-actin (β-a) was used as a loading control. Shown is one representative blot of three reproducible replicates.

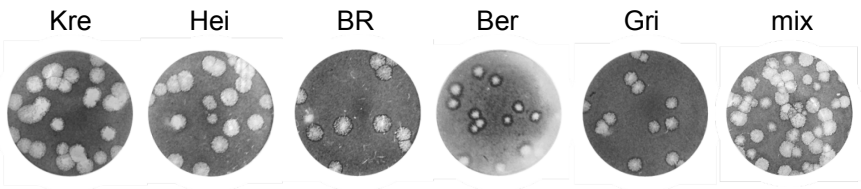

Figure S3. Plaque morphology of different CPXV strains. Shown are plaques of different CPXV strains (Kre, Hei, BR, Ber and Gri). Mix: equal mix of the five CPXV strains.

Supplementary Tables

Table S1: Determination of the GE-to-PFU ratio.

Sample	GE/mL	PFU/mL	GE/PFU ratio	Mean	SD[a]
HEp-2, replicate 1	2.48E+10	3.50E+08	70.8	82	9
HEp-2, replicate 2	2.61E+10	3.33E+08	78.3		
HEp-2, replicate 3	2.47E+10	2.83E+08	87.2		
HEp-2, replicate 4	3.62E+10	4.00E+08	90.6		
Rat-2, replicate 1	2.50E+09	1.75E+08	14.3	17	8
Rat-2, replicate 2	3.28E+09	1.17E+08	28.2		
Rat-2, replicate 3	2.09E+09	2.17E+08	9.6		
Rat-2, replicate 3	4.00E+09	2.33E+08	17.1		

[a] Standard deviation

Table S2. Overview of poxvirus reads and coverage.

Sample[a]	Pox reads[b]	Coverage[c]	Genome size	Sample[a]	Pox reads[b]	Coverage[c]	Genome size
HP1	3.27E+06	2432.6	216,329	RP1	1.74E+06	1338.4	209,458
HP2	4.28E+06	3596.3	216,478	RP2	6.80E+06	5624.3	216,476
HP3	3.15E+06	3233.1	216,230	RP3	6.94E+06	6114.5	216,481
HP4	3.01E+06	3014.3	216,626	RP4	8.54E+05	722.1	216,479
HP5	1.13E+06	891.3	216,476	RP5	7.97E+05	793.4	216,899
crust	1.30E+06	1290.3	216,458				

[a] H: HEp-2; R: Rat-2; P: passage
[b] Trimmed reads after quality control
[c] Mean coverage across viral genome

Table S4. Ubiquitinated CPXV IMV proteins without conserved ubiquitination sites.

Protein name	Protein description	Function
A34	EEV glycoprotein	Entry into host cell
A47	3 beta-hydroxysteroid dehydrogenase/$\Delta^{5\rightarrow4}$-isomerase	Immune evasion
C9	Ankyrin repeat domain-containing protein, host range CP77	Unknown
E2	Core protein	Unknown
E8	Cell surface-binding protein	Transcription
G11	RhoA signaling inhibitor	Unknown
G4	Ribonucleoside-diphosphate reductase small chain	DNA replication
H9	Late transcription factor 1	Transcription
J4	RNA polymerase-associated protein	Transcription
M4	Phospholipase-D-like protein	DNA replication
O2	DNA-directed RNA polymerase 22 kDa subunit	Transcription

Table S3. Distinct conserved ubiquitination sites in CPXV IMV proteins.

Protein name	diGly(K) position in protein (CPXV BR)
A11	149; 189; 194; 367; 437; 511; 560; 739; 791; 797
A14	49; 56
A17	258
A19	88
A1	36
A23	44
A24	154; 283; 330; 357
A25	139
A26	15; 77; 239; 246; 255
A28	37
A30	174
A35	125
A36	64
A44	13; 16; 26; 29; 42; 59
A4	111; 185; 189; 270; 311; 471
A50	83
A52	143
A53	394
A6	70
A7	86; 136; 137; 194; 297; 299; 331
A8	513
B2	370
B4	41
C17	62
C3	273; 274
C8	66; 76
D12	96; 108; 109
E13	172; 231; 354; 419; 436; 469
E5	124; 647
F3	45
F4	62
F6	90; 94
F8	13; 187
G13	168; 226; 231
G17	17; 25; 74
H10	236
H1	7; 96; 109; 369; 370; 478
H2	89; 111
H3	107
H4	54; 96; 99
H5	282
H8	36; 224; 246; 268; 292
J1	22; 40; 51; 159; 165; 170
J3	47; 109; 148; 225; 254
L1	59; 100; 109; 174; 203; 232
L7	97
M1	21; 262
N1	21
N3	272
N4	175; 202; 207; 212; 240; 250
O1	234
O4	37
Q1	70; 78
S1	82; 78

Figures

Tables

Abbreviations

Common abbreviations are not listed separately.

ABC	Ammonium bicarbonate
ACN	Acetonitrile
ATI	A-type inclusion body
Ber	CPXV strain HumBer07/1
BR	CPXV strain Brighton Red
BRFseR	RFP/GFP-expressing CPXV strain
CAA	2-Chloroacetamid
CCHF	Crimean-Congo haemorrhagic fever virus
CDS	Coding sequence
CI	Cell index
CID	Collision-induced dissociation
CLSM	Confocal laser scan microscopy
CMC	Carboxymthylcellulose
CMV	Cytomegalovirus
CNV	Copy number variation
CPE	Cytopathic effect
CPXV	Cowpox virus
CsCl	Cesium chloride
diGly	Di-glycine
DMEM	Dulbecco's Modified Eagle Medium
DMSO	Dimethylsulfoxid
EEV	Extracellular enveloped virion
EMEM	Eagle's Minimal Essential Medium
EtOH	Ethanol
FA	Formic acid
FCS	Fetal calf serum
FDR	False discovery rate
GE	Genome equivalents
GFP	Green fluorescent protein
Gri	CPXV strain HumGri07/1
Hei	CPXV strain RatHei09/1
iBAQ	Intensity Based Absolute Quantification
IFN	Interferon
IL	Interleukin
IMV	Intracellular mature virion
IRF	Interferon regulatory factor
ISG	Interferon-stimulated gene
ITR	Inverted terminal repeat
Kre	CPXV strain RatKre08/2
LB	Lateral body
LC	Liquid chromatography
LDH	Lactate dehydrogenase
LFQ	Label free quantification
LTQ	Linear trap quadrupole
MBR	Match between runs
MeOH	Methanol
MOI	Multiplicity of infection
MS	Mass spectrometry
MS/MS	Tandem mass spectrometry
m/z	Mass-to-charge ratio
NGS	Next-generation sequencing
nLC	Nano liquid chromatography
OPV	Orthopoxvirus
p.i.	Postinfection
PBS	Phosphate buffered saline
PCA	Principal component analysis
PFA	Paraformaldehyde
PFA	Paraformaldehyde
PFU	Plaque forming units
PKR	Protein kinase R
PMSF	Phenylmethylsulfonylfluorid
Pol	Polymerase
PTM	Posttranslational modification
RFP	Red fluorescent protein
SDS	Sodium dodecyl sulfate
TCEP	Tris(2-carboxyethyl)phosphine
TEM	Transmission electron microscope
TFA	Trifluoroacetic acid
TNF	Tumor necrosis factor
TPA	Total protein approach
UPS	Ubiquitin-proteasome system
VACV	Vaccinia virus
VARV	Variola virus
VF	Virus factory

Publications

The author's publications are listed in the following.

1. Grossegesse, M., Doellinger, J., Fritsch, A., Laue, M., Piesker, J., Schaade, L. and Nitsche, A. Global ubiquitination analysis reveals extensive modification and proteasomal degradation of cowpox virus proteins, but preservation of viral cores. Manuscript submitted to *Scientific Reports*.

2. Grossegesse, M., Doellinger, J., Tyshaieva, A., Schaade, L. and Nitsche, A. Combined proteomics/genomics approach reveals proteomic changes of mature virions as a novel poxvirus adaptation mechanism. *Viruses* **2017**, 9(11).

3. Grossegesse, M., Doellinger, J., Haldemann, B., Schaade, L. and Nitsche, A. A next-generation sequencing approach uncovers viral transcripts incorporated in poxvirus virions. *Viruses* **2017**, 9(11).

4. Doellinger J., Grossegesse, M., Nitsche, A. and Lasch, P. DMSO as a mobile phase additive enhances detection of ubiquitination sites by nanoLC-ESI-MS/MS. *Journal for Mass Spectrometry*, **2017**.

5. Grossegesse, M., Doellinger J. and Nitsche A. Adaptation of DNA viruses in cell culture on the example of poxviruses. Manuscript in preparation.

6. Doellinger J., Grossegesse M., Schlenther I., Lasch P., Schaade L. and Nitsche A. Proteomics identifies rat-isolated CPXV strain with high adaptation to inhibit human IFN-type I signaling. Manuscript in preparation.

Acknowledgments

Above all, I am very grateful to Prof. Dr. Andreas Nitsche not only for supervision and support, but also for giving me many freedoms. Moreover, I would like to thank Prof. Dr. Juri Rappsilber and Prof. Dr. Roland Lauster for supervising and reviewing my dissertation.

Many thanks to my scientific advisor Dr. Jörg Döllinger for that you had always time and for introducing me to the field of proteomics. Thanks also to Annemarie Fritsch, who made a considerable contribution to my project during her internship and her master's thesis "The role of the ubiquitin-proteasome system in CPXV infection". Thanks to all my wonderful colleagues in ZBS 1 who facilitated my work in so many ways, especially my doctoral colleagues Andreas Andrusch, Annika Brinkmann, Doreen Vollandt, Ilka Schlenther, Margarita Voskanian, Markus Neumann, Robert Koban and Simon Tausch. Very special thanks to Jeanette Klenner for your honesty and for always encouraging me and making me smile. I would also like to thank the NGS team, above all Julia Hinzmann, for handling my NGS samples. Moreover, I am grateful to Dr. Wojtek Dabrowski, Alona Tyshaieva, Berit Haldemann, Dr. Lei Mao and Dr. Bernhard Renard for support with bioinformatics analysis. Thanks to Dr. Michael Laue, Janett Piesker, Gudrun Holland and Kazimierz Madela for excellent EM pictures and support with confocal laser scanning microscopy. Also great thanks to Ursula Erikli for copy-editing of manuscripts.

Moreover, in particular, I would like to thank Juliane Rudeck, who took care of my dear horse Avalon during my thesis. And thank you Avalon for relaxing rides in the evening.

Finally, I am deeply grateful to my whole family, the Bürgers and the Grossegesses, for supporting me in whatever I do. Thanks to my parents Regina Bürger and Andreas Czajka for always believing in me and enabling me to live my dreams. Greatest thanks to my husband Maximilian Grossegesse for your daily support and for bearing my limited free-time. Thanks to my sister Leandra Bürger for making me see the world from a different point of view and for being such a good friend.